Summer 8-15-2019

The Role of Mitofusins in the Osteoclast Lineage

Anna Ballard
Washington University in St. Louis

WASHINGTON UNIVERSITY IN ST. LOUIS

Division of Biology and Biomedical Sciences
Molecular Genetics and Genomics

Dissertation Examination Committee:
Deborah J. Veis, Chair
Gabriel Mbalaviele, Co-Chair
Gerald W. Dorn, II
Roberta Faccio
Jason M. Held

The Role of Mitofusins in the Osteoclast Lineage

by
Anna A. Ballard

A dissertation presented to
The Graduate School
of Washington University in
partial fulfillment of the
requirements for the degree
of Doctor of Philosophy

August 2019
St. Louis, Missouri

Table of contents

List of Figures

Acknowledgements

This study was supported by NIH/NIAMS AR052705, NIH/NIAMS R01 AR070030-01A1, and funding from the Shriners Hospitals awarded to D. Veis, as well as 5T32AR060719-05 awarded to A. Ballard and R. Zeng. μCT and histological analysis was made possible by the Musculoskeletal Research Center site grant P30 AR057235. Additional support for the TFEB and Osteomyelitis projects was from NIH/NIDDK DK067145 awarded to S. Mumm, and NIH/NIAMS R21 AR073507, awarded to D. Veis.

I want to thank the Deborah Veis Laboratory at Washington University in St. Louis for their support of my graduate journey. Current members Ali Zarei, D.Phil, Phil Roper, Ph.D., Jennifer Davis, Ph.D., Linda Cox, and Christine Shao, have constantly helped me troubleshoot experiments and offer insight on the implications of my data. Former member Rong Zeng, Ph.D., spearheaded this project and helped me take it over. Jianqiu Xiao and Crystal Idleberg were instrumental in generating retroviral mutants and histological sections. Guidance by Deb Veis, M.D., Ph.D. has helped me grow as a scientist and I am grateful for her mentorship and generosity in allowing me to pursue work in her laboratory. I am thankful for the Faccio lab next door, as these individuals offer support on a daily basis and participate in helping promote scientific rigor in my project through comments at laboratory meetings. Roberta Faccio, Ph.D., has been a strong force in shaping our work into a story, and providing countless suggestions to improve our methods and interpretation of results. I have learned so much from meetings with her and Dr. Veis, as these two women are incredible role models and experts in the field.

In addition, my thesis committee has helped guide our work forward and I am grateful for the support of Gabriel Mbalaviele, Ph.D. in leading this group, as well as past committee chairman Fanxin Long, Ph.D. Roberta Faccio, Ph.D., and Jason Held, Ph.D. have been strong

supporters of our work at committee meetings and I am fortunate to also have exceptional assistance from Gerald Dorn, II, M.D. He has generously provided $Mfn1^{fl/fl}$; $Mfn2^{fl/fl}$ breeders and Mfn2 WT, EE, and AA plasmids for our work, and his expertise in mitofusin biology aided intellectual support to our studies.

This work could not have been completed without the support of the Division of Bone and Mineral Diseases and Musculoskeletal Research Center, as I received financial support from the division's T32 training grant, and benefitted from the community on our floor. Colleagues constantly offered camaraderie throughout the years and random smiles and waves in the hallway were always appreciated. In particular, my labmates Linda and Jenn were lifesavers in that they could always heighten my spirits and cause laughter in the lab. Lunch buddies, Linda, Samantha Coleman, and Michael Brodt did the same and I'm appreciative of their friendships. Kirsten Brenner served as my number one support system in St. Louis, and I appreciate her support on a daily basis for coffee breaks and for being my indoor cycling and stress-relief partner in crime.

Lastly, I could not have completed my Ph.D. training without the unyielding support and love of my parents, Steve Ballard, D.D.S., and Sandy Ballard, M.S. They have allowed me to chase my love of genetics from Colorado, through Minnesota, and then to Missouri, and continually share their support from afar by to listening to lab stories and drama on the phone and then enduring hot St. Louis summers on yearly visits. Knowing they believe in me on this journey keeps me moving forward every day. I am extraordinarily lucky to have them on my side and am forever grateful for their strength and love.

Thank you, all! Best, Anna

Washington University in St. Louis
August 2019

Dedicated to my incredible parents,
Steve and Sandy Ballard.

Abstract of the Dissertation

Mitochondria exist in a highly dynamic network in many cell types, and mutations in mitochondrial transmembrane GTPase mitofusin2 (MFN2), a key factor that mediates mitochondrial tethering, cause defects in the nervous system. Intriguingly, the skeleton has been overlooked in patients with such mutations. Because expression of MFN2 and its homolog, mitofusin1 (MFN1) increase with maturation of osteoclasts (OCs), which are rich in mitochondria, we sought to determine the role of mitofusins in the OC lineage. Double knockout of *Mfn1* and *Mfn2* in OC precursors by Lysozyme-M cre reveals that mitofusin activity is required for OC function and maintenance of bone mass in female mice *in vivo. In vitro,* double knockout bone marrow macrophages are unable to differentiate into mature OCs. Here, OC formation in dcKO BMMs is restored when *Mfn2* but not *Mfn1* is retrovirally overexpressed. To further explore the role of MFN2 in the OC lineage, we conditionally deleted *Mfn2* with LysM-cre and find bone mass is increased in aged female Mfn2 cKOs compared to cre-only littermates. Challenging these single MFN2 knock out animals with acute RANKL injection indicates that Mfn2 is important in female, but not male, OCs, because female Mfn2 cKOs are protected from bone loss with this osteolytic stimuli. Specific MFN2 functions were further assessed in culture. While a MFN2 mutant defective in mitophagy is able to promote osteoclastogenesis, another unable to tether mitochondria is not. This suggests that tethering of mitochondria to eachother and/or the ER by MFN2 is required for osteoclast differentiation, at least in culture. Taken together, our results reveal a sexually divergent role of MFN2-mediated control of mitochondrial dynamics in OC biology. Given the differences in female mice, there may be therapeutic potential to target MFN2 activity for treatment of postmenopausal osteoporosis.

Chapter 1 – Introduction

Part 1 – Osteoclasts

Skeletal homeostasis

The skeleton is an organ constantly remodeling and responding to interactions with other bodily systems and external factors. Bone homeostasis relies on the coupled activity of osteoblast (OB) and osteoclast (OC) cells that build and resorb the bone matrix, respectively. During development, organic matrix is deposited and subsequently mineralized by OBs to form hydroxyapatite from calcium and phosphate. The OC destroys both the organic and inorganic components of the bone matrix through release of acids and proteases at sites of bone remodeling. When skeletal integrity is properly maintained, these two cell types constantly remodel bone at a rate of complete bone turnover every 10 years (reviewed in (Novack, 2011).

The bone environment includes chondrocytes that reside on joint surfaces and maintain articular cartilage. Osteocytes are imbedded in the bone matrix and are OB-derived, functioning to relay signals from mechanical stimuli. In response to mechanical demands and fracture healing, bone formation is favored. Without these stimuli, bone mass decreases in conditions of unloading. OC formation and function are regulated by a number of factors in the body, and hormonal or inflammatory stimulation of OC activity that is not matched by OBs can lead to pathogenic decreases in bone mass (reviewed in (Novack, 2011; Ono, 2018)). Under homeostatic conditions, bone remodeling is coupled, whereby products released by OC-mediated matrix degradation recruit OBs, and OBs in turn secrete factors that induce OC differentiation (Henriksen et al., 2013; Martin and Sims, 2005; Novack and Teitelbaum, 2008).

Cellular morphology/components

The unique morphology of the mature OC allows it to efficiently resorb the bone. These multinuclear cells become polarized when in contact with the bone surface creating an area, termed the resorption lacuna, where the section of bone to be excavated is isolated. At this junction, called the ruffled border, numerous expansions of the membrane allow large surface areas for transport of cargo into the lacuna by trafficking down microtubules and microfilaments, which is controlled by small GTPases (reviewed in (Cappariello et al., 2014; Novack and Faccio, 2011)).

Inorganic and organic components make up the bone matrix. Inorganic crystalline hydroxyapatite mineral, $[(Ca_3(PO_4)_2]_3Ca(OH)_2$, must be dissolved acidically. This is achieved by the transport of protons to the resorption lacuna by the vacuolar H^+-ATPase on the ruffled border that creates a pH of ~4.5 and liberates calcium from hydroxyapatite (Gay and Mueller, 1974; Silver et al., 1988). Because H_2CO_2 is utilized as a proton source, it dissociates into H^+ which is pumped into the lacuna, and the remaining bicarbonate is removed from the OC cytoplasm via a chloride-bicarbonate exchanger on the basolateral membrane. This also brings Cl^- into the cell which is also delivered to the resorption lacuna by Cl^- channels charge coupled to the H^+-ATPase (Blair et al., 1991). Proteolytic enzymes, primarily cathepsin K (CatK), are active at low pH and degrade type I collagen and other organic components of the bone matrix (Bossard et al., 1996; Drake et al., 1996).

The membrane at the sealing zone is anchored to the bone surface via integrin-mediated adhesion, primarily by integrin αvβ3. In close proximity to integrin αvβ3 is a belt of podosomes that form a ring around the periphery of the resorption lacuna (Destaing et al., 2003). Comprised of F-actin and microtubules, these structures are highly dynamic and isolate only areas being

actively resorbed (SALTEL et al., 2008). Here, when OCs migrate, cytoskeletal remodeling includes disassembly of sealing zones and lamellipodial movement, then subsequent attachment to a new location with integrin αvβ3 adherence and nascent podosome formation (reviewed in (Novack and Faccio, 2011; Teitelbaum, 2011)) (Fig. 1.1).

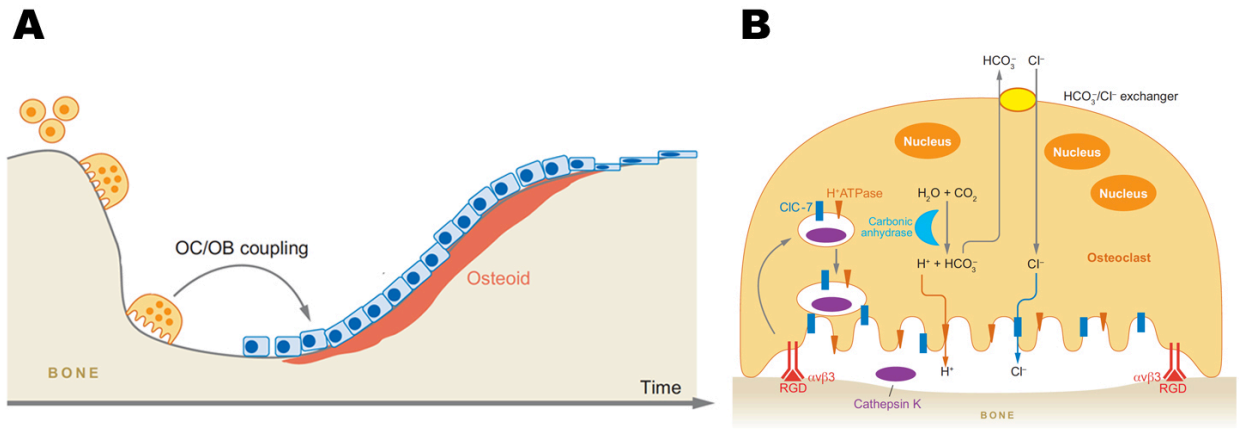

Figure 1.1: Bone remodeling

A). Under homeostatic conditions OB build the bone resorbed by OCs at an equal rate to maintain bone mass. B). Cellular components that allow for proper acidification of the resorption lacuna, adapted from (Novack and Teitelbaum, 2008).

Differentiation/activation signaling

OCs are derived from hematopoietic stem cells in the bone marrow by way of c-Kit^{+}CD11b^{lo}c-Fms^{+} common myeloid progenitors (Arai et al., 1999). Cells from this macrophage/monocyte lineage become committed to an OC fate when exposed to two cytokines, macrophage-colony stimulating factor (M-CSF) and receptor activator of NF-κB ligand (RANKL). Both factors are required for OC formation, and are sufficient to form OCs from bone marrow macrophage precursors *in vitro* (Quinn et al., 1998). While M-CSF works through tyrosine kinase receptor c-Fms to promote survival and proliferation of OC lineage cells,

RANKL interacts with the RANK receptor to initiate differentiation through alternative NF-κB signaling (Novack and Teitelbaum, 2008). RANKL (encoded by *Tnfsf11*), a transmembrane protein member of the TNFR superfamily that harbors several TRAF-binding domains, is produced most highly by osteoblasts and osteocytes (Nakashima et al., 2011; Nelson et al., 2012). Although osteoclastogenesis is aided by co-stimulatory action of ITAM signaling that with RANKL modulates calcineurin, MAPK, PI3K and Src signaling, NF-κB remains indispensable for OC formation (Novack, 2011). When NF-κB is activated by membrane-bound or soluble RANKL interacting with the RANK receptor on OC precursors, RANK binds TNF receptor-associated factor 3 (TRAF3), which stabilizes NF-κB inducing kinase (NIK). Because NIK is ubiquitinated and degraded in the absence of RANKL activation, its stabilization allows NIK to phosphorylate and activate IκB kinase alpha (IKKα). Consequently, IKKα activation leads to p100 and RelB processing in the proteasome so that p52 (resulting from partial degradation of p100) and RelB can translocate to the nucleus. Of most importance, this results in the activation of two transcription factors required for osteoclastogenesis, c-Fos, and NFATc1 (reviewed in (Novack, 2011; Ono, 2018)).

NFATc1 is a master regulator of osteoclastogenesis, and with its induction and auto-amplification, transcription of multiple osteoclast-specific genes are induced (Ishida et al., 2002; Takayanagi et al., 2002). To name a few, cathepsin K is important for bone resorption as described above, tartrate resistant acid phosphatase (TRAP) is a potent OC marker, and DC-STAMP mediates OC fusion (BURSTONE, 1959; Yagi et al., 2005). Interestingly, NFATc1 is highly susceptible to Ca^{2+} fluxes and requires dephosphorylation by calcineurin for translocation to the nucleus (Hogan et al., 2003). Here, many groups have demonstrated that heightened Ca^{2+}

oscillations in the cytoplasm following RANKL stimulation are associated with increased osteoclastogenesis (Kim et al., 2013; Takayanagi et al., 2002; Yang et al., 2009).

Bioenergetics in the OC

Compared to other cells, OCs have the ability to function in low oxygen conditions between 1.5-6.3% pO_2 (atmospheric O_2 = 21% and majority of tissues operate between 5-12%) (Spencer et al., 2014). Hypoxia actually increases osteoclastogenesis *in vitro* (Arnett et al., 2003). With their ability to function in a variety of cellular conditions, OCs may use fatty acids and glucose to support both aerobic and anaerobic respiration during osteoclastogenesis (reviewed in (Arnett and Orriss, 2018)). Further, metabolic byproducts of H^+ ions and reactive oxygen species have beneficial effects on OCs by stimulating OC activity and aiding acidification of the resorption lacuna (Arnett and Dempster, 1986; Callaway and Jiang, 2015).

OCs are rich in mitochondria and differentiation from bone marrow macrophage precursors to OCs is associated with significant increase in mitochondria copy number, oxidative phosphorylation (OxPhos) subunits, and oxygen consumption (Zeng et al., 2015). Alternative NF-κB signaling that is crucial for osteoclastogenesis also regulates mitochondrial biogenesis and function in skeletal muscle, and modulates the expression of mitochondrial biogenesis factor, PPARγ cofactor 1β (PGC-1β), in the OC (Bakkar et al., 2012; Zeng et al., 2015). Loss of PCG-1β in the OC results in impaired cytoskeletal organization and bone resorption in addition to decreased mitochondrial biogenesis (Zhang et al., 2018).

OCs require vast amounts of energy to resorb bone, and these cells utilize glucose and glutamine as primary sources for respiration (Indo et al., 2013). As OCs operate in the hypoxic environment of the bone, resorption becomes an energy-intensive operation. Upon differentiation from bone marrow macrophage precursors, pre-OCs exposed to RANKL undergo

a metabolic shift toward accelerated glycolytic and oxidative metabolism, ultimately leading to increased ATP production and electron transport chain activity (Kim et al., 2007; Morten et al., 2013). Accordingly, metabolic enzymes are upregulated during osteoclastogenesis and oxygen consumption rates increase compared to macrophages in mouse-derived cells (Czupalla et al., 2005; Zeng et al., 2015).

Additional functions of the OC

In addition to bone resorption, studies have also shown OCs to have roles in regulating hematopoiesis, bone formation, intraosseous angiogenesis, and osteocalcin hormonal functions. Cathepsin K and matrix metalloproteinase MMP9 produced by the OCs mobilize CXCL12 and c-Kit that regulate hematopoietic stem cells (HSCs), and treatments targeting the OCs such as strontium, prostaglandin, and bisphosphonates, have additional effects on HSCs (Frisch et al., 2009; Lymperi et al., 2011; 2008). During resorption OCs release products from the bone matrix that induce bone formation. These are termed "clastokines" and are anabolic agents that recruit OB precursors to the bone matrix such as TGFβ, bone morphogenetic proteins, fibroblast growth factors, and insulin-like growth factor (reviewed in (Cappariello et al., 2014; Teti, 2013). Other factors such as VEGF-A and HIF1α induce angiogenesis (Chim et al., 2013; Trebec-Reynolds et al., 2010).

Mouse models and cres

Cre-Lox technology allows researchers to selectively delete genes of interest in specific tissues through mating genetically engineered animals harboring a *floxed gene* and cre recombinase expressed by tissue-specific transcription factors (Yarmolinsky and Hoess, 2015).

The study of factors important in OC formation and function has been aided by the development of multiple cre drivers in the OC lineage. Early deletion of floxed alleles can be achieved with use of Lysozyme M-cre, CD11b-cre, and RANK-cre, while genes may be conditionally deleted in mature OCs via Cathepsin K-cre (reviewed in (Elefteriou and Yang, 2011)).

While mice display highest levels of bone mass at 4 months of age, OCs generally have greatest activity at 2 months, as evidenced by serum CTX, a marker for bone resorption, reaching peak elevation in B6 mice (Amend et al., 2015). Common experimental techniques to induce OC differentiation and activity include exposing mice to RANKL injected subcutaneously or intraperitoneally (Shashkova et al., 2016). Induction of inflammatory arthritis has also been shown to induce OC activity (Decker et al., 2015; Seeling et al., 2013). Such induction of pathological bone loss can produce robust OC phenotypes, and uncover phenotypes not apparent under basal physiological conditions (Novack et al., 2003; Vaira et al., 2008). This is also seen in models of ovariectomy (OVX), a model of postmenopausal osteoporosis that induces OC activity through estrogen deficiency (Anginot et al., 2007; Wu et al., 2007).

Mouse models have been immensely useful in elucidating the impact of signaling components of the osteoclast and overall bone health. For example, ablation of NF-κB components, RANK, RANKL, Cathepsin K, αvβ3 integrin, NFATc1, in murine models all lead to high bone mass osteopetrotic phenotypes (reviewed in (Novack and Teitelbaum, 2008; Xu and Teitelbaum, 2013)).

In contrast to osteoporosis, osteopetrosis is a genetic condition in which bone mass and density are increased because of a failure of bone resorption by OCs. Most often, humans present with forms of either OC-poor or OC-rich osteopetrosis whereby the disease manifests due to a failure of OCs to differentiate or function, respectively. Either form of the disease is

often accompanied by hematological impairment and decreased life expectancy (reviewed in (Sobacchi et al., 2013)). As mouse models closely phenocopy human ailments, it is critical that mouse models of OC dysfunction be studied closely.

Part 2 – Mitochondrial dynamics

Mitochondrial networks

Mitochondria exist within a dynamic network in most cell types and are highly regulated. Here, termed mitochondrial dynamics, the processes of tethering/fusion, fission, and mitophagy play an important role in mitochondrial homeostasis. Changes in mitochondrial networks are frequent, and this architecture is varied depending on the developmental or metabolic needs of a cell (reviewed in (Dorn et al., 2015; Schrepfer and Scorrano, 2016; Ventura-Clapier et al., 2008)).

As the organelles become more connected with increased fusion, ATP production increases because networks allow exchange of mtDNA and metabolites between once-separated mitochondria. In particular, fusion of mitochondria under stressful conditions prevents autophagy and allows ATP production to be optimized due to increased cristae density favoring ATPase oligomerization (Gomes et al., 2011; Rambold et al., 2011). Fusion is accomplished through coordinated rearrangement of both the outer and inner mitochondrial membranes (OMM and IMM, respectively), which are mediated by MFN1/MFN2, and OPA1, respectively. Mammalian mitofusins MFN1 and MFN2 are ~80% homologous, each consisting of an N-terminal cytosolic GTPase domain, a coiled coil heptad-repeat (HR1) domain, two transmembrane domains, and heptad-repeat domain (HR2) at the C-terminus (reviewed in (Filadi et al., 2018b)).

Accumulation of mitofusins in regions of contact in neighboring mitochondria precedes fusion events (Mozdy and Shaw, 2003). It is generally accepted that fusion is achieved first through antiparallel binding of the carboxy-terminal α-helical HR domains of MFN1 and/or MFN2. This brings GTPase heads together for subsequent GTP hydrolysis and dimerization

(reviewed in (Dorn, 2019; Koshiba et al., 2004). Intriguingly, MFN2 exhibits two alternative conformations that make its state tethering-permissive or tethering-non-permissive. Only tethering-permissive intramolecular interactions of MFN2 allow the HR2 domain exposure into the cytosol to tether with the HR2 of an adjacent mitofusin protein (Franco et al., 2016). When tethering is successful, GTP hydrolysis then induces OMM fusion of the two mitochondria (Koshiba et al., 2004; Lee and Yoon, 2016). Following OMM fusion, OPA1 anchored on one IMM binds to cardiolipin on another IMM, whereby subsequent tethering and GTP hydrolysis by OPA1 fuses the two membranes (Ban et al., 2017; Lee and Yoon, 2018).

Conversely, networks become fragmented to prevent nutrient overload. In this state, oxidative stress and mitochondrial depolarization increase, and ATP production is blunted with an increase in mitochondrial uncoupling and nutrient storage (Jheng et al., 2012; Molina et al., 2009). Mitochondrial fission requires recruitment and post-translational modifications of DRP1, a cytosolic GTPase dynamin 1-like protein, to the OMM, where it promotes fission with interaction of fission proteins, MFF, MID51, MID49, and FIS1 (reviewed in (Hu et al., 2017)).

Additionally, mitochondrial dynamics allow for strict quality control of organelles, as damaged mitochondria can be sequestered from the network and degraded via a specialized form of autophagy referred to as mitophagy (reviewed in (Ashrafi and Schwarz, 2013; Shirihai et al., 2015). Here, it is generally accepted that PINK1 kinase responds to mitochondrial depolarization, ROS production, and protein misfolding to induce mitophagy ((Jin and Youle, 2013; Matsuda et al., 2010; Narendra et al., 2010)). PINK1 phosphorylates MFN2 on three residues to promote removal of damaged mitochondria. Ser378 phosphorylation induces the tethering-non-permissive state, prohibiting mitochondrial fusion (Rocha et al., 2018). Phsosphorylation on Thr111 and Ser442 recruits E3 ubiquitin ligase PARKIN to bind MFN2

(Chen and Dorn, 2013). With mutation of these threonine and serine residues to glutamic acid or alanine, mitophagy signaling is either constitutively activated or repressed, respectively (Gong et al., 2015). When recruited by MFN2, PARKIN subsequently mediates mitochondrial targeting to the autophagosome (reviewed in (Dorn et al., 2015; Gustafsson and Dorn, 2019)). Independent of PINK1/PARKIN signaling, mitochondria can also be cleared by direct engulfment into the lysosome or through clearance by the endosomal sorting complexes required for transport (ESCRT) machinery that ultimately delivers mitochondria to the lysosome (reviewed in (Moyzis and Gustafsson, 2019).

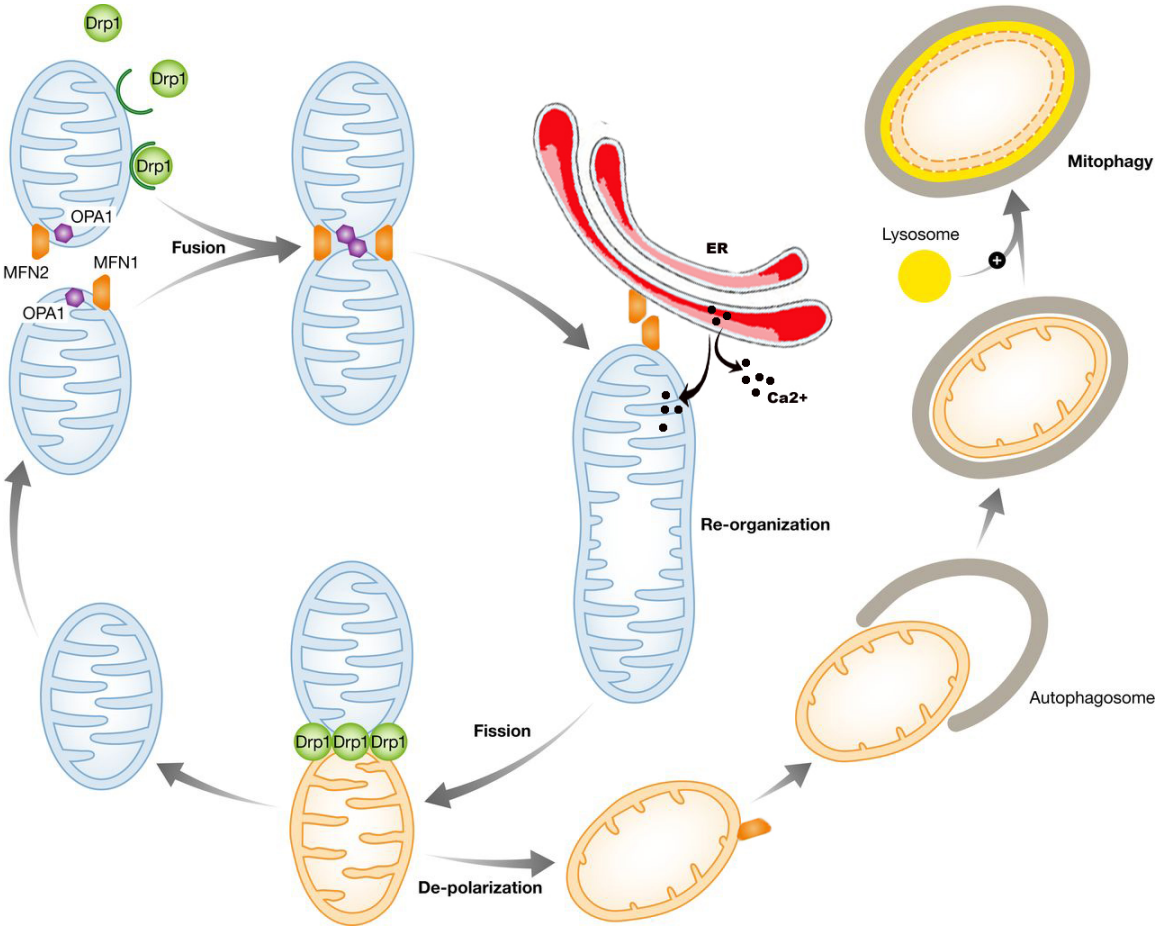

Figure 1.2: Depiction of mitochondrial dynamics and key players

Mitochondrial dynamics includes the fission, fusion, and mitophagy of mitochondria. Of note, MFN1 and MFN2 participate in the tethering/fusion of one mitochondria to another, and tethering of mitochondria to the ER by MFN2 impacts Ca^{2+} signaling. Adapted from (Gao et al., 2014).

Mitofusins

As introduced above, transmembrane GTPases MFN1 and MFN2 are key players in mitochondrial dynamics. Both are necessary for survival, as deletion of either mitofusin is embryonic lethal, at mid-gestation in murine models. The majority of *Mfn1* or *Mfn2* knock out (KO) embryos are resorbed prior to E12.5, and in the case of *Mfn2* KO, placenta formation is impaired. Double deletion of *Mfn1* and *Mfn2* leads to even earlier mortality (Chen et al., 2003). Morphologically in MEFs, knockout of *Mfn1* or *Mfn2* leads to severely fragmented mitochondrial networks (Chen et al., 2003). Decreased oxygen consumption is also a feature of cells lacking *Mfn1* and *Mfn2* in murine cell cultures (Chen et al., 2005; Song et al., 2015).

To combat the lethality associated with global mitofusin knockout, floxed alleles have been generated to study *Mfn1* and/or *Mfn2* loss conditionally. Similarly to whole body single and double KO of *Mfn1* and/or *Mfn2*, systems such as cardiac muscle display more robust defects in morphology and function when both *Mfn1* and *Mfn2* are deleted compared to deletion of either homolog alone (Chen et al., 2010; Papanicolaou et al., 2012a; Song et al., 2015).

Changes in mitofusin expression can be observed as the connectivity of mitochondria decreases. This generates mitochondrial aspect ratios that can be compared, as higher ratios indicate a greater degree of fused/networked organelles (Gong et al., 2015). While MFN1 solely participates in mitochondrial tethering/fusion, MFN2 mediates mitophagy as well as assists in mitochondrial transport and serves as a mitochondrial tether to the ER (Figure 1.2). Transport of mitochondria down axons also requires functional MFN2 whereby MFN2 interacts with MIRO and MILTON motor proteins that allow mitochondrial attachment to microtubules (Misko et al., 2010). Branching and enervation of nerve fibers to dopamine neurons is also compromised in dopamine neuron specific *Mfn2* cKO (Lee et al., 2012).

The connection between mitochondria and the ER is important for regulation of many cellular functions including Ca^{2+} signaling, lipid biosynthesis, apoptosis, and the ER stress response (reviewed in (Filadi et al., 2018a; van Vliet and Agostinis, 2018)). Studies using *Mfn2* knockdown cells have revealed that ablation of *Mfn2* increases mitochondria distance to the ER, and loss of the protein leads to impaired Ca^{2+} calcium uptake in the mitochondria (de Brito and Scorrano, 2008; Filadi et al., 2016; Naon et al., 2016). Buffering of Ca^{2+} by the mitochondria functions to maintain cellular functions including metabolism and survival, further implicating the importance of *Mfn2*. Accordingly, mouse heart and hematopoietic stem cell models lacking *Mfn2* sustain defects in calcineurin signaling including aberrant induction of downstream transcription factors NOTCH1 and NFAT, respectively (Kasahara et al., 2013; Luchsinger et al., 2016). Recently, structural insights into MFN2 GTPase and HR domains have allowed groups to probe the specific function of particular residues *in vitro*. For example, MFN2 K416R mutation disallows ubiquitination by Parkin that required for the physical interaction between mitochondria and ER, as K414R increases distance between organelles and reduces mitochondrial Ca^{2+} uptake in MEFs (Basso et al., 2018). Another mutant, MFN2 F223L, represses mitochondrial fusion, but does not alter mitochondrial proximity to one another by tethering assay. Tethering to the ER was not assessed in this model (Engelhart and Hoppins, 2019).

Mfn2 disease importance

The nervous system is highly impacted by *Mfn2* defects, and *Mfn2* mutations are linked to disorders of the central and peripheral nervous system that lead to neuropathies and sensory loss (reviewed in (Celsi et al., 2009; Filadi et al., 2018b)). One of the leading neuropathies

associated with mutations in *Mfn2* is Charcot-Marie-Tooth type 2A syndrome (CMT2A), a neurodegenerative disease in which motor and sensory defects develop within the first two decades of life. Over 100 dominant *Mfn2* mutations are linked to CMT2A, and are responsible for nearly 100% of cases. In the clinic, these patients generally present with sensory loss in the feet, lack of tendon reflexes, and postural tremors (Adam et al., 1993; Züchner et al., 2004). On a molecular level, axonal degeneration is observed and mitochondrial transport along microtubules is impaired with CMT2A, and often, mitochondria are reported accumulating abnormally in distal sites of axons, making the longest axons most severely affected (Cartoni et al., 2010; Funalot et al., 2009; Misko et al., 2010).

Mitochondrial fusion defects are observed in CMT2A as well (Funalot et al., 2009; Sole et al., 2009), with the majority of *Mfn2* missense mutations arising near or within the coiled-coil and GTPase regions of the protein important for initial tethering between mitochondria and completion of fusion, respectively. These defects have been modeled in zebrafish and drosophila, as well as mice (Sandoval et al., 2014; Vettori et al., 2011). Mouse models corroborate the phenotypes seen in humans as mice perform poorly in open field tests (Strickland et al., 2014), and cultured human cells from CMT2A patients have decreased electrical properties and reduced mitochondrial membrane potential (Loiseau et al., 2007; Saporta et al., 2015).

Apart from the nervous system, decreased mitofusin expression is associated with Alzheimer's Disease, poor prognosis in breast cancer, and insulin resistance in diabetes (Bach et al., 2003; Manczak et al., 2011; Wang et al., 2009; Xu et al., 2017). Parkinson's Disease has also been linked to PINK1/PARKIN mutations (Lee et al., 2012). Intriguingly, two families with Charcot-Marie-Tooth Syndrome have been reported to also suffer from dilated cardiomyopathy (Sevillano Fernández et al., 1994; Yoshida et al., 1991). Apart from these cases, defects in

mitochondrial dynamics have not been specifically linked to irregularities in human hearts (Dorn, 2016). However, model organism and human cell culture models lacking mitofusins yield conditions of myocardial hypertrophy, heart tube contractile dysfunction, and vascular smooth muscle cell proliferation, to name a few (Dorn, 2016; Eschenbacher et al., 2012; Guo et al., 2007).

Studies in cardiomyocytes have revealed an important role for MFN2 function during development whereby mitophagy is a requisite for metabolic reprogramming of mammalian hearts as glycolytic mitochondria are replaced with ones optimized for fatty acid metabolism (Gong et al., 2015). Here, post-natal conditional knock out of *Mfn2* in cardiomyocytes begets cardiomyopathy with accumulated dysfunctional mitochondria, and in adults, *Mfn2* cKO in cardiomyocytes manifests with enlarged hearts and dilated cardiomyopathy (Papanicolaou et al., 2011; 2012a). Furthermore, defects in MFN2 or PINK1/PARKIN machinery can lead to myocardial injury and cardiomyopathy (Billia et al., 2011; Kubli et al., 2013). Accordingly, selective loss of MFN2 mitophagy function in mice leads to cardiomyopathy and lethality by 8 weeks of age, but pups with fusion-deficient MFN2 are indistinguishable from wild type littermates (Gong et al., 2015). Of note, human *Mfn2* mutations identified through sequencing databases produce phenotypes such as mitochondrial fragmentation in MEFs and dilation of the heart tube in *Drosophila* (Eschenbacher et al., 2012).

Part 3 – Study Goals

Rationale for study of mitofusins in the OC

OCs are an incredibly dynamic cell type and during osteoclastogenesis, BMMs go through many conformational changes including fusion to become mature multinucleated OCs. Here, we anticipate that mitochondrial networks will be remodeled and ultimately increased tethering/fusion may be required for completion of this differentiation process. Preliminary studies in our laboratory using MitoTracker Green FM staining have demonstrated that control pre-OCs derived from $Mfn2^{+/+}$; $LysM^{c/c}$ mice have highly networked mitochondria, confirming what others have has been shown with elongated mitochondria in human OCs by TEM and anti-mitochondria antibodies (Lemma et al., 2016). In contrast, we find that pre-OCs of $Mfn2^{fl/fl}$; $LysM^{c/c}$ mice where *Mfn2* is conditionally deleted in the OC lineage lose this degree of connectivity in mitochondrial networks, suggesting the absence of *Mfn2* compromises the ability of mitochondria in the OC to fuse with one another.

To our knowledge, the consequence of this observation has never been investigated. Further, bone phenotypes have never been evaluated in humans with *Mfn2* mutations such as in CMT2A, likely because when faced with neurodegenerative ailments, skeletal effects are presumed to be secondary to the immobility and/or neurological changes patients experience. In other cell types, the effect of *Mfn1* vs. *Mfn2* knockout are not always identical, and in particular, double knock out of *Mfn1* and *Mfn2* produce more severe phenotypes than single knockout of either mitofusin alone. We anticipate this could be the case in the OC lineage as well. Therefore, we have generated mouse models in which *Mfn1* and *Mfn2* are conditionally deleted in the OC lineage separately and in combination. In Aims I and II of our study, we explore how bone mass is affected in these three murine models and expect this will inform how the mitofusin

proteins support osteoclast formation and/or function. It is possible that the efficiency of OCs to resorb bone is heightened with highly networked mitochondrial architecture, therefore requiring mitochondria-to-mitochondria tethering and fusion. Alternatively, *Mfn1* and/or *Mfn2* could be necessary for OCs to form, possibly due to altered Ca^{2+} signaling when tethering of mitochondria to the ER is altered. We hypothesize that mitochondrial tethering might accompany OC cell fusion during osteoclastogenesis, and that tethering of mitochondria to each other or the ER is important for OC formation and/or function.

In addition, considering that in other cell types one function of MFN2 is seemingly predominant over the other, we hypothesize that tethering/fusion is more important than mitophagy for OC function. Though autophagy proteins are essential for generating the ruffled boarder and for bone resorption in OCs (DeSelm et al., 2011), we suspect fusion events for OCs to become large multinucleated will also require tethering and fusion of mitochondrial networks. Therefore, in Aim III, we investigate which function is dominant in the OC lineage through utilizing different *Mfn2* mutants that selectively disable tethering or mitophagy. Since MFN2 residues T111 and S442 are phosphorylated in order for mitophagy signaling to proceed, mutagenesis of both to alanine (designated as Mfn2-AA) ablates PARKIN recruitment to the mitochondria and prevents mitophagy from occurring. Alternatively, T111E and S442E mutations (designated Mfn2-EE) promotes spontaneous mitophagy and with the absence of a fusion signal, mitochondrial networks become fragmented (Gong et al., 2015).

Uncoupling the function of tethering/fusion and mitophagy in the OC lineage will elucidate the mechanism through which MFN2 modulates OC formation and/or function. Such knowledge regarding MFN2 action in the OC lineage will inform the novel relationship between this mitochondrial GTPase and skeletal integrity, a connection that may have the potential to be

exploited therapeutically for patients suffering from diseases of bone remodeling like osteoporosis and osteopetrosis.

Specific Aims:

Aim 1 – How is bone mass affected when *Mfn2* is deleted from the OC lineage?

Aim 2 – Is there redundancy between MFN1 and MFN2 in the OC lineage?

Aim 3 – Are tethering/fusion and mitophagy functions of MFN2 important in the OC lineage?

Chapter 2 –
Loss of mitofusins in the OC lineage inhibits OC formation and function in murine models and cell culture systems

Introduction

To investigate the role of mitofusins in the OC, we explore the how loss of Mfn1 and Mfn2 alone and in combination affect the ability of OCs to form and function *in vivo* and *in vitro*. Specifically, we test whether the activities of MFN1 and MFN2 are redundant and address which homolog has a greater impact on bone mass and osteoclastogenesis. To our knowledge, this is the first investigation of these genes in the osteoclast lineage. We use three conditional mouse models in which *Mfn1*, *Mfn2*, or both mitofusins are deleted in the lineage by LysozymeM-cre. μCT analysis of murine femurs is used as our primary readout of changes in bone mass in these models. Cell culture experiments are also undertaken to differentiate BMMs from these mice to OCs *in vitro*. We find that while deletion of *Mfn1* and *Mfn2* singularly does not affect bone mass in young animals, double knockout increases bone mass in female but not male mice. This corresponds with an inability of OCs to form in culture. Further, as rescue of osteoclastogenesis occurs with the overexpression of MFN2 but not MFN1 in these double knockout BMMs, we report that in the OC lineage, Mfn2 plays a dominant role. Accordingly, stressing Mfn2 cKO mice with age and induced osteolysis reveals MFN2 presence supports OC activity.

Materials and methods

Reagents and mice

Double floxed *Mfn1*$^{fl/fl}$*; Mfn2*$^{fl/fl}$ animals were mated to C57Bl/6 mice harboring the LysM-cre allele, and all mice used for study had two copies of LysM-cre (Chen et al., 2007; Clausen et al., 1999). To generate dcKOs, double heterozygous (*Mfn1*$^{fl/+}$*; Mfn2*$^{fl/+}$*;LysM*$^{c/c}$) mice were first bred together and dcKO (*Mfn1*$^{fl/fl}$*; Mfn2*$^{fl/fl}$*; LysM*$^{c/c}$) female progeny mated to double heterozygous males to generate the cohort of double heterozygous controls and dcKOs. In parallel, cre-only (*Mfn1*$^{+/+}$*; Mfn2*$^{+/+}$*; LysM*$^{c/c}$) females from the original double heterozygous mating were bred to double heterozygous males to generate the cohort of cre-only and control animals. The single Mfn2 cohort was generated using heterozygous breeding pairs so that progeny genotypes included cre-only (*Mfn2*$^{+/+}$*; LysM*$^{c/c}$) and cKOs (*Mfn2*$^{fl/fl}$*; LysM*$^{c/c}$). The same strategy was employed to generate Mfn1 cre-only and cKO littermates (*Mfn1*$^{+/+}$*; LysM*$^{c/c}$ and *Mfn1*$^{fl/fl}$*; LysM*$^{c/c}$, respectively)

Mice were housed communally with ad libitum access to fresh chow and water in a pathogen-free temperature controlled barrier facility. Daily observation and weekly cage change was provided by staff of the Division of Comparative Medicine (DCM). Lab members coordinated animal husbandry and breeding, and the DCM veterinarian assessed all health concerns. All protocols were approved by Washington University School of Medicine's Animal Studies Committee (ASC protocol #20170025).

Micro-computed tomography

Following dissection of right femurs from 2, 4, and 12-month old animals, bones were fixed in 10% neutral buffered formalin (Di Ruscio & Associates, Inc., Fenton, MO) for 24 hours, and

then stored in 70% ethanol. *Ex vivo* trabecular and cortical scans were acquired proximal to the growth plate and at the mid-shaft of the femur, respectively (μCT40, Scanco, Brüttisellen, Switzerland) (10 μm resolution, 55kVp, 145 μA, 300 seconds integration time). *In vivo* scanning of tibias was performed at 21.5 μM resolution (70 kVp, 114 μA, 8W, 100ms integration time) on VivaCT 40 (Scanco, Brüttisellen, Switzerland). Trabecular bone compartment was analyzed distal to the end of the tibial growth plate. Thresholds for VivaCT and μCT were determined in a blinded manner and analyzed with reference to accepted guidelines (Bouxsein et al., 2010; Nazarian et al., 2008).

CTX1 and P1NP

Serum was collected from animals fasted overnight via mandibular bleed (BD Microtainer), and stored at -80˚C. RatLaps CTX-1 and P1NP EIA assays was conducted according to manufacturer's instructions (Immunodiagnostic Systems, Gaithersburg, MD, USA; AC-06F1 and AC-33F1, respectively).

Histomorphometry

2 month-old mice were injected intraperitoneally (IP) with 10mg/kg calcein (C0875; Sigma, USA) and 30 mg/kg alizarin red (A3882; Sigma, USA) seven and two days prior to sacrifice. Intact femur/tibias were fixed in 10% neutral buffered formalin for 24 hrs prior to storage in 70% ethanol. Tissues were embedded in methymethacrylate and sectioned sagittally by the Washington University Musculoskeletal Histology and Morphometry Core. 20X high-resolution slide images were acquired using a NanoZoomer 2.0 with brightfield and FITC/TRITC (Hamamatsu Photonics, Japan). Images were then analyzed via Bioquant Osteo

software according to manufacture's instructions and published standards (v18.2.6; Bioquant Image Analysis Corp., Nashville, TN, USA)(Dempster et al., 2012).

Bone marrow macrophage isolation and osteoclast differentiation

BMMs were harvested by collecting bone marrow from dissected long bones via centrifugation at 10,000 rpm, passed through a 40μm filter and cultured with α-MEM (Sigma M0894, St. Louis, MO, USA) containing 10% FBS (Gibco, Grand island, NY, USA), 100 IU/ml penicillin/streptomycin, and 1:10 dilution of CMG 14-12 cell supernatant (containing equivalent of 100ng/ml M-CSF) (Novack et al., 2003; Takeshita et al., 2000).

Expanded BMMs were plated at a density of 9,000 and 300,000 cells per well for 96 and 6 well plates, respectively. Purified GST-RANKL at 30ng/ml was added to α-MEM containing 10% FBS, 100 IU/ml penicillin/streptomycin, and 1:50 dilution of CMG 14-12 cell supernatant. Media was changed every alternate day until wells were filled with multinucleated OCs. TRAP stains were employed following 10 minute fixation with 4% paraformaldehyde (Polysciences, Warrington, PA, USA) and 0.1% Triton X-100 in PBS according to manufacturer's instructions (Sigma 387A, St. Louis, MO, USA).

Actin Rings

Expanded BMMS were seeded on bovine bone slices and differentiated to OCs with purified GST-RANKL as above. At maturity, bone slices were fixed for 10 min with 4% paraformaldehyde and 0.1% Triton X-100 in PBS, washed 3x in PBS and stained with Alexa fluor 488 Phalloidin (Thermo Fisher Scientific A12370, Waltham, MA, UWA) for 30 min. Slices were imaged for FITC at 20X on an Olympus BX41 fluorescent microscope.

Resorption assay

Expanded BMMS were seeded on bovine bone slices and differentiated to OCs with purified GST-RANKL as above. At maturity, bone slices were fixed for 10 min with 4% paraformaldehyde and 0.1% Triton X-100 in PBS. Bone slices were incubated in 0.5 NaOH for 30 seconds and kept hydrated in PBS. Cells were scraped off bone slices with a cotton swab, and incubated with 20µg/ml peroxidase conjugated wheat germ agglutinin in PBS (Sigma-Aldrich 61767, St. Louis, MO, USA) for 30 min. Subsequently, slices were washed 3x in PBS and incubated with DAB chromogen kit (Biocare Medical BDB2004H, Pacheco, CA, USA) at 37˚C for 30 min. Slices were left to dry and imaged under brightfield at 20X on an Olympus BX41 fluorescent microscope.

Quantitative real-time PCR

Following collection of cells with TRIzol (Life Technologies), solutions were centrifuged at 12,000xg and aqueous layer extracted with phenol:chloroform. An equal volume of 70% ethanol was added, and remaining RNA isolation done via NucleoSpin RNA II kit (Clontech Laboratories, Palo Alto, CA, USA, 740955.50). 1µg of RNA was input into cDNA Ecodry premix kit prior to qPCR program run on ABI QuantStudio 3 with iTaq Universal SYBR Green Supermix (Bio-Rad Laboratories 1725121, Hercules, CA, USA). Each reaction proceeded at 50˚ for 2 min, 95˚ for 10 min, then 40 cycles of 95˚ for 15 sec and 60˚ for 1 min. Relative expression was calculated as $100*2^{-(\text{target CT-B2M CT})}$ for mouse and $100*2^{-(\text{target CT-HBMS CT})}$ for human. Primer sequences (murine unless otherwise specified) -

Mfn1: F – TTGGCAGGACAAGTAGTGGC, R – AGCAGTTGGTTGTGTGACCA

Mfn2: F – AAGCACTTTGTCACTGCCAAG, R – TTGTCCCAGAGCATGGCATTG

Human *Mfn2* F – CGCGCTTATCCACTTCCCTC, R – CCAGTCCTGACTTCACCTTCC

Nfatc1: F – GGTAACTCTGTCTTTCTAACCTTAAGCTC, R – GTGATGACCCCAGCATGCACCAGTCACA

DC-Stamp: F – ACAAACAGTTCCAAAGCTTGC, R – TCCTTGGGTTCCTTGCTTC

CatK: F –AGGCAGCTAAATGCAGAGGGTACA, R – AGCTTGCATCGATGGACACAGAGA

B2m: F – CTGCTACGTAACACAGTTCCACCC, R – CATGATGCTTGATCACATGTCTCG

Human *Hbms*: F – CACCCACACACAGCCTACTT, R – CCCACGCGAATCACTCTCAT

Western blot

RIPA buffer (20mM Tris, pH 7.5, 150mM NaCl, 1mM EDTA, 1mM EGTA, 1% Triton X-100, 2.5 mM sodium pyrophosphate, 1mM β-glycerophosphate, 1mM Na_3VO_4, 1mM NaF) with 1:50 HALT protease and phosphatase inhibitor (Thermo Fisher Scientific 1861280, Waltham, MA, USA) was used to lyse BMM and OC cells following 2x washes in PBS. Lysates were vortexed, centrifuged at 700xg and supernatant quantified with BCA assay (Bio-Rad Laboratories, Hercules, CA, USA), and 20 µg loaded to 10% SDS PAGE gel. Gels were run at 80 V for 2 hrs, and transferred to nitrocellulose by wet transfer at 100V for 90 minutes. Blocking was done in TBS+0.1% Tween 20 with 5% milk. Membranes were probed with 1˚ antibodies overnight at 4˚C (1:500 Mfn1 - Santa Cruz Biotechnology sc-50330, Dallas, TX, USA; 1:1,000 Mfn2 - Abcam ab56889, Cambridge, UK). Actin was used as a loading control at 1:10,000 (Sigma-Aldrich A228, St. Louis, MO, USA). Imaging was done using SuperSignal West Femto substrate (Thermo Fisher Scientific 34095, Waltham, MA, USA) and a chemiluminescence imager (Syngene, Cambridge, UK).

Retroviral overexpression

Mfn1-Myc and *Mfn2-Myc* were obtained from Addgene (plasmids #23212 and #23213, respectively, Watertown, MA, USA)(Chen et al., 2003). Each gene was cloned into the pMX retroviral vector and transfected into Platinum-E (platE) cells by calcium phosphate precipitation (Morita et al., 2000; Zou et al., 2012). PlatE supernatant was harvested 48 and 72 hrs post-transfection, filtered through 0.45μm and added to BMMs with α-MEM, 10% FBS, and 100 IU/ml Penicillin/Streptomycin, 1:10 CMG, and 8μg/ml polybrene (Sigma H9268, St. Louis, MO, USA) on 2 consecutive days. 24 hrs following the final viral addition, 1μg/ml blasticidin (Sigma 203350, St. Louis, MO, USA) was added to select for infected BMMs.

Seahorse

BMMs were seeded on Seahorse XF96 Cell Culture Microplates at a density of 8,000 cells/well (cre-only and Mfn2 cKO) or 4,000 cells/well (ctrl and dcKO) in α-MEM, 10% FBS, and 100 IU/ml Penicillin/Streptomycin, 1:10 CMG. Pre-osteoclasts were treated with 30ng/ml RANKL for 3 days. Seahorse XF Cell Mito Stress Test Kit was used according to manufacturer's instructions using 1μM of oligomycin, FCCP, and rotenone/antimycinA (Agilent Technologies 103015-100, Santa Clara, CA). Seahorse assay was run on Seahorse Biosciences XF96 Flux Analyzer in the Washington University Tissue Culture Support Center.

Mitotracker

For live cell imaging BMMs were seeded onto Lab TeK II 8-well Chambered Coverglass dishes at 40,000 cells/chamber (Thermo Fisher 155409, Waltham, MA). Following differentiation to pre-OCs with 30ng/ml RANKL for 3 days, cells were stained with 100nM MitoTracker Green

FM per product instructions (Molecular Probes M5714, Eugene, OR). For fixed imaging, BMMs were seeded at 100,000 cells/well in 24-well plates containing circular coverglass (FisherScientific 12-545-81, Hampton, NH), and differentiated with 30ng/ml RANKL. Live mitotracker stained cells were imaged using a Nikon Spinning Disk Confocal and Nikon Elements software at the Washington University Center for Cellular Imaging (WUCCI). WUCCI imaging was supported by the Washington University School of Medicine, The Children's Discovery Institute of Washington University and St. Louis Children's Hospital (CDI-CORE-2015-505) and the Foundation for Barnes-Jewish Hospital (3770).

CD14$^+$ cell isolation

Human peripheral blood collected in sodium heparinized vacutainers was transferred to histopaque (Ficoll Histopaque, Sigma # 10771) and centrifuged at 2,200xg for 15 min. Buffy coat was then collected and washed twice with PBS. Per every 10^7 cells, cells were resuspended in 20µl CD14 MicroBeads and 80µl MACS buffer (PBS pH7.2, 0.5% BSA, 2mM EDTA) (Miltenyi Biotec 130-050-201, Bergisch Galdbach, Germany). Following 15 min incubation at 4˚, cells were washed and isolated via positive selection columns per manufacturer's instructions (LS columns: #130-042-401, MiniMACS separator kit: #130-090-312, Miltenyi Biotec, Bergisch Galdbach, Germany). Collected CD14$^+$ cells were plated in α-MEM (Sigma M0894, St. Louis, MO, USA) containing 10% FBS (Gibco, Grand Island, NY, USA), 100 IU/ml penicillin/streptomycin, 40 ng/ml hMCSF (BioLegend 574806, San Diego, CA) and 100ng/ml RANKL for osteoclastogenesis.

Induced osteolysis

2 month old ctrl and Mfn2 cKO animals were injected intraparitoneally (IP) with 1mg/kg body weight GST-RANKL twice, 24 hrs apart, as previously published (Shashkova et al., 2016). 50 hrs after the first injection, animals were sacrificed.

Statistics

Two-way ANOVA with Tukey's multiple comparisons and student's unpaired t-tests with Welch's correction were performed with GraphPad Prism built-in statistical analysis (GraphPad Software, Inc., La Jolla, CA, USA). All data are represented as mean ± standard deviation with 3+ biological replicates. P values are designated at *$p<0.05$, **$p<0.01$, ***$p<0.001$.

Results

Bone mass is increased in female mice lacking Mfn1 and Mfn2 in the OC lineage

Because OCs are rich in mitochondria, we expected that disrupting mitochondrial dynamics in these cells would manifest in global changes in bone mass. We used LysM-cre to target OC precursors to delete *Mfn1* and *Mfn2*. Double heterozygous ($LysM^{c/c}$; $(Mfn1/2)^{fl/+}$ = ctrl) and double knockout ($LysM^{c/c}$; $(Mfn1/2)^{fl/fl}$ = dcKO) pups were born at normal Mendelian ratios. In parallel, double heterozygous ctrl mice were bred to cre-only ($LysM^{c/c}$;$(Mfn1/2)^{+/+}$) mice to generate a cohort of ctrl and cre-only littermates.

Male and female animals were sacrificed at 2 months of age, a time of high OC activity. Basal bone morphology was assessed by μCT of dissected femurs. We find a strong phenotype in female animals at this age, with all trabecular and cortical parameters consistent with a high bone mass (significantly increased BV/TV, BMD, Tb. Th., Tb. N., Cort. Th., TMD, and decreased Tb. Sp.) (Fig. 2.1 A-B, Fig. 2.2 A-D). Interestingly, males show no significant differences between ctrl and dcKO groups (Fig 2.1 C-D)(Fig. 2.3 A-D). Ctrl and dcKO mice were undistinguishable by eye, and weights between groups were identical (Fig 2.2 E, Fig 2.3 E). These data suggest that in females, mitochondrial dynamics mediated by MFN1 and MFN2 activity contribute to OC formation and/or activity. Further, bone parameters were not significantly different between cre-only and ctrl double heterozygous mice at the same age, indicating that loss of one allele of each mitofusin does not negatively affect the OC of either sex *in vivo* (Fig. 2.2 F-L, Fig 2.3 F-L).

Serum CTX-1 levels were decreased in female dcKOs compared to ctrls, indicating an impairment of OC activity (Fig. 2.4 A). Histomorphometry was undertaken for these same animals to determine whether OC abundance was altered by the double knockout of *Mfn1* and

Mfn2 by LysM-cre. Although not statistically significant, the dcKO OC surface and OC number per bone surface trend lower than ctrls (Fig 2.4 B-C). Bone accrual in this cohort was assessed first by serum P1NP. These levels remained unchanged, suggesting a decrease in bone catabolism alongside no change in bone anabolism for the dcKOs (Fig 2.4 D). Consistently, OB activity is unchanged between ctrl and dcKO samples, as measured by dynamic histomorphometry for MS/BS, MAR, and BFR/BS (Fig. 2.4 E-G). Taken together, these data suggest that in female mice, blunted OC activity in the dcKOs is partly explained by decreases in OC presence. However, OB-OC coupling is not affected because P1NP, MS/BS, MAR, and BFR/BS are unchanged between groups.

Taken together, these data suggest that in female mice, loss of mitofusin activity in the OC lineage disrupts the ability of OCs to form, and as a consequence, resorption is depressed without affecting OB-OC coupling.

Ostoclastogenesis is inhibited in Mfn1/2 –deficient BMMs

To more closely characterize the impact of mitofusin loss in the OC lineage, BMMs were expanded from the bone marrow of ctrl and dcKO 2 month old female mice, in which mitofusin protein and RNA expression is decreased (Fig. 2.5). Treating BMMs with RANKL for up to 5 days to differentiate cells to OCs revealed osteoclastogenesis is defective in dcKO cultures compared to ctrls, leading to an inability of these cells to resorb bone (Fig 2.6 A-B). Consistently, qPCR expression of *Nfatc1*, *DC-Stamp*, and *CatK* are repressed in dcKOs throughout 5 days of differentiation (Fig 2.6 C-E). We posit that this defect in osteoclastogenesis is the primary mechanism for increased bone mass observed in dcKO female animals.

As in other cell types loss of mitofusin activity is associated with decreased oxygen consumption, we analyzed female BMM and pre-OCs via Seahorse analysis. Contrary to our expectations, no clear trends in oxygen consumption rate were discerned between genotypes in BMM or OC samples (Fig. 2.7). However, high variability among replicates in this preliminary assay does not allow us to make a definitive conclusion, and additional samples will be evaluated in the future.

We sought to determine whether MFN1 or MFN2 was dominant in contributing to the dcKO phenotype. Expression of both homologs by protein and gene expression increases as osteoclastogenesis progresses in culture, though MFN2 to a slightly higher degree (Fig. 2.8 A-B). Next we attempted to rescue the dcKO osteoclastogenesis phenotype by retrovirally expressing either *Mfn1* or *Mfn2* in BMMs. We found that addition of *Mfn2* to the dcKO cells rescues osteoclastogenesis while *Mfn1* does not, suggesting that MFN2 is the dominant mitofusin homolog responsible for OC differentiation (Fig 2.2 C-E).

To further assess the difference between loss of *Mfn1* or *Mfn2* alone, we generated single knockout colonies. We generated a Mfn1 cohort to assess bone parameters in cre-only and Mfn1 cKO littermates ($LysM^{c/c}$; $Mfn1^{+/+}$ and $LysM^{c/c}$; $Mfn1^{fl/fl}$, respectively). Pups were aged to 2 months and femurs collected for µCT analysis. We find no differences in trabecular or cortical parameters in males or females at this age (Fig. 2.9). Paired with the inability of *Mfn1* to rescue dcKO osteoclastogenesis, lack of a phenotype in this cohort prompted us to discontinue further study of the single Mfn1 cKOs.

Stress by aging and stimulated osteolysis reveals a Mfn2 cKO phenotype *in vivo*

To investigate whether loss of Mfn2 alone would have an effect on the OC lineage *in vivo*, we generated cohorts of Cre-only and Mfn2 cKO littermates ($LysM^{c/c}$; $Mfn2^{+/+}$ and $LysM^{c/c}$;

Mfn2$^{fl/fl}$, respectively). At 2 months of age, no differences were observed in femurs of female or male cre-only compared to Mfn2 cKOs by mCT (Fig. 2.10 A-B). Female bones were analyzed by historphometry and while no difference was observed between BV/TV, Oc.S/BS and OcN./BS both trend downward in Mfn2 cKO compared to cre-only bones (Fig. 2.11).

Our group has previously observed that challenging animals with pathological bone loss can produce robust OC phenotype even when basal changes are not present (Anginot et al., 2007; Novack et al., 2003; Vaira et al., 2008; Wu et al., 2007). Therefore, we hypothesized this may be the case for Mfn2 cKO animals, and explored the consequences of two models of physiological stress in our cohort. First, we aged male and female Mfn2 cre-only and cKO mice to 4 and 12 months of age, and assessed femoral trabecular and cortical bone parameters by μCT after sacrifice. While we observed no differences in bone parameters in either sex at 4 months when mice exhibit peak bone mass, female Mfn2 cKOs have significantly increased trabecular bone mass compared to cre-only animals at 12 months of age (n=9-17/group). Hence, in females, loss of MFN2 alone in the OC lineage impacts bone resorption with aging, as the percent trabecular bone retained from 4 months at 12 months is for 24% for ctrls and 46% for cKOs (64% and 63% in males, respectively) (Fig. 2.10 C-F). Holistically, in females, most trabecular and cortical parameters trend upwards in the Mfn2 cKOs, even at 2 months of age. Because no such trends are apparent in males, we suggest that our phenotype is sex-specific (Fig. 2.12).

Next, we induced osteolysis to evaluate how OCs lacking MFN2 function when stimulated. 2-month-old male and female control and cKO mice were challenged with intraperitoneal RANKL injection, a model that stimulates OC activity and induces between 30-50% loss in trabecular bone mass in 2 days (Fig. 2.13). Male controls, male cKOs, and female controls lost significant amounts of bone, 30-45%, following RANKL injection. Female cKOs

were protected from induced osteolysis, as they only appear to lose a small, but statistically insignificant, amount of bone following treatment (Fig. 2.14-2.15). Thus, MFN2 is required for the response of female, but not male, OCs to an acute osteolytic stimulus. The same result is seen for stress by aging, suggesting the presence of MFN2 promotes the ability of female OCs to resorb bone.

Loss of Mfn2 alone in the OC lineage does not reproducibly affect OC formation or function *in vitro*

To probe whether loss of MFN2 impacts osteoclastogenesis *in vitro*, nearly 30 pairs of cre-only and Mfn2 cKO BMMs were treated with RANKL. We find that a defect in differentiation occurs frequently in cells harvested from 12 month old animals but less so in those from 2 month old mice (Fig. 2.16, 2.17 A-B). Although TRAP expression levels by RNA are not different between cre-only and Mfn2 cKO differentiating OCs from 2 month old animals, day 4 OCs from female cKOs have significantly lower *Nfatc1* expression than cre-only OCs (Fig. 2.17 C-F). However, when these cells are grown on bone slices, no differences are seen between bone resorption at normoxia or low oxygen conditions (Fig. 2.18 A-B). Oxygen consumption rates are also identical between BMMs and OCs of either group (Fig. 2.18 C-F).

Despite an inconsistent defect in osteoclastogenesis between cre-only and Mfn2 cKO cells, Mfn2 cKO pre-OCs exhibit altered mitochondria network morphology compared to cre-only pre-OCs by MitoTracker green staining. The appearance of more punctate mitochondria suggests the distance between organelles may be increased when *Mfn2* is deleted from the OC lineage (Fig. 2.19).

Mfn2 gene expression rises during osteoclastogenesis in humans

As all of our studies thus far have been in murine cells, we isolated $CD14^+$ monocytes from the peripheral blood of healthy donors and exposed cells to RANKL *in vitro*. In assaying Mfn2 expression in differentiated OCs we find modest increases from M-CSF-treated monocytes to RANKL-treated OCs (Fig. 2.20). Additional samples will be required to verify whether the increase in *Mfn2* expression following OC differentiation is reproducible.

Discussion

OCs are an incredibly dynamic cell type and during osteoclastogenesis, BMMs go through many conformational changes including fusion of pre-OC cells to become mature multinucleated OCs. We theorized that mitochondrial networks in differentiating OCs are remodeled and that increased mitochondrial tethering/fusion is required for completion of this process. To test this, we dually knocked out *Mfn1* and *Mfn2* in the OC lineage by Lysozyme-M cre, finding that deletion of both homologs manifests in increased bone mass in 2 month old female mice *in vivo*, which is accompanied by modest decreases in OC numbers and serum CTX-1 levels. Further, BMMs harvested from these animals do not differentiate to OCs *in* vitro.

In humans, mutations in *Mfn2* are most commonly associated with CMT2A. With the severity of these neurodegenerative phenotypes, it is not surprising that the skeleton has yet to be evaluated. While reduced mobility in these patients likely has adverse effects on the skeleton, bone mass has not been evaluated to determine whether any changes that occur or are related to lack of weight-bearing activity or altered MFN2 function. In other cell types, the effect of *Mfn1* vs. *Mfn2* knock out are not always identical, but in particular, double knock out of *Mfn1* and *Mfn2* produce more severe phenotypes than single knockout of either mitofusin alone. Of note, while cardiac specific conditional knockout of *Mfn1* or *Mfn2* alone display minor functional deterioration of the heart, double deletion of *Mfn1* and *Mfn2* by the same cre-driver provokes lethal cardiomyopathy (Chen et al., 2011; Papanicolaou et al., 2011; 2012a; 2012b). As a similar situation is observed in skeletal muscle with a higher degree of muscle atrophy with double compared to single mitofusin knockouts, we expected to observe a similar trend in the bone (Chen et al., 2010). Like the heart and skeletal muscle, OCs are rich in mitochondria, and in female animals, we make a comparable observation that double knockout of *Mfn1* and *Mfn2* in

OC precursors halts osteoclastogenesis and ultimately begets increases in bone mass. Although deletion of *Mfn2* alone had no effect on young cohorts basally, the loss of *Mfn2* in the female OC lineage becomes protective against trabecular bone loss with age and induced osteolysis *in vivo*. This is not uncommon in OC biology, as our group and others have demonstrated that despite certain models having undetectable changes in OC activity under basal conditions, challenge by stress and pathological bone loss produces robust OC phenotypes (Anginot et al., 2007; Novack et al., 2003; Vaira et al., 2008; Wu et al., 2007).

To our knowledge, this is the first evaluation of mitofusin function in the OC lineage, and expands our understanding of how these genes contribute to the formation of this specialized cell type. Our data highlights the fact that we can no longer discount the importance of the elongated organelles observed in human OCs by TEM and anti-mitochondria antibodies (Lemma et al., 2016). This functional necessity of mitochondrial fusion is likely beneficial for proper OC function as fused mitochondria in other models have been shown to prevent autophagy and allow ATP production to be optimized due to increased cristae density favoring ATPase oligomerization (Gomes et al., 2011; Rambold et al., 2011). While we did not observe differences between oxygen consumption in ctrl compared to dcKO cells, we confirm that OCs have higher oxygen consumption rates compared to BMMs, as we and others have previously documented (Czupalla et al., 2005; Kim et al., 2007; Zeng et al., 2015).

Although we find that MFN2 alone is able to rescue the osteoclastogenesis phenotype in dcKO cells, an OC differentiation defect is not consistently affected with loss of MFN2 alone in the OC lineage. With functional MFN1 in the system *in vitro* cells derived from bone marrow of 2 month old animals maintain the ability to resorb bone and respire, indicating a compensation effect by MFN2. The mitochondria in these cells, however, take on a striking network

appearance in which mitotracker signal is highly aggregated. This could indicate that mitochondrial architecture is impacted but not to a level that produces a functional response.

Figures and tables

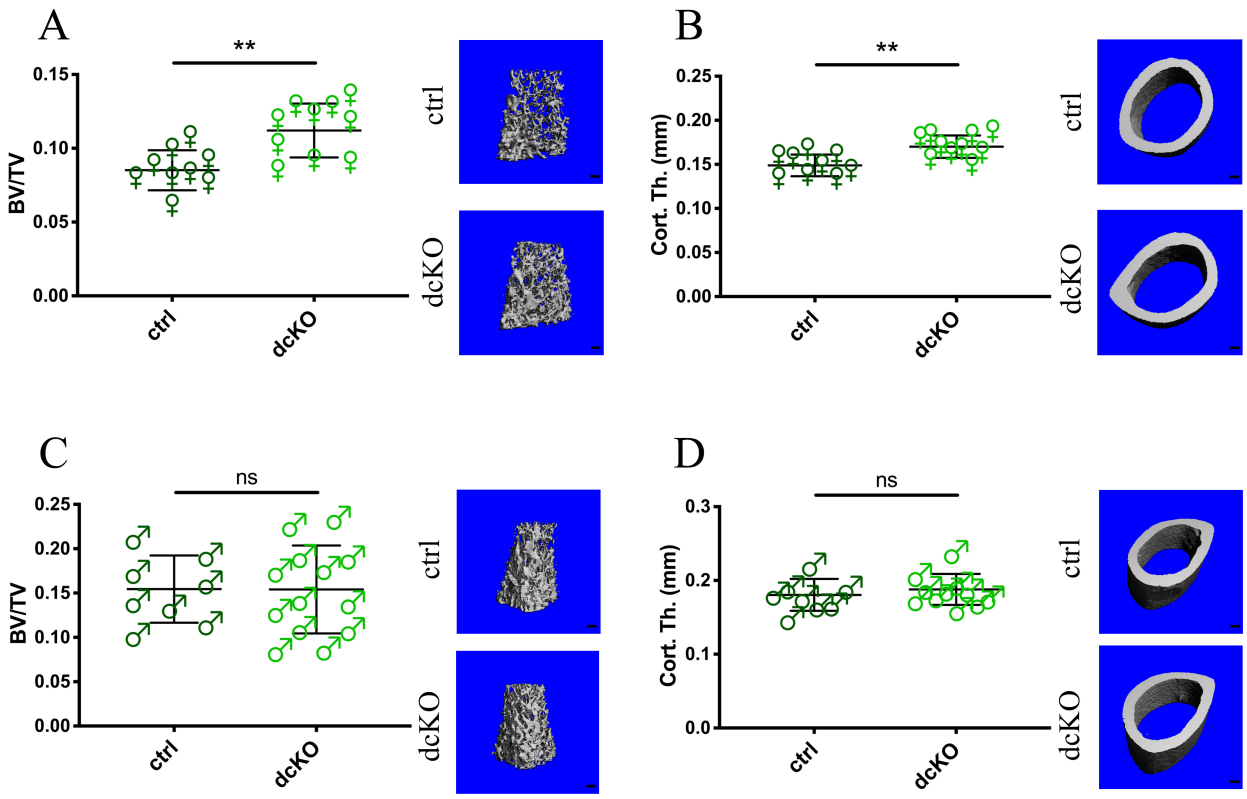

Figure 2.1: Trabecular and cortical bone is increased in 2 month old female mice lacking Mfn1 and Mfn2 in the OC lineage

Female BV/TV (A) and Cort. Th. (B) is significantly elevated in dcKOs compared to ctrls by µCT of femurs. Representative reconstructions of analyzed regions below the growth plate and mid-shaft are shown, scale=200µm. C-D). males as in A-B. **p<0.01, unpaired t-test with Welch's correction.

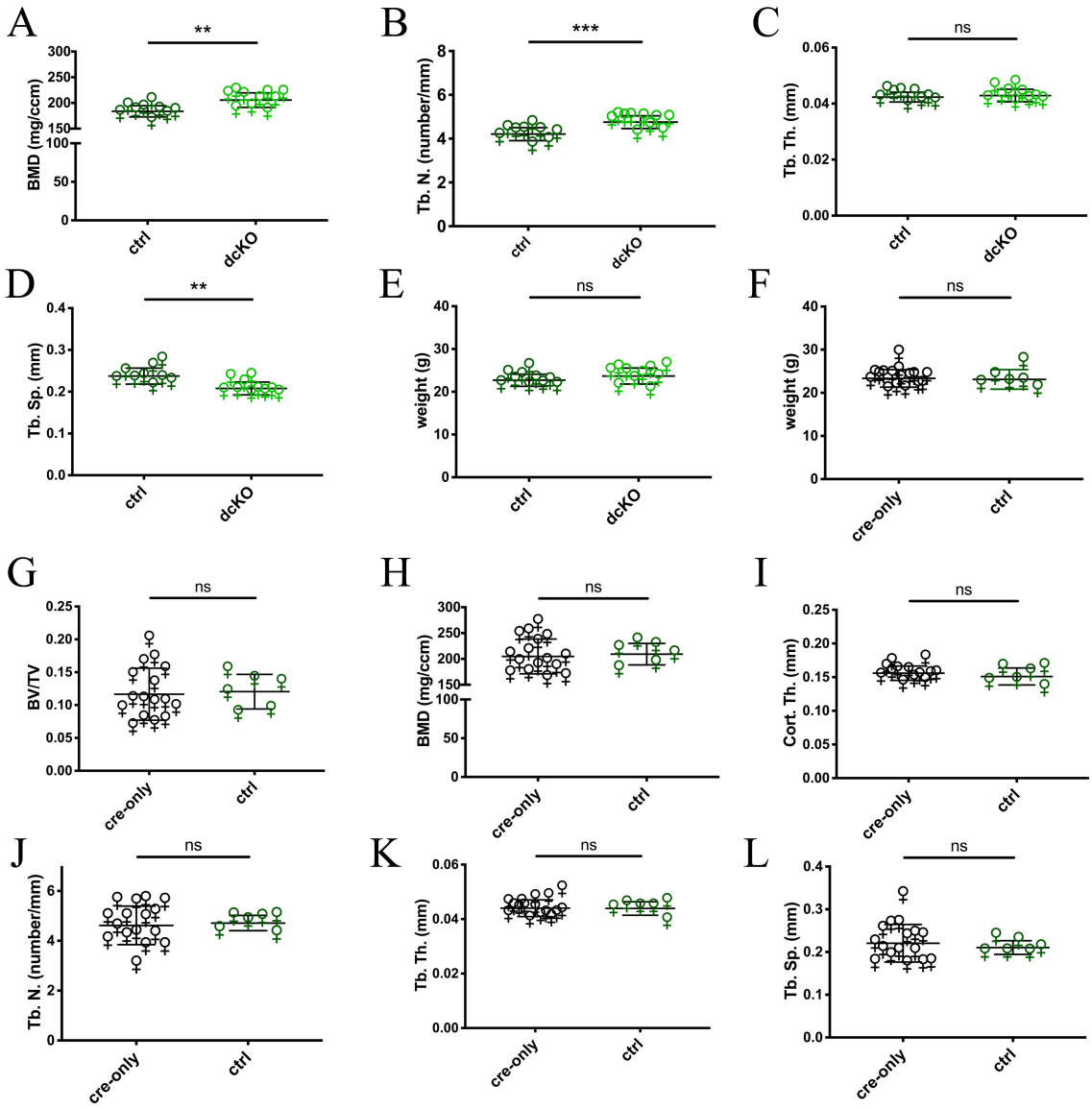

Figure 2.2: µCT analysis of ctrl, dcKO, and cre-only female cohorts

Additional analyses between ctrl and dcKO females at 2 months for BMD (A), Tb.N. (B), Tb.Th. (C), Tb.Sp. (D) and weight (E). Identical analyses were undertaken for cre-only and ctrl littermates with weight (F), BV/TV (G), BMD (H), Cort.Th. (I), Tb.N. (J), Tb.Th. (K), and Tb.Sp. (L). **p<0.01, ***p<0.001, unpaired t-test with Welch's correction.

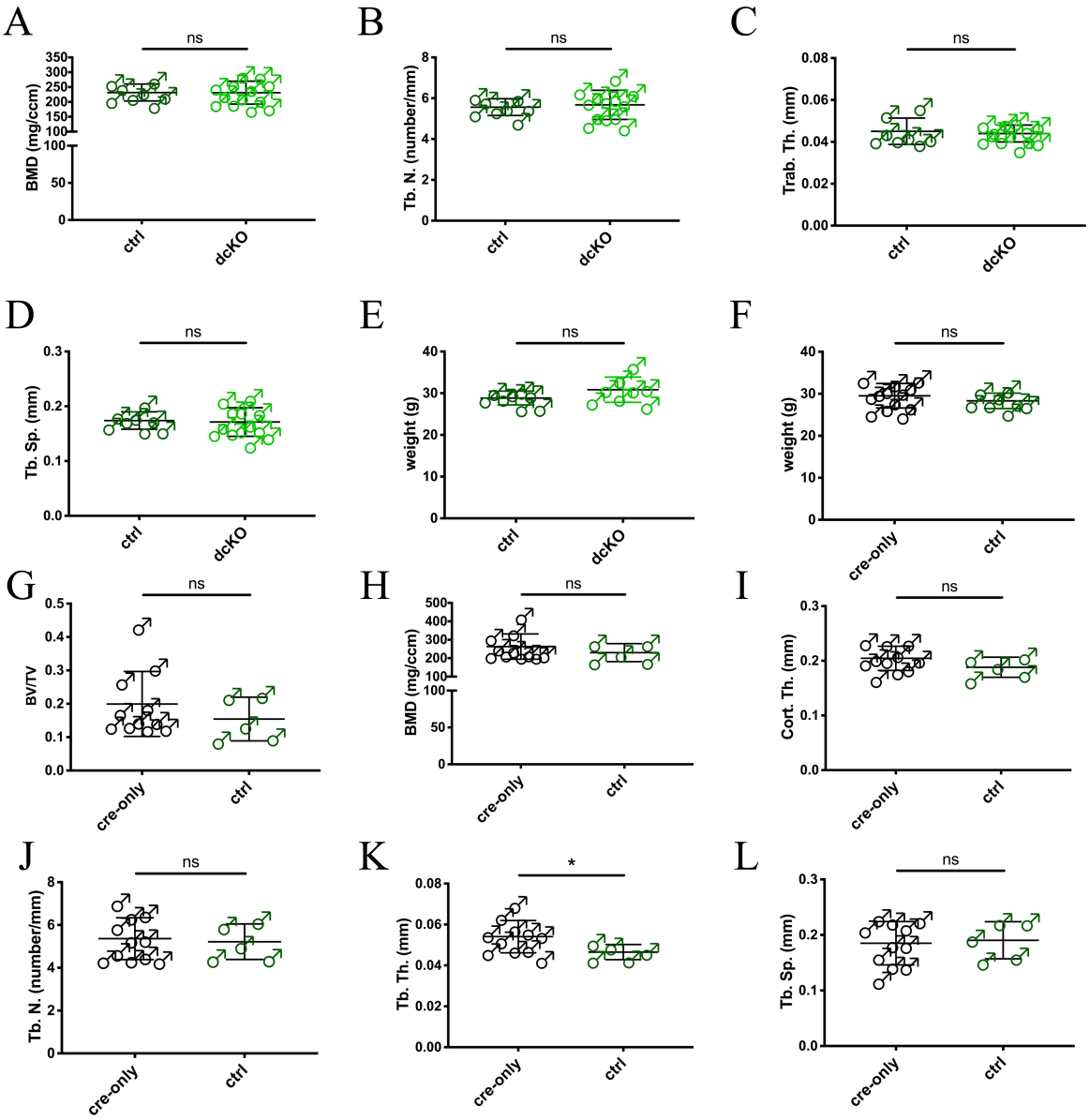

Figure 2.3: µCT analysis of ctrl, dcKO, and cre-only male cohorts

Additional analyses between ctrl and dcKO males at 2 months for BMD (A), Tb.N. (B), Tb.Th. (C), Tb.Sp. (D) and weight (E). Identical analyses were undertaken for cre-only and ctrl littermates with weight (F), BV/TV (G), BMD (H), Cort.Th. (I), Tb.N. (J), Tb.Th. (K), and Tb.Sp. (L). *$p<0.05$, unpaired t-test with Welch's correction.

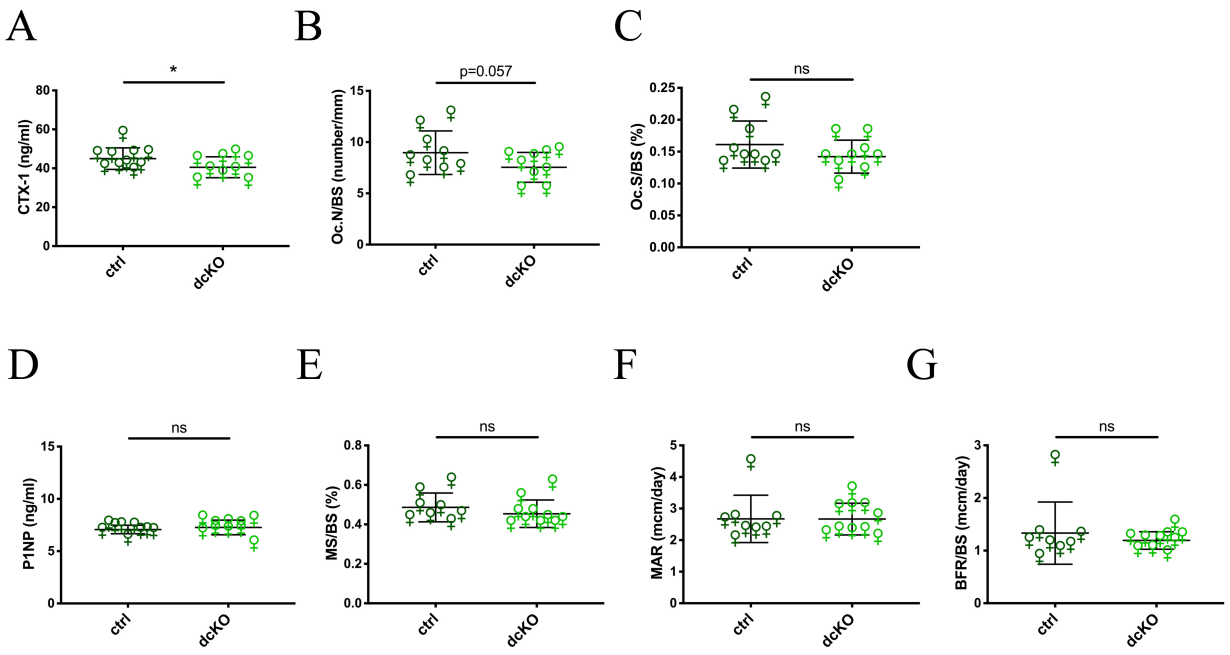

Figure 2.4: Female Mfn1/2 dcKOs have decreased OC numbers and activity, but no change in bone formation

Bone turnover in 2 month old females was assessed with serum CTX-1 (A), and histomorphometry of TRAP-stained tibiae for OC.S/BS (B) and OC.N/BS (C). Bone accrual was assessed with serum P1NP (D), and dynamic histomorphometric analysis of unstained tibiae for MS/BS (E), MAR (F), and BFR/BS (G). *$p<0.05$, one-tailed unpaired t-test with Welch's correction.

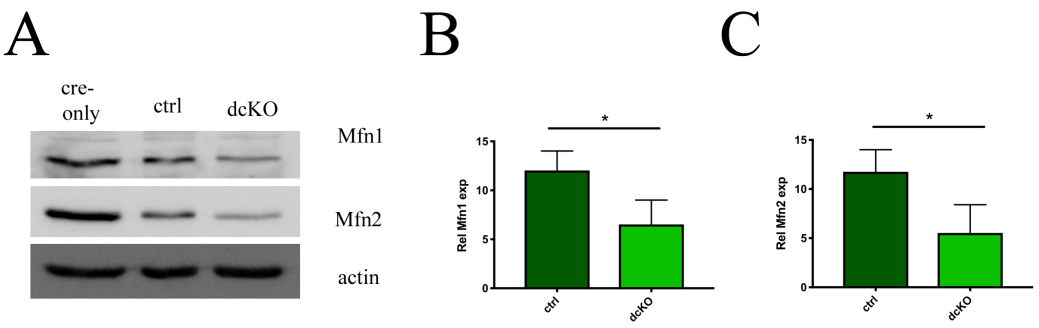

Figure 2.5: Confirmation of Mfn1 and Mfn2 knockdown by western blot and qPCR

A). Protein harvested from OCs derived harvested from ctrl and cKO animals are blotted against Mfn1 and Mfn2, and expression by qPCR is shown in (B-C). Loading controls = actin (A), B2M (B-C), *$p<0.05$, unpaired t-test with Welch's correction.

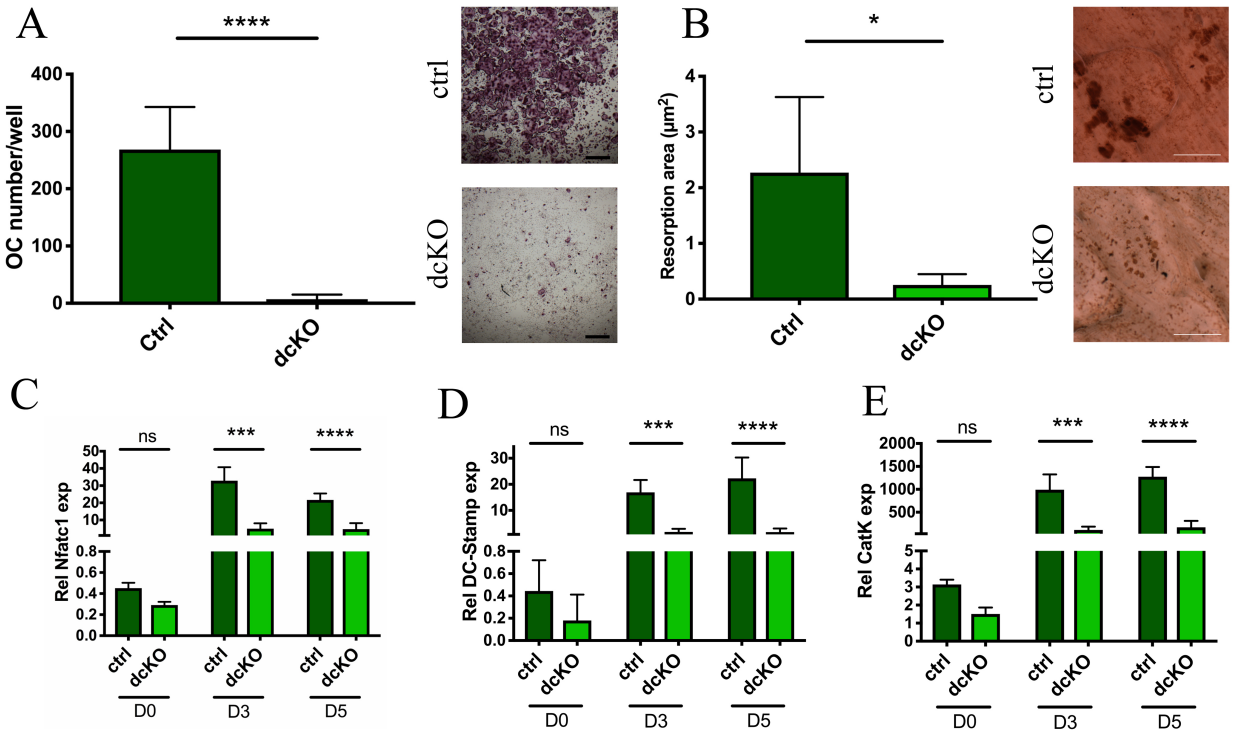

Figure 2.6: Osteoclastogenesis is defective in BMMs derived from dcKO bone marrow.

BMMs cultured with RANKL for 5 days allow OC formation in ctrls but not in dcKOs (A), and bone resorption is congruently inhibited in dcKOs (B). Representative images are displayed (scale = 400µm in A, 200µm in B). OC markers NFATc1 (C), DC-Stamp (D), and CatK (E) are blunted in dcKOs throughout 5 days of osteoclastogenesis. *p<0.05, ***p,0.001, ****p<0.0001, unpaired t-test with Welch's correction.

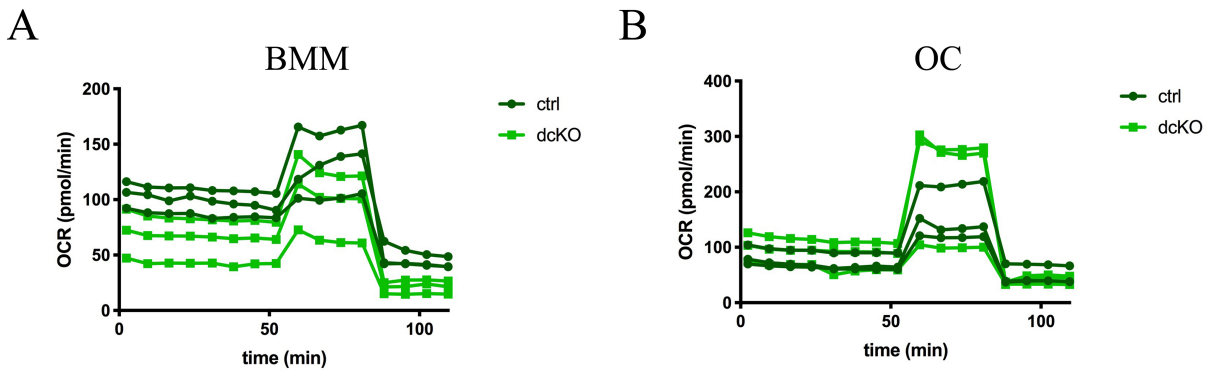

Figure 2.7: Oxygen consumption rates in BMMs and OCs are not disrupted by loss of Mfn1 and Mfn2

Oxygen consumption rates of ctrl and dcKO were assessed in BMM (A) and OC (B) cultures by Seahorse analysis, n=3 biological replicates/group.

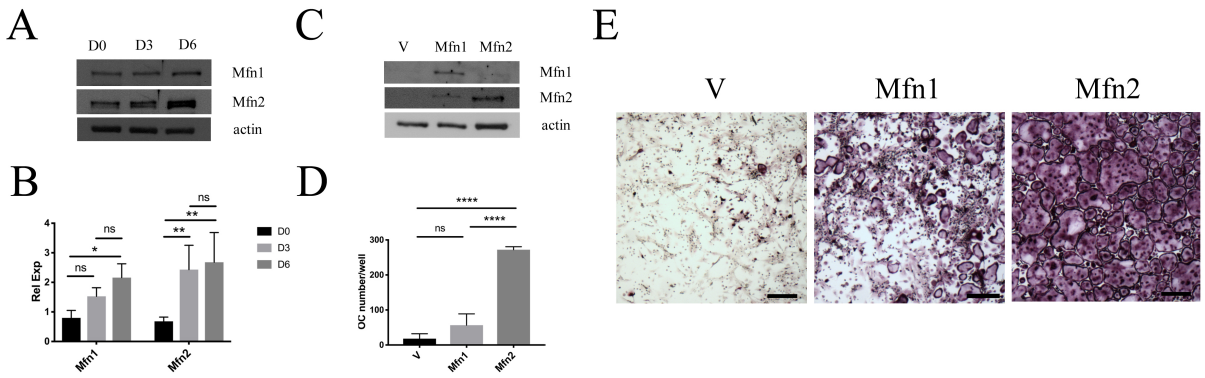

Figure 2.8: Though both homologs increase during OC formation, addition of Mfn2 alone drives osteoclastogenesis *in vitro*

A). Timecourse though 6 days of osteoclastogenesis in wild type BMMs shows increases of Mfn1 and Mfn2 expression by protein (A) and RNA (B). C.) pMX-Vector, V, pMX-Mfn1, Mfn1, and pMX-Mfn2, Mfn2, were retrovirally transduced into dcKO BMMs. D). Enumeration of TRAP+ OCs staining following RANKL treatment of dcKO BMMs transduced with V, Mfn1, or Mfn2, indicates Mfn2 but not Mfn1 alone enables OC formation, scale=400µm. Representative TRAP-staining images are shown in (E). *p<0.05, **p<0.01, ****p<0.0001, Two-way and one-way ANOVA with multiple comparisons in A and C, respectively.

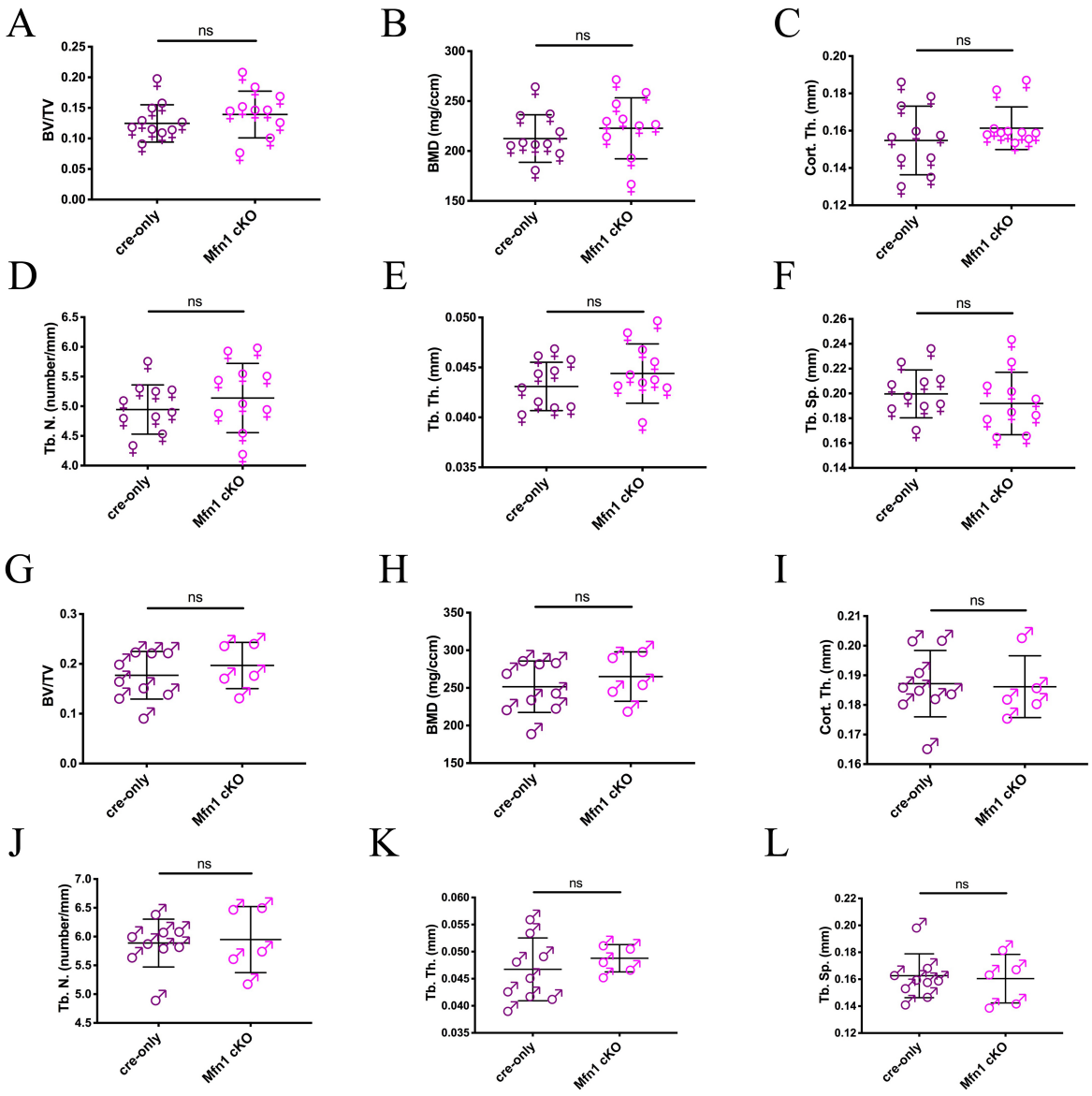

Figure 2.9: Bone mass of 2 month old mice is not altered when Mfn1 is lost in the OC lineage

Femoral µCT analysis of 2 month old female mice reveals no difference between cre-only and Mfn1 cKOs for BV/TV (A) BMD (B), Cort. Th. (C), Tb.N. (D), Tb.Th. (E), and Tb.Sp. (F). Further, no differences in males are seen by BV/TV (G) BMD (H), Cort. Th. (I), Tb.N. (J), Tb.Th. (K), and Tb.Sp. (L). ns=no significance, unpaired t-test with Welch's correction.

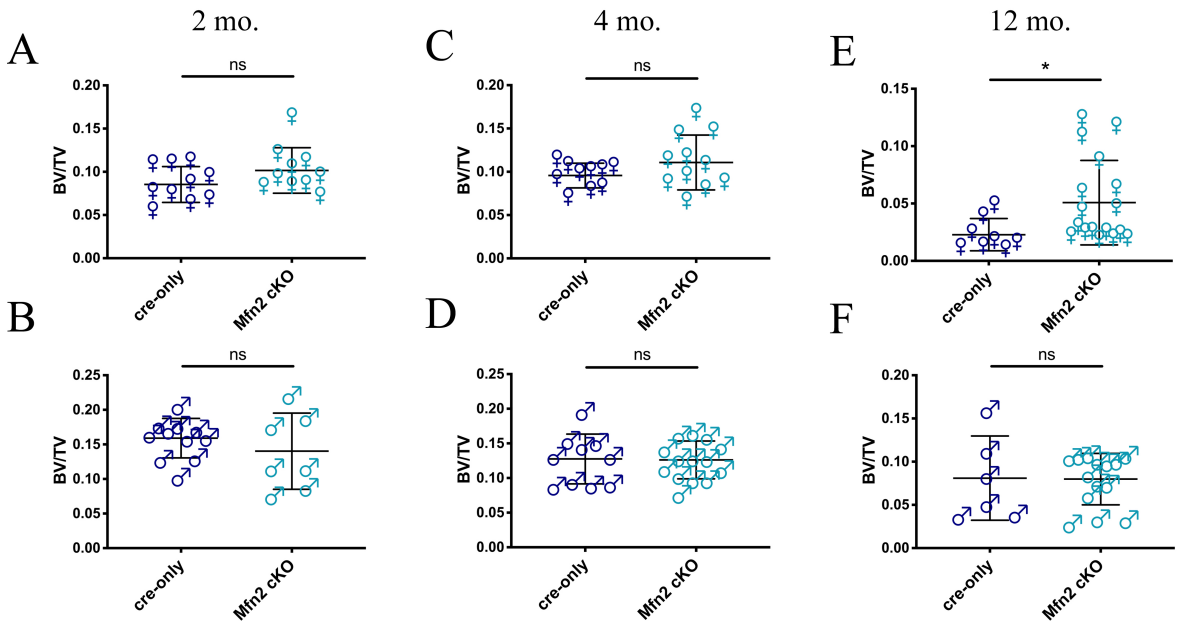

Figure 2.10: Female mice lacking Mfn2 alone in the OC lineage are protected from bone loss with age

Femurs from male and female cre-only and Mfn2 cKO mice were analyzed by μCT at 2 months (A-B), 4 months (C-D), and 12 months (E-F). *p<0.05, **p<0.01, unpaired t-test with Welch's correction.

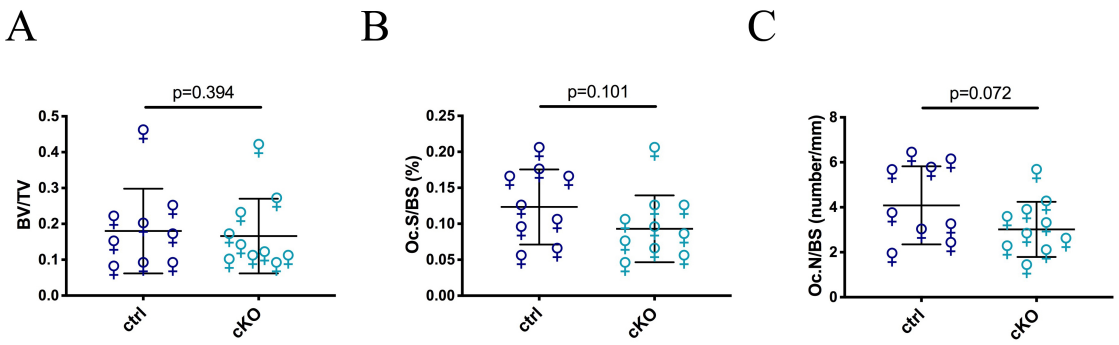

Figure 2.11: Osteoclast presence trends downward in 2 month old females lacking Mfn2 in the OC lineage

TRAP stained sagittal tibial sections from 2 month old female mice were analyzed via histomorphometry for BV/TV (A), Oc.S/BS (B), and Oc.N./BS (C).p-values are indicated, one-tailed t-test with Welch's correction.

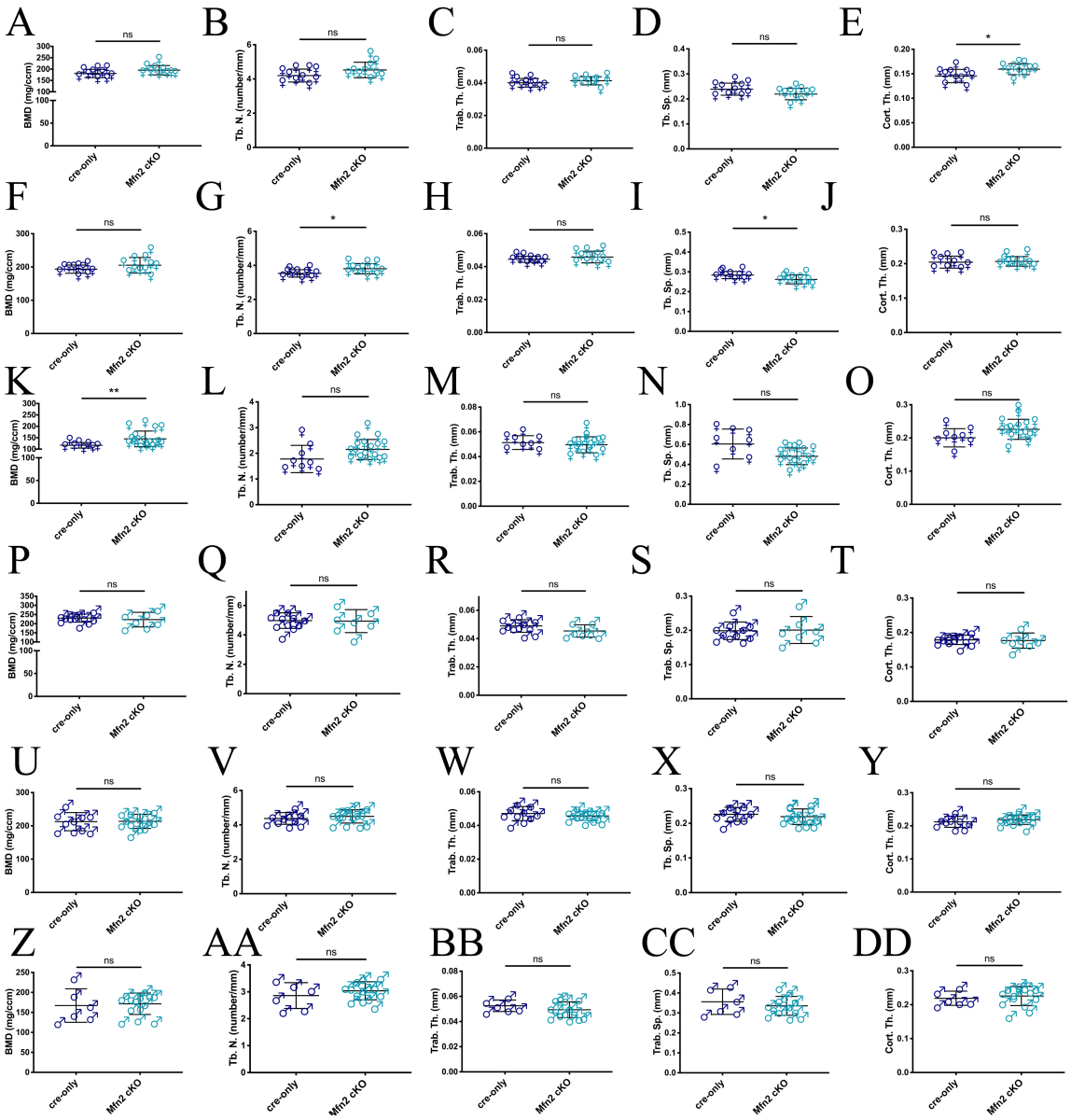

Figure 2.12: µCT analysis of cre-only and Mfn2 cKO female and male cohorts

Additional analyses between cre-only and Mfn2 cKO females at 2 months for BMD (A), Tb.N. (B), Tb.Th. (C), Tb.Sp. (D) and Cort.Th. (E). Identical analyses were undertaken for females at 4 months (F-J), females at 12 months (K-O), males at 2 months (P-T), males at 4 months (U-Y), and males at 12 months (Z-DD). *$p<0.05$, unpaired t-test with Welch's correction.

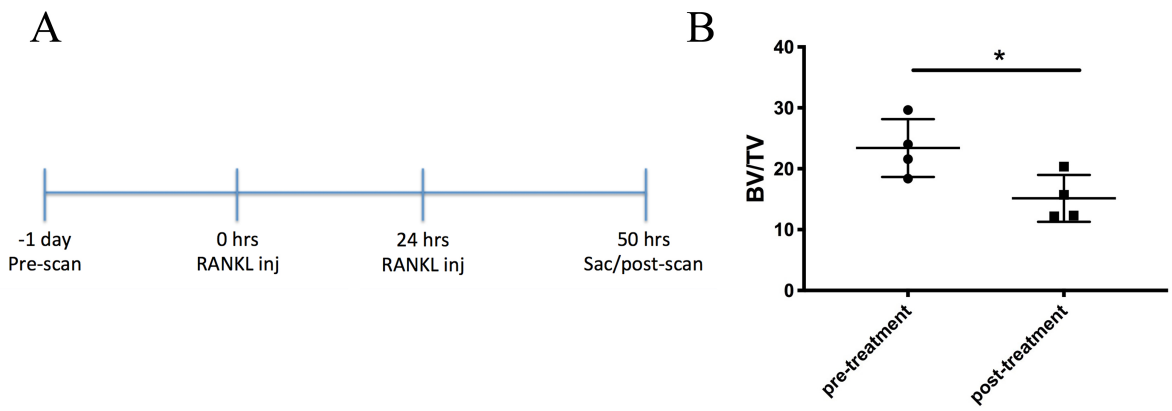

Figure 2.13: acute osteolysis model

A). Schematic of protocol with VivaCT scan one day prior to first RANKL injection. A second RANKL injection is administered 24 hrs after the first, and mice are sacrificed 50 hours after the first injection. B). Pilot B6 animals were scanned pre- and post-treatment, and lose trabecular bone volume. *p>0.05, unpaired t-test with Welch's correction.

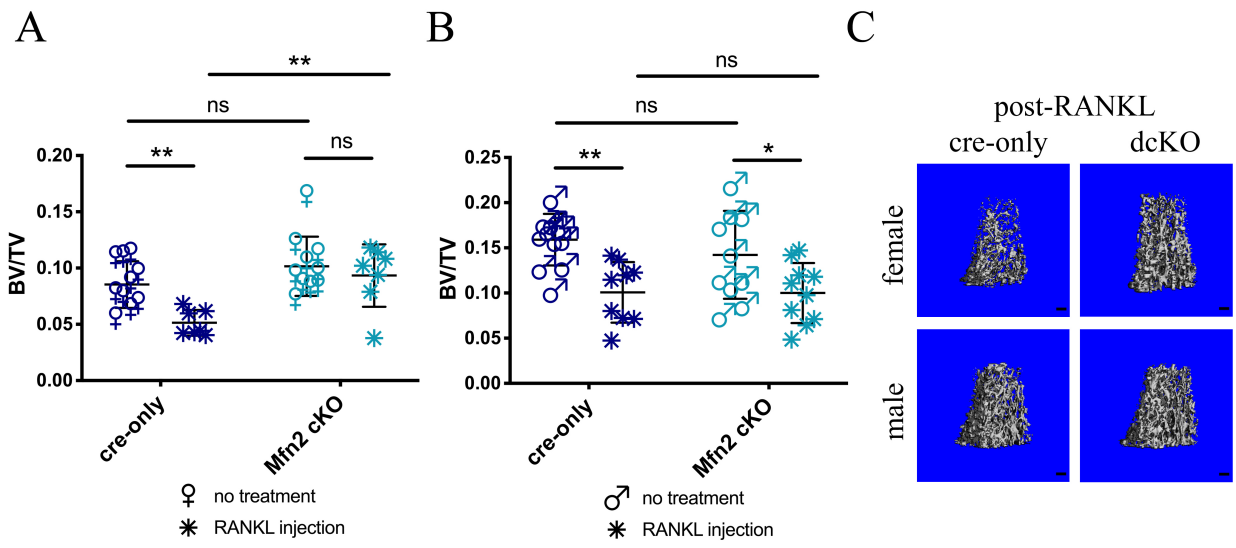

Figure 2.14: Female mice lacking Mfn2 in the OC lineage are protected from acute osteolysis

A model of acute bone loss by RANKL injection performed on 2 month old cre-only and Mfn2 cKO mice induces significant bone loss in all males, cre-only females, but not Mfn2 cKO females (A-B). C). Representative post-RANKL µCT reconstructions from A-B, scale=200µm. *p<0.05, **p<0.01, ordinary two-way ANOVA with multiple comparisons.

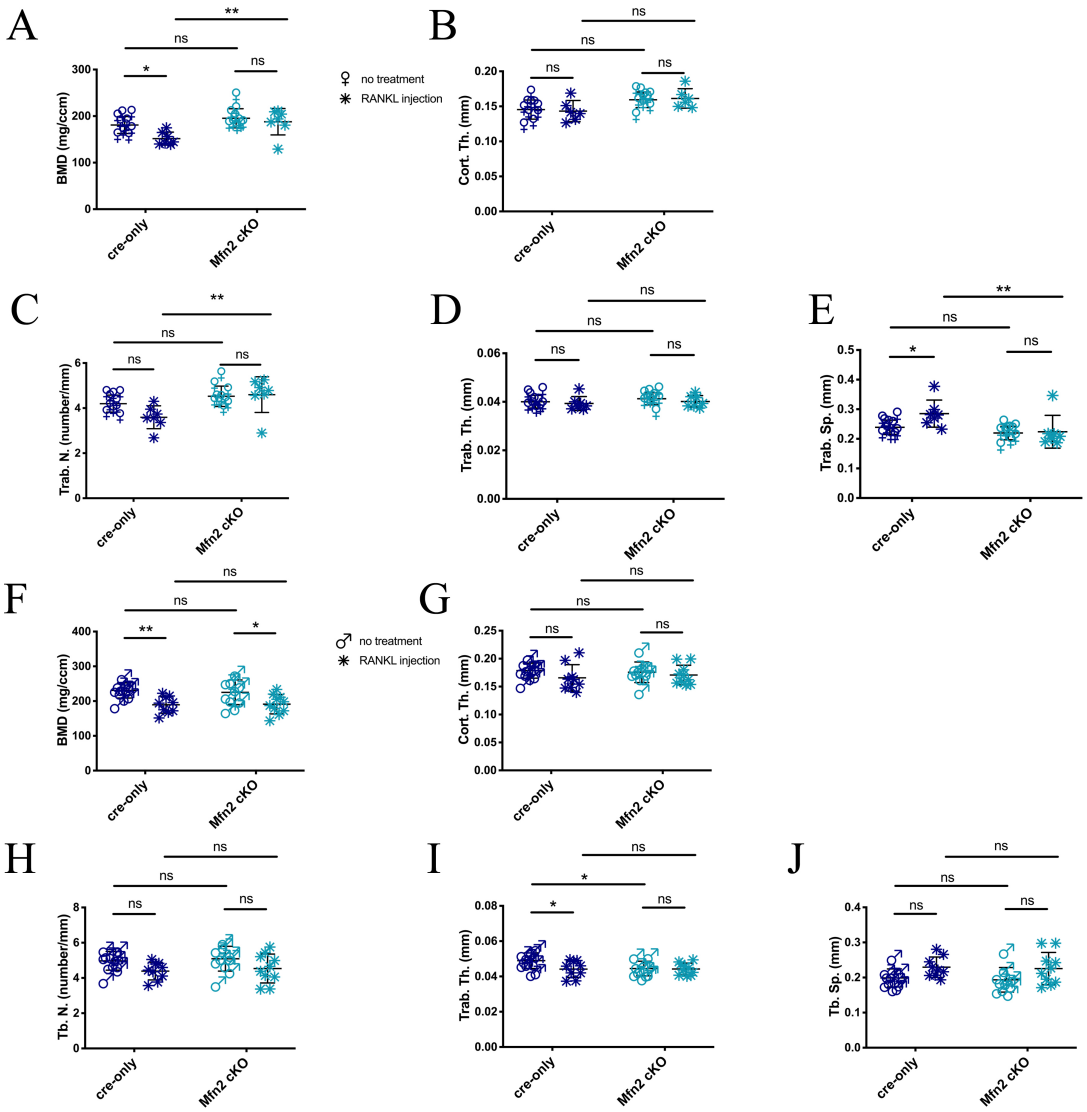

Figure 2.15: µCT analysis of induced osteolysis in female and male cohorts

Additional analyses between cre-only and Mfn2 cKO females with no treatment or acute RANKL challenge for BMD (A), Cort.Th. (B), Trab.N. (C), Trab.Th. (D), and Trab.Sp. (E). Identical analyses for males are shown in F-J. *p<0.05, **p<0.01, ordinary two-way ANOVA with multiple comparisons.

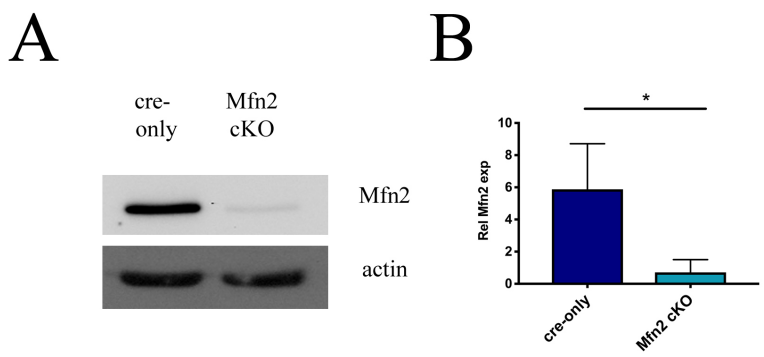

Figure 2.16: Confirmation of Mfn2 knockdown by western blot and qPCR

A). Protein harvested from OCs derived from cre-only and Mfn2 cKO animals are blotted against Mfn2, and expression by qPCR is shown in (B). *$p<0.05$, unpaired t-test with Welch's correction.

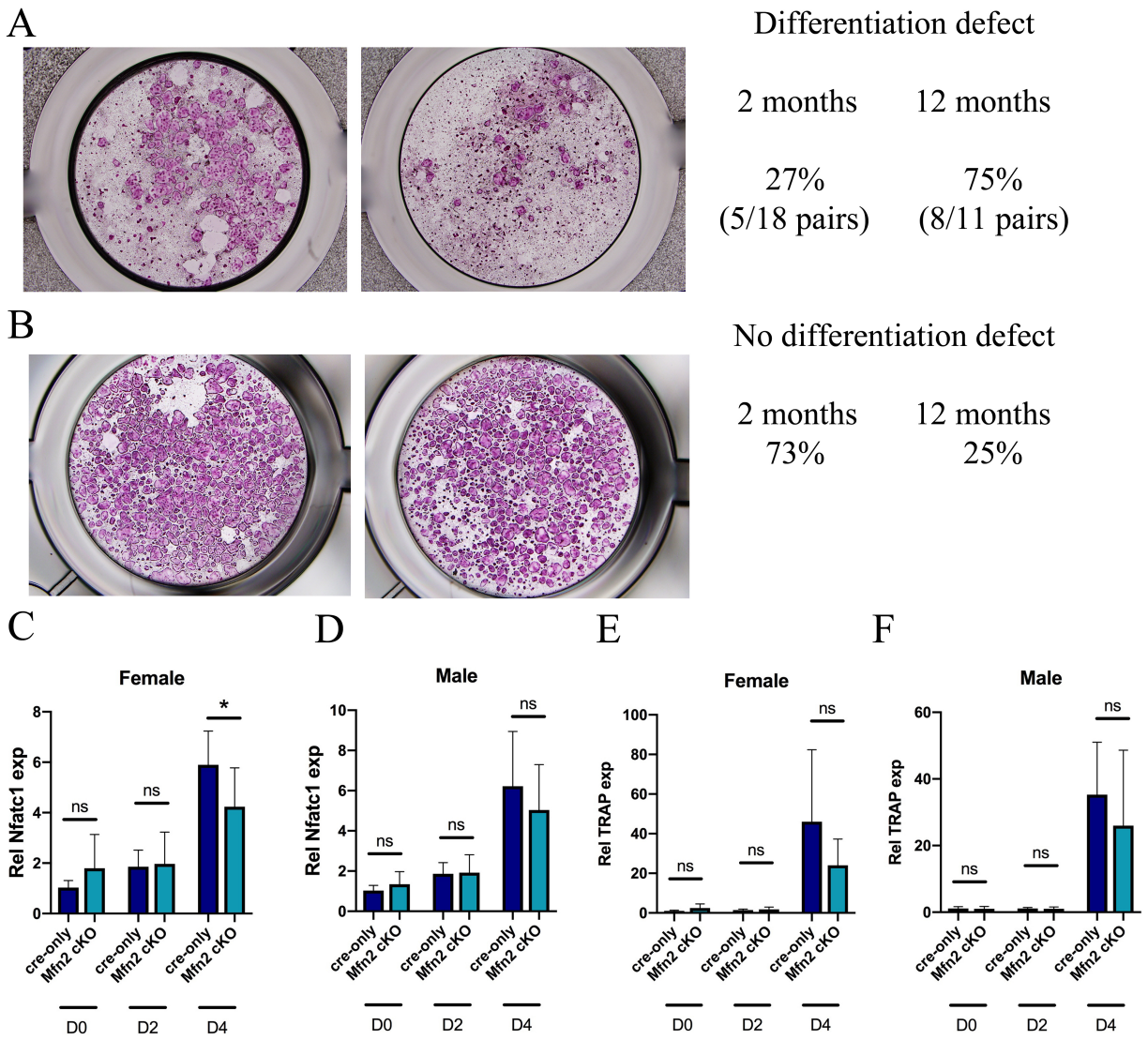

Figure 2.17: Loss of Mfn2 in the OC lineage does not consistently impede osteoclastogenesis by TRAP and gene expression

A). Representation of experiment yielding defect in OC formation when Mfn2 is deleted in the OC lineage and percentage of this phenotype occurring in samples derived from bone marrow of 2 and 12 month old animals. B). Representation of experiment yielding no defect in OC formation when Mfn2 is deleted in the OC lineage and percentage of this phenotype occurring in samples derived from bone marrow of 2 and 12 month old animals. In differentiating OCs from 2 month old bone marrow Nfatc1 (C-D) and TRAP (E-F) expression are assessed by qPCR (n=4 biological replicates per group), *$p<0.05$, two-way ANOVA.

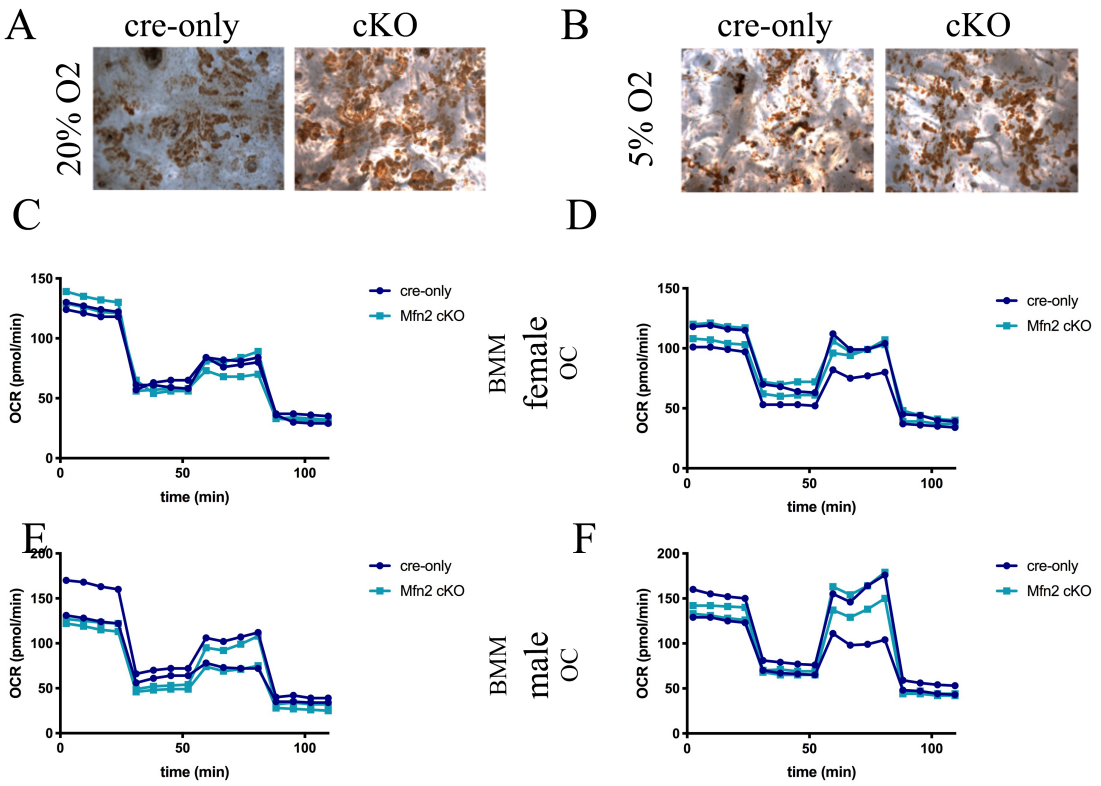

Figure 2.18: Lack of Mfn2 in the OC lineage does not affect bone resorption or oxygen consumption.

Pit staining after cre-only and Mfn2 cKO BMMs were differentiated on bovine bone slices in 20% O_2 (A) or 5% O_2 (B). Female BMMs (C) and OCs (D) were analyzed by Seahorse analysis. Males in E-F.

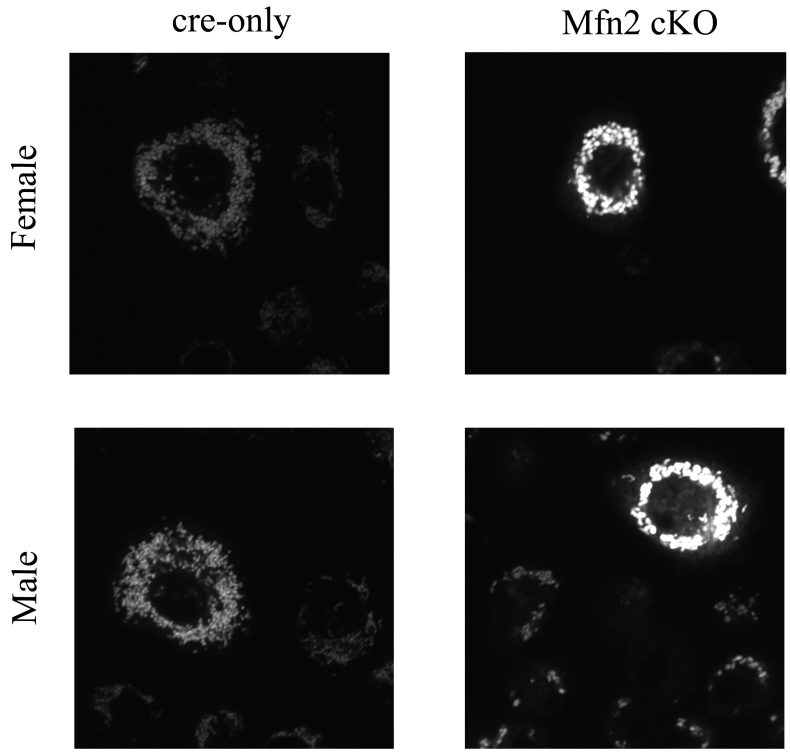

Figure 2.19: Pre-OCs lacking Mfn2 display altered mitochondrial networks compared to cre-only pre-OCs

BMMs from cre-only and Mfn2 cKO mice were differentiated with RANKL and stained with Mitotracker Green to illuminate mitochondria. Image are 100X.

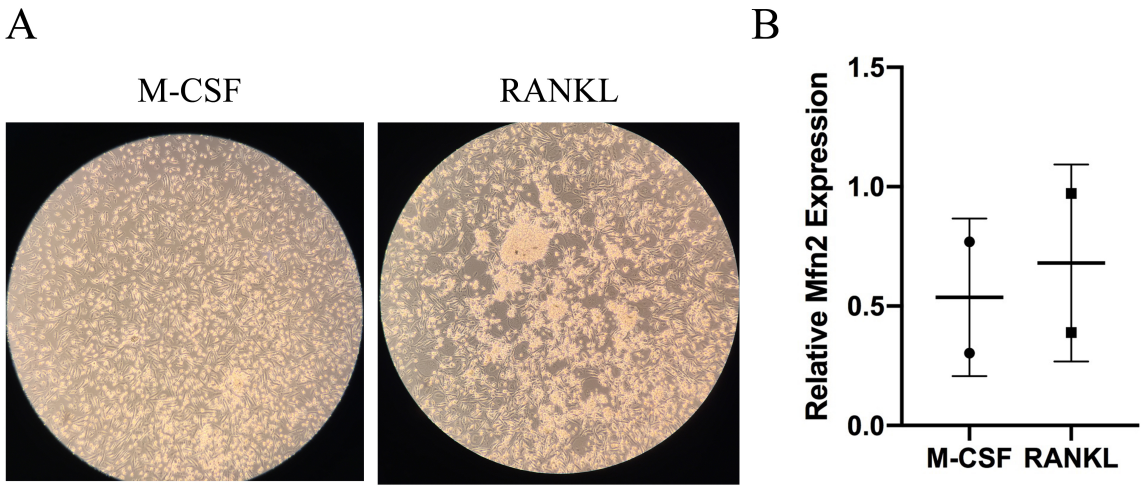

Figure 2.20: Mfn2 expression increases from human monocytes to OCs *in vitro*.

A). CD14^{+} cells isolated from human peripheral blood differentiated to mature OCs are shown via brightfield microscopy at 4X B). Mfn2 expression was assayed by qPCR in two patient samples and is increased in RANKL-treated OCs compared to CD14^{+} precursors.

Chapter 3 –
Tethering function of Mfn2 is required for osteoclastogenesis *in vitro*

Introduction

In this chapter, we aimed to determine which function of MFN2 is responsible for promoting osteoclastogenesis. One function of MFN2 is to promote tethering of mitochondria to mitochondria and mitochondria to the ER, leading to mitochondrial fusion and altered signaling such as Ca^{2+}, respectively. The other function of the protein is to stimulate PINK1/PARKIN signaling to remove defective organelles via mitophagy. In non-OC-forming Mfn1/2 dcKO BMMs, we overexpress mutants that selectively disable tethering (Mfn2-EE) or mitophagy (Mfn2-AA). We show that in this cell lineage, tethering/fusion by MFN2 is required for OC differentiation. Because Ca^{2+}-dependent *Nfatc1* levels are decreased in our Mfn2 cKO cells, further experiments are undertaken to begin probing whether MFN2-mitochondria tethering and subsequent Ca^{2+} signaling plays a role in our system. While work in this area is still ongoing, we are confident that the specific role of MFN2 is crucial and possibly unique in the OC compared to other cell types. We are determined to elucidate this mechanism in future studies beyond the scope of this dissertation.

Materials and methods

Retroviral overexpression

Mfn2-WT, Mfn2-EE, and Mfn2-AA were gifts from Gerald Dorn II, M.D. (Washington University in St. Louis). Each gene was cloned into the pMX retroviral vector and transfected into Platinum-E (platE) cells by calcium phosphate precipitation (Morita et al., 2000; Zou et al., 2012). PlatE supernatant was harvested 48 and 72 hrs post-transfection, filtered through 0.45μm and added to BMMs with α-MEM, 10% FBS, and 100 IU/ml Penicillin/Streptomycin, 1:10 CMG, and 8μg/ml polybrene (Sigma H9268, St. Louis, MO, USA) on 2 consecutive days. 24 hrs following the final viral addition, 1μg/ml blasticidin (Sigma 203350, St. Louis, MO, USA) was added to select for infected BMMs. Retroviral NFATc1-WT and NFATc1-CA were acquired from Addgene (plasmid #11101 and #11102, respectively, Watertown, MA, USA)(Monticelli and Rao, 2002).

Mitotracker staining

BMMs were seeded at 100,000 cells/well in 24-well plates containing circular coverglass (FisherScientific 12-545-81, Hampton, NH), and differentiated with 30ng/ml RANKL. Prior to fixation, cells were washed once with PBS and stained with 100nM Mitotracker Deep Red FM per product instructions (Molecular Probes M22426, Eugene, OR). Wells were then fixed with 4% paraformaydehyde for 10 min, and coverglass adhered to slides with ProLong Diamond Antifade Mountant with DAPI P36962 (Invitrogen, Carlsbad, CA). Slides were imaged using a Zeiss LSM 880 Confocal with Airyscan with 63x magnification and optical zoom of 1.8 at the Washington University Center for Cellular Imaging (WUCCI). WUCCI imaging was supported by the Washington University School of Medicine, The Children's Discovery Institute of

Washington University and St. Louis Children's Hospital (CDI-CORE-2015-505) and the Foundation for Barnes-Jewish Hospital (3770).

Ca^{2+} Oscillations

BMMs seeded on 29 mm glass bottom dish at a density of 300,000 cells/dish, and exposed to 30ng/ml RANKL for 2 days. Dishes were washed in 1X HBSS containing 1 mM Mg^{2+} and 2 mM Ca^{2+}, then stained with the same buffer and 2μM Fura-2 AM and 10 ng/ml hMCSF for 30 min at 37˚C (Life Technologies F-1221, Carlsbad, CA, USA; BioLegend 574806, San Diego, CA, USA). Following three washes with 1X HBSS containing 1 mM Mg^{2+}, cells were kept in this buffer with additional 10ng/ml hMCSF. Ratiometric Ca^{2+} was performed with a Till Photonics digital microscope at the Center for Investigation of Membrane Excitability Diseases (CIMED) Live Cell Imaging Core (Washington University in St. Louis). 100uM and 2 mM $CaCl_2$ were added following baseline collection to induce increases in cytosolic $Ca2^{+}$ when data is presented as 240/380 ratios.

Results

Mitochondrial tethering is the dominant Mfn2 mechanism contributing to osteoclastogenesis *in vitro*

MFN2 has two main molecular functions – tethering and mitophagy – that can be selectively disabled via mutation to examine the ability of either to impact OCs. As we consistently observe a decrease in osteoclastogenesis in cells derived from female dcKO bone marrow, we infected these BMMs with each of the following retroviral constructs: Vector, Mfn2-WT, Mfn2-EE (T11E-S442E; defective tethering due to spontaneous mitophagy without a fusion signal), and Mfn2-AA (T111A-S442A; defective mitophagy without impacting fusion)(Gong et al., 2015). Cultures were stained for TRAP as OC differentiation progressed. We find that transduction of dcKO BMMs with Mfn2-AA restores osteoclastogenesis to a comparable level as Mfn2-WT, indicating that the mitophagy function of MFN2 is dispensable for osteoclastogenesis. In contrast, transduction with Mfn2-EE has only a modest effect on osteoclastogenesis, suggesting that tethering is necessary for osteoclastogenesis to occur (Fig. 3.1). When assessing mitochondrial networks by Mitotracker Red staining, however, gross differences between staining in Mfn2-EE and Mfn2-AA are not observed. Here, mitochondria display a rather intermediate phenotype between densely aggregated mitochondria in Vector cells and uniformly organized organelles in Mfn2-WT cells (Fig. 3.2). This implies fusion of mitochondria partially accounts for MFN2 support of osteoclastogenesis, and that tethering may play a greater role.

Tethering defect does not impact Nfatc1 through a mitochondrial calcium buffering mechanism

Because tethering of MFN2 promotes mitochondria-mitochondria interactions as well as mitochondria-ER interactions, we hypothesized that ER-mitochondria proximity is important for OC formation, as this is an exclusive function of MFN2 that MFN1 does not share. This appears plausible because oscillation in cytosolic Ca^{2+} is known to regulate *Nfatc1* induction, and we detect significantly decreased *Nfatc1* levels in OCs from Mfn2 cKO and Mfn1/2 dcKO compared to cre-only and ctrls, respectively (Fig. 2.6 and Fig. 2.17) (Hogan et al., 2003; Kim et al., 2013). Previously, we tried to rescue the osteoclastogenesis defect seen in Mfn2 cKO BMMs derived from 12 month old animals by overexpressing *Nfatc1*. Irrespective of RANKL dose used, TRAP staining of Mfn2 cKO cells treated with *Nfatc1* was identical to those infected with the vector control (Fig. 3.3). This result, however, did not exclude the possibility that NFATc1 localization the nucleus was impaired.

To assess whether Ca^{2+}-dependent regulation of NFATc1 targeting to the nucleus was impacted by Mfn2 loss in BMMs, dcKO BMMs were infected with wild type (WT) or constitutively active (CA) forms of *Nfatc1* and treated with RANKL. In two independent experiments pilot experiments, while no striking differences between WT and CA are seen, we cannot discount the observation that CA OCs counts per well are elevated compared to WT (Fig. 3.4). Lack of effect could be attributed to the fact that lack of a mammalian selection gene in these vectors did not allow elimination of uninfected BMMs prior to addition of RANKL. We are currently working to clone these genes into a selectable vector as well as collect protein for NFATc1 western blot to definitively conclude the effect of WT vs. CA *Nfatc1* in our *in vitro* system.

To further explore Ca^{2+} signaling in the model, cytosolic Ca^{2+} was measured via ratiometric imaging in one pilot experiment. Here, although ctrl pre-OCs may appear to have higher amplitude in oscillations, we cannot claim any definitive differences are consistent seen between groups (Fig. 3.5). We note that this is one trial, and due to difficulty placing ATP and Ca^{2+} stimuli directly in the line of the camera, another trial of this experiment is needed before ruling out the possibility of differing Ca^{2+} handling when mitofusins are deleted in the OC lineage.

In another effort to examine wither Mfn2-directed mitochondrial tethering to the ER is responsible for decreased osteoclastogenesis in our dcKO cells, two additional retroviral *Mfn2* mutants were constructed. First, an Italian group recently identified a substitution mutation in MFN2, K416R, that disrupts the mitochondria-ER distance and mitochondrial Ca^{2+} uptake (Basso et al., 2018). However, this study does not explicitly assess whether mitochondrial fusion is disrupted with MFN2 K416R mutation, though we infer from seemingly networked images that mitochondria-mitochondria tethering and subsequent fusion is not affected in this model. Nevertheless, lack of such specific information means our osteoclastogenesis results to be interpreted with caution. We cloned this mutant and overexpressed it in dcKO BMMs via retroviral infection. No differences in OC formation are seen between cells with overexpressed Mfn2-WT and Mfn2-K416R in our standard OC formation assay (Fig. 3.6). Here, these results suggest that impaired ER-mitochondria tethering by MFN2 in the OC may not be the mechanism sole mechanism that drives OC formation.

Second, *in vitro* assays using Mfn2-F223L mutation in MEFs revealed that this mutant has normal ability of mitochondria to tether into dimers, but have impaired homotypic fusion of Mfn2-F223L to Mfn2-F223L mitochondria, even when Mfn1-WT is present in the system, due

to a potential defect in GTP hydrolysis disallowing nucleotide-dependent self-assembly of the MFN2 molecules (Daumke and Roux, 2017; Engelhart and Hoppins, 2019). Though it is not clear whether this applies to MFN2 on the ER membrane, the data suggest that association of Mfn2-F223L proteins is not affected. Retroviral overexpression of Mfn2-F223L in dcKO BMMs does not promote osteoclastogenesis, indicating that solely tethering but not fusion of MFN2 may be dispensable in the OC lineage (Fig. 3.7).

Discussion

We sought to determine the mechanism through which mitofusin activity contributes to OC formation. Because we see that high bone mass phenotypes in knockouts compared to littermate controls in our animal models are more pronounced in Mfn1/2 dcKOs than Mfn1 or Mfn2 cKOs, this could suggest that the effect on the OC lineage is solely an effect of mitofusin dose. Here, loss of one homolog could be compensated for by the presence of the other in single Mfn1 and Mfn2 cKO animals. This does not, however, explain why overexpression of *Mfn2* but not *Mfn1* rescues osteoclast formation *in vitro*. We therefore postulated that MFN2 contributes in a way that MFN1 cannot. MFN2-specific functions include initiation of mitophagy, following phosphorylation of MFN2 by PINK, and regulation of mitochondrial-ER interactions, a consequence of tethering. Our demonstration that overexpressing Mfn2-AA (defective mitophagy) but not Mfn2-EE (defective fusion) rescues osteoclastogenesis pointed us toward mitochondria-ER interactions as a possible mechanism.

MFN2 is present not only on the outer mitochondrial membrane, but on the ER membrane, facing the cytoplasm. Interactions between ER-located MFN2 with mitofusins on mitochondria control the proximity of these two organelles (Filadi et al., 2018b). Mitochondrial tethering to the ER by MFN2 is known to specifically regulate cellular functions such as Ca^{2+} signaling and the ER stress response (reviewed in (Filadi et al., 2018a; van Vliet and Agostinis, 2018). Studies using *Mfn2* knockdown cells have revealed that loss of *Mfn2* is associated with increased distance between the mitochondria and ER as well as impaired mitochondrial Ca^{2+} uptake, which hinders calcineurin and apoptosis pathways (de Brito and Scorrano, 2008; Karbowski et al., 2006; Kasahara et al., 2013; Naon et al., 2016). Here, because the decreased *Nfatc1* levels we observe in Mfn1/2 dcKO and Mfn2 cKO OCs *in vitro* directly implicate Ca^{2+}

signaling in our cultures, we postulate that changes in Ca^{2+} may be the link to decreased OC formation in our model. Although Ca^{2+} oscillations in ctrl and dcKO cells were not grossly different in a pilot experiment of n=1/group and overexpression of Nfatc1-CA did not wholly imprive osteoclastogenesis over Nfatc1-WT in mitofusin-deficient dcKO BMMs, future studies in the laboratory will probe these with additional rigor. This will include measuring changes in mitochondrial Ca^{2+} in addition to cytosolic Ca^{2+} when *Mfn2* presence is altered, and repeating rescue experiments using selectable Nfatc1-WT and Nfatc1-CA vectors.

Our *in vitro* investigation of MFN2 mutations K416R and F223L could naively imply that tethering of adjacent MFN2 molecules either between neighboring mitochondria or mitochondria and the ER is not necessary for OC differentiation. Here, disabling ER-mitochondria tethering with K416R did not inhibit osteoclast formation, and disabling fusion while leaving tethering intact with F223L produced no OCs. Accepting these data would prompt us to conclude that fusion between mitochondria is the primary mechanism through which mitofusins support osteoclastogenesis, at least in culture. This simplistic interpretation however does not consider the fact that both of these mutants were primarily evaluated by others solely in MEF cells and in purified mitochondrial fractions lacking a native cell environment. Mutants could plausibly behave differently in the context of a differentiating OC and more work is needed to further probe the effect of these substitution mutations.

Figures and tables

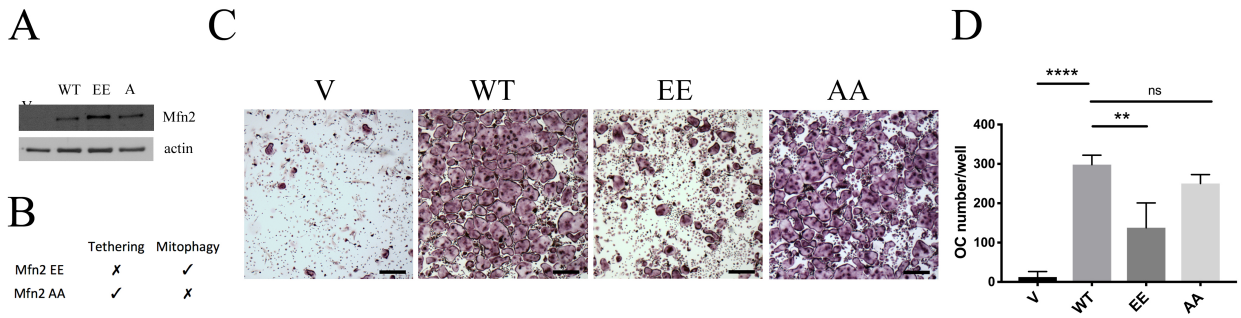

Figure 3.1: Restoration of Mfn2 tethering function restores osteoclastogenesis in dcKO BMMs

A). dcKO BMMs were transduced with retroviral pMX-Vector, V, tethering-defective mutant pMX-Mfn2-EE, EE, and mitophagy defective pMX-Mfn2-AA, and Mfn2 protein detected via western blot. B). While Mfn2-EE allows mitophagy, Mfn2-AA allows tethering/fusion. C). Cultures were TRAP-stained following 6 days of RANKL exposure. OC numbers are quantified in D. *p<0.05, **p<0.01, ***p<0.001, ****p<0.0001, ordinary one-way ANOVA.

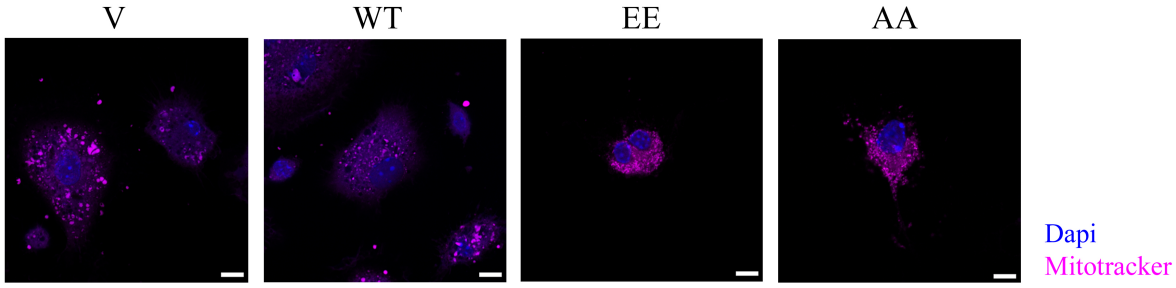

Figure 3.2: Mitochondrial fusion is modestly altered with overexpression of Mfn2 mutants *in vitro*

Following transduction pMX-Vector, V, pMX-Mfn2-WT, WT, pMX-Mfn2-T111EE-S442E, EE, and pMX-Mfn2- T111A-S442A, AA, into dcKO BMMs and treated with RANKL, pre-OCs were stained with Dapi and Mitotracker Red. Mitochondrial networks are illuminated, scale = 7μm.

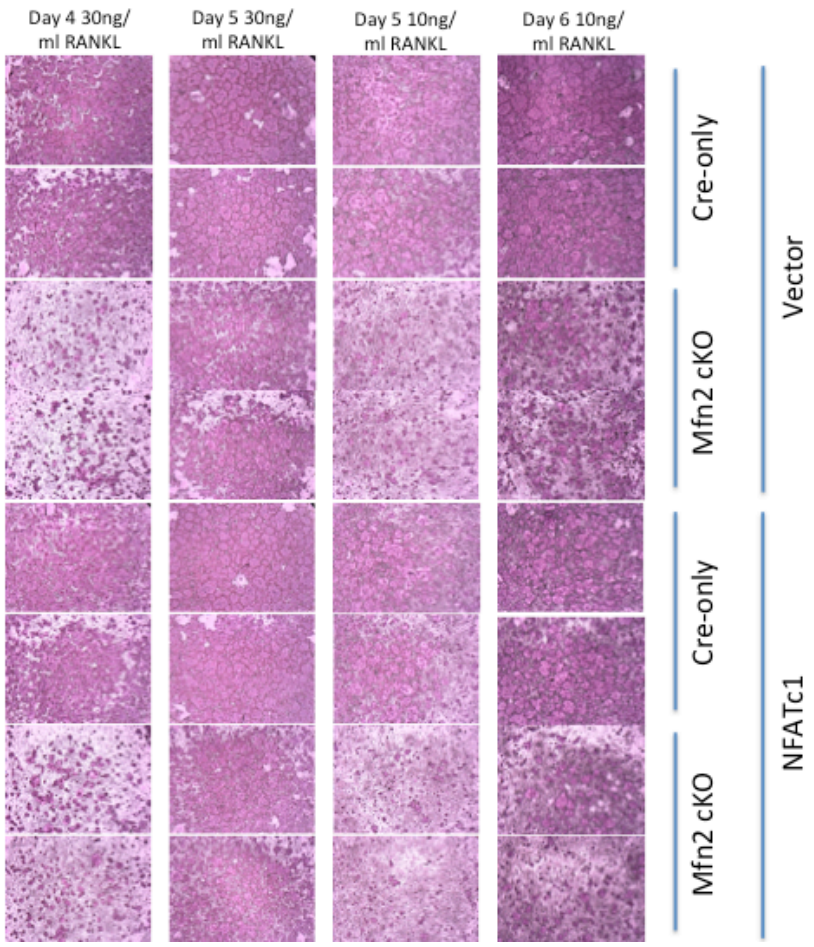

Figure 3.3: Nfatc1 overexpression does not rescue osteoclastogenesis defect in BMMs derived from 12 month old Mfn2 cKO mice

Cre-only and Mfn2 cKO BMMs harvested from 12 month old animals were infected with empty vector or Nfatc1 and cultured with RANKL. Representative TRAP images are shown over a number of days and RANKL doses at 2X.

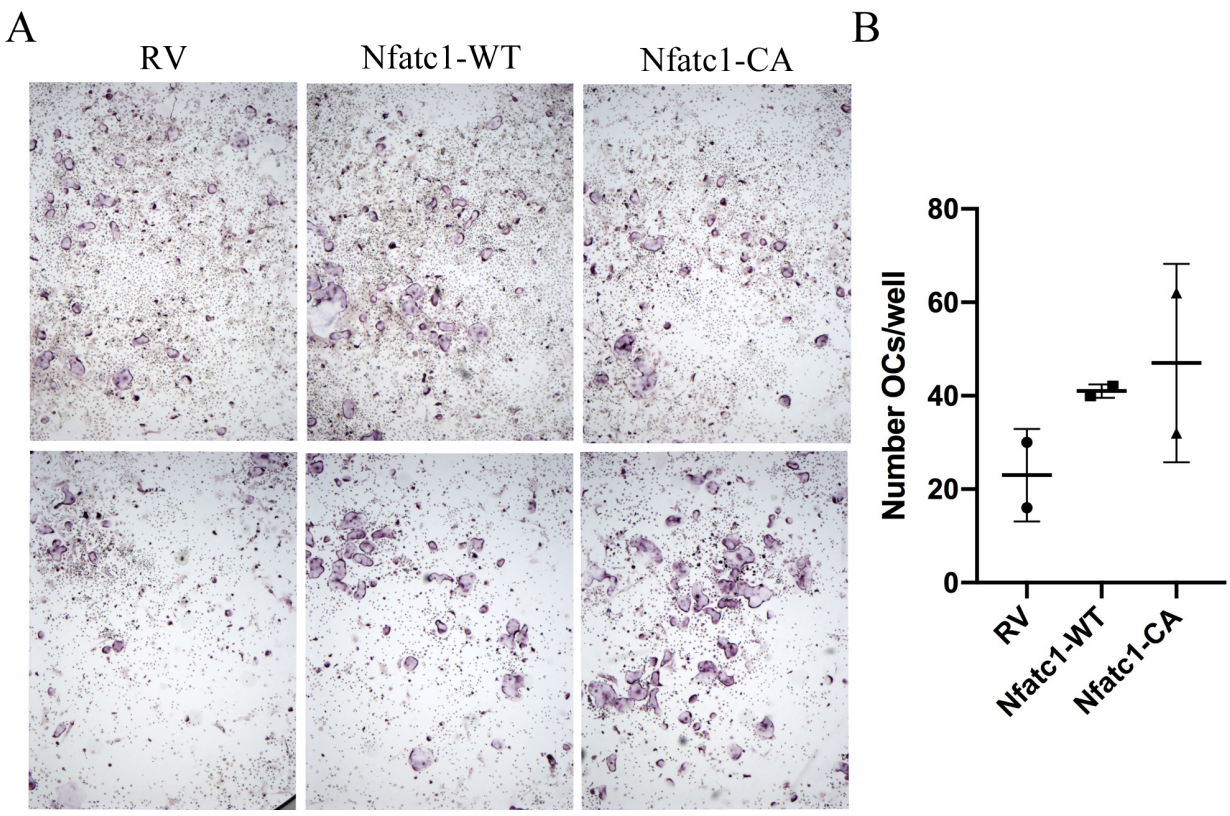

Figure 3.4: Wild type and constitutively active Nfatc1 induce osteoclastogenesis to the same degree in dcKO BMMs.

A). dcKO BMMs were infected with a retroviral vector, Nfatc1-WT, or Nfatc1-CA, and stained for TRAP. Osteoclast numbers are shown in (B). Representative images from both trials are shown at 2X.

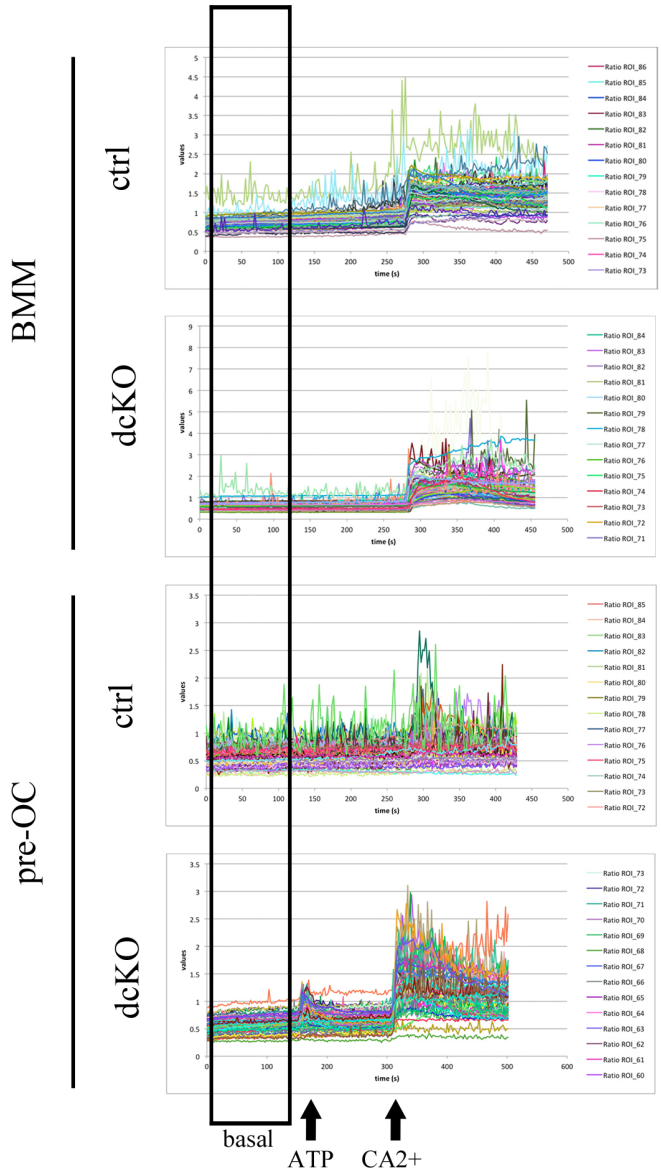

Figure 3.5: No differences are seen in basal Ca^{2+} oscillations between ctrl and dcKO cells

Female ctrl and dcKO BMMs and OCs were loaded with Fura-2 dye and cytosolic calcium measured over time. Basal represents oscillations prior to ATP or CA^{2+} stimuli.

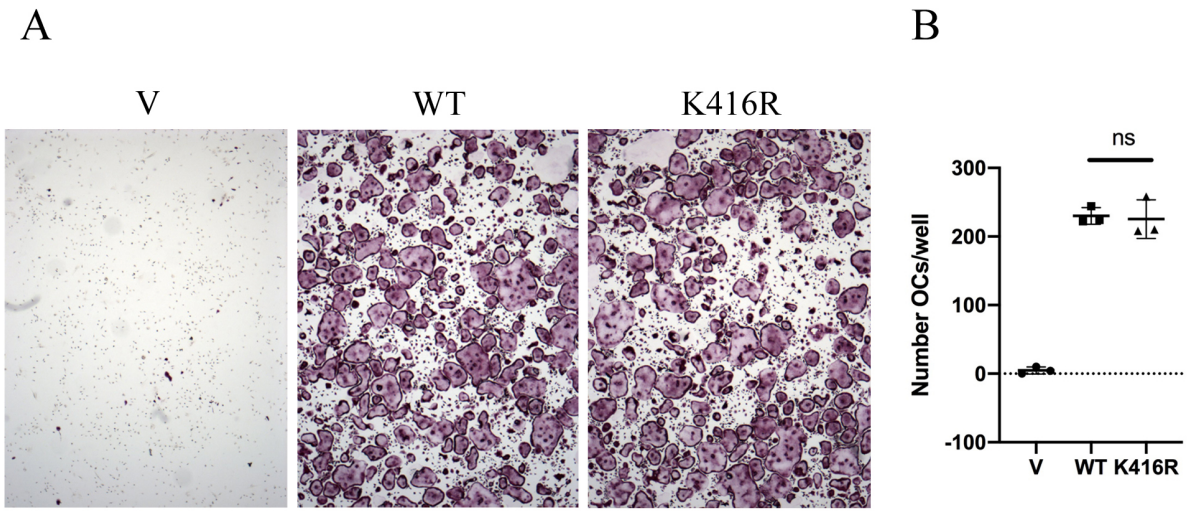

Figure 3.6: Disabling Mfn2 tethering to the ER does not impact osteoclastogenesis.

A). Female dcKO BMMs were retrovirally infected with the overexpression of vector, Mfn2-WT, or Mfn2-K416R, treated with RANKL, and TRAP stained. Number of OCs per well are plotted in (B).

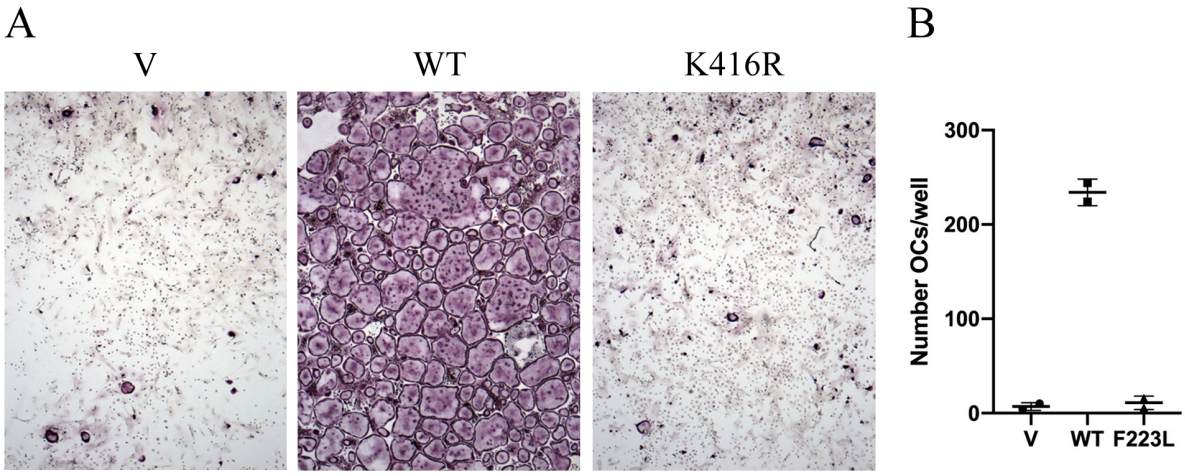

Figure 3.7: Restoring tethering but not fusion functions of Mfn2 does not support osteoclastogenesis.

A). Female dcKO BMMs were retrovirally infected with the overexpression of vector, Mfn2-WT, or Mfn2-F223L, treated with RANKL, and TRAP stained. Number of OCs per well are plotted in (B).

Chapter 4 –
Discussion and future directions

Part 1 – Role of mitofusins in the OC lineage

Our data reveals that mitofusin activity is an important component of OC formation *in vivo* and *in vitro*. In murine models, dual loss of *Mfn1* and *Mfn2* causes a high bone mass phenotype in female animals, and single loss of *Mfn2* offers protection from bone loss with age and induced osteolysis in females. In culture, expression of *Mfn2* on a double Mfn1/Mfn2 knockout background induces osteoclastogenesis to a greater degree than *Mfn1*. Further, selectively disabling the mitophagy function of MFN2 has no effect on OC formation, but osteoclastogenesis is impaired when the tethering ability of MFN2 is ablated. Therefore, because OC differentiation ensues when solely MFN2, but not MFN1, is present, we hypothesize MFN2 must have a non-redundant function from MFN1 that allows this to occur. This could be the unique ability of MFN2 to tether mitochondria to the ER, because changes in ER-MFN2 juxtaposition are known to modulate cytosolic Ca^{2+} levels (Naon et al., 2016). In turn, Ca^{2+} modulates translocation of NFATc1 to the nucleus, and our dcKO and Mfn2 cKO have decreased *Nfatc1* expression (Hogan et al., 2003). However, our mechanistic studies thus far have not been able to confirm or refute the hypothesis that abnormal ER-MFN2 juxtaposition in our knockouts alters Ca^{2+} handling and therefore reduces NFATc1-driven OC differentiation.

In assessing the effect of Mfn2-K416R and Mfn2-F223L mutations *in vitro*, preliminary experiments suggest that Mfn2 association with the ER does not have an effect on osteoclastogenesis, because dcKO cells overexpressing Mfn2-K416R (mutant that disables mitochondria-ER tethering) generate mature OCs. Conversely, and when Mfn2-F223L (mutant that allows tethering but inhibits fusion) is added, the ability of BMMs to differentiate to OCs is abolished. It remains unclear, however, in the original studies of these mutants whether Mfn2-K416R permits mitochondrial fusion or whether the tethering ability of Mfn2-F223L relates to

ER-mitochondria relationship in addition to mitochondria-mitochondria interactions. Answering these questions is imperative to fully assess and interpret the effect of these mutants in our system. To begin additional characterization of these mutations, retroviral rescue experiments will be repeated in a single Mfn2 cKO background to evaluate whether K416R and F223L mutations have different effects when interactions with endogenous MFN1 are allowed. Future exploration will also include study of [Ca^{2+}] in the cytoplasm and mitochondria of pre-OCs with varying MFN2 mutations to determine whether changes in mitochondrial juxtaposition to the ER with K416R mutation culminates in biologically meaningful changes in signaling on the Ca^{2+} /NFATc1 axis. It could also be the case that decreases in dcKO and Mfn2 cKO *Nfatc1* expression is due to Ca^{2+}-independent mechanisms. Because changes in Ca^{2+} oscillations that affect NFATc1 might be difficult to detect, EM microscopy can be simultaneously employed to precisely measure ER to mitochondria distances in our cells and understand how tethering changes by Mfn2 may impact osteoclastogenesis.

We cannot rule out that Mfn2 activity *in vitro* may not be indicative of how the protein operates *in vivo*, and that tethering/fusion of MFN2 could alter OC function in addition to or instead of OC differentiation when in a biological setting. In particular, *in vitro* osteoclastogenesis phenotypes are inconsistent between BMMs derived from cre-only and Mfn2 cKO animals. We have assessed whether *in vivo* and *in vitro* phenotypes are correlated, but BMMs derived from high bone mass animals are not consistently defective in OC formation (R. Zeng, unpublished observation).

Critical interpretation could be attained through generating knock-in mice harboring the Mfn2-K416R or Mfn2-F223L mutations. Knock-in of mutations to the Rosa26 locus would allow cre-driven induction and overexpression of *Mfn2* mutants in OC lineage cells at birth, or

genes could be activated or deleted at different stages with incorporation of rtTA or diphtheria toxin transgenes, respectively (Belteki et al., 2005; Ivanova et al., 2005). This would allow tighter control of expression during murine development or experimental timelines. Alternatively, allowing *Mfn2* mutations to be expressed and regulated at physiological levels through global CRISPR-mediated point mutations could offer relevant and powerful study of disabled ER juxtaposition and tethering by MFN2. Combining such knock-ins of K416R and F223L on a background in which *Mfn1* is deleted in the OC lineage might have further potential to dissect this specific role of Mfn2 tethering on bone mass.

Additional options could include crossing cKO or *Mfn2* mutation-containing animals with those harboring fluorescent mitochondria to further assess changes in mitochondrial architecture during osteoclast formation (Pham et al., 2012; Sun et al., 2015). In particular, mitochondrial fusion maybe evaluated *in vivo* using PhAM^{excised} animals in which mitochondria constitutively express GFP unless exposed to 405 nm laser light where they express RFP. By exposing sub-populations of mitochondria to light, fusion events of green and red organelles may be characterized by yellow fluorescence (Pham et al., 2012). Differentiating BMMs from these animals would allow quantification and comparison of fusion events when different *Mfn2* mutants are introduced *in vitro.*

An unexplored area in this thesis is additional signaling pathways in which MFN2 is involved. For example, mTOR is reported to be enriched in the mitochondria-associated ER membranes (MAM), and its activity is suppressed when bound by the HR1 domain of MFN2 (Betz et al., 2013; Xu et al., 2017). This in turn inhibits mTORC2 signaling through PI3K and Akt (Xue et al., 2018). Intriguingly other groups have demonstrated that inhibition of mTOR and downstream Akt signaling supports OC formation and survival in animal and cell culture

models (Dai et al., 2017; Glantschnig et al., 2003; Sugatani and Hruska, 2005; Tiedemann et al., 2017). It is tempting to speculate that without the tethering function of MFN2 linking mitochondria to the ER in the OC, the MAM is disrupted and therefore hinder OC differentiation via lack of MTORC2 activity.

Wnt signaling might also have implications in MFN2 activity as our laboratory finds increased β-catenin protein levels in OBs with conditional deletion of *Mfn2* compared to controls (A. Zarei, unpublished observation). This correlates with increased osteogenesis we see *in vitro* from bone marrow stromal cells lacking *Mfn2* and increased mitochondrial activity that others have documented (An et al., 2010; Shares et al., 2018). If β-catenin levels are altered in our OC model as well, disruption of β-catenin protein regulation by MFN2 could be detrimental to OC formation. β-catenin decreases OC through direct inhibition of RANKL-induced NF-κB signals and *Nfatc1* induction in the OC (Kobayashi et al., 2016; Lerner and Ohlsson, 2015; Movérare-Skrtic et al., 2014; Shares et al., 2018). Moreover, glycolytic enzyme pyruvate kinase (PKM2) was recently shown to interact with MFN2 downstream of mTOR to not only promote mitochondrial fusion, but also attenuate glycolysis while stimulating OxPhos (Li et al., 2019). We cannot rule out the possibility that inability of MFN2 to associate with PKM2 in the OC could singularly disrupt mitochondrial fusion and normal metabolic properties of this cell type.

Future studies will probe the relationship between MFN2 and MTORc2, β-catenin, and PK2M in the OC lineage. We will start by conducting *in vitro* timecourse experiments to determine how RNA and protein expression of these factors change during osteoclastogenesis in BMMs derived from ctrl and dcKO bone marrow. Anticipating MTORC2, β-catenin, and/or PK2M expression will change with MFN2 levels during osteoclastogenesis, we can move forward in activating or disabling these components in the presence or absence of *Mfn2*.

Because knockdown of PK2M increases mitochondrial fragmentation, we could also try rescuing mitofusin deficiencies with PKM2 overexpression *in vitro* (Li et al., 2019). Such experiments have the potential to pinpoint how MFN2 converges with other signaling pathways to support OC formation in our model.

We are intrigued by the striking sexual differences in our model, and to our knowledge this is the second report of differences in male vs. female response to mitofusin loss. Conditional ablation of *Mfn2* in brown adipose tissue (BAT) leads to dysfunction of the tissue and protection from insulin resistance and obesity by high-fat diet. Here, a sex-specific remodeling of BAT mitochondrial function was reported after *Mfn2* deletion as females displayed increased ATP-synthesizing fat oxidation while males experienced increased glycolytic capacity (Boutant et al., 2017; Mahdaviani et al., 2017). This suggests that female mitochondria may have an inherent bias toward oxidative phosphorylation over glycolysis in the bone, and with the induction of stress, tethering-compromised mitochondria may be unable to respond and accommodate to stress by maximizing ATP output through efficiently fusing OMM and IMM. As mitochondrial differences in male and female mammals have been documented in other organs, is it unsurprising that this also manifests in the OC lineage. For example, female murine cardiomyocyte mitochondria are more efficient than male cells despite having lower mitochondrial content (reviewed in (Ventura-Clapier et al., 2017)). Sex differences in mitochondria can plausibly be due to the fact that mitochondrial DNA is only under selection in females, therefore allowing hormones like estrogens to have a protective effect on female mitochondria.

Intriguingly, a major regulator of the OC is estrogen. In menopause, estrogen production by the ovaries falls and leads to increased bone resorption by the OC. Estrogen deficiency

reverses the pro-apoptotic effect of the molecule on the OC and enables upregulation of TNFα and IL-1β cytokines as well as RANKL that promote OC differentiation. Estrogen deficiency also disfavors the commitment of mesenchymal progenitors to the OB lineage and fails to block OB apoptosis, further leading to the overabundance of OC activity and bone resorption in post-menopausal women (reviewed in (Khosla et al., 2011; Novack, 2010). Congruently, we theorize that sex differences in our model may be inherent to OC biology. We have previously observed that compared to males, female mice have more numerous OCs in the trabecular compartment compared to males (Zarei et al., 2018). We anticipate that a higher abundance of OCs might make females more susceptible to the impact of mitochondrial defects in the cell lineage. It would be interesting to further investigate the role of estrogen in mitochondrial dynamics. Depletion of estrogen with ovariectomy (OVX) surgeries could determine if estrogen is responsible for female phenotypes. If so, we would expect Mfn2 cKO females post-OVX to have identical bone mass to ctrls post-OVX, similar to how males respond to loss of bone mass with RANKL-injection. We could consider approaching the interplay of estrogen and MFN2 in culture by supplementing culture media with or without estrogen, and undertaking transcriptional profiling of cellular populations. *In vivo*, laser capture microdissection of frozen skeletal tissues would allow isolation of male or female OCs and confirmation of differences observed *in vitro*.

Part 2 – Final comments

In sum, our studies highlight the importance of mitochondrial tethering/fusion in OC lineage cells and bring the skeleton into light for the field of mitochondrial dynamics. With continued investigation, our work opens the possibility that regulation of mitochondrial dynamics in the osteoclast could modulate bone mass in humans. Especially as women are more

prone to osteoporosis then men, altering mitofusin activity has the potential to be exploited for preservation of bone mass in this post-menopausal population.

Appendix A –
Transcription Factor EB

Abstract

In 2011, a 3-year old boy born to consanguineous parents presented to physicians at Shriners Hospitals for Children in St. Louis with clinical signs of osteopetrosis (OPT). His bones were abnormally dense, as reflected by a lumbar spine z-score of +13.4. A bone core biopsy of the dsistal metaphasys of the tibia revealed the abundance of OBs and a complete absence of OCs. Active bone formation by tetracycline labeling along with a disorganized trabecular compartment suggested the patient presented with OC-poor OPT (Fig. A.1). Further, RANKL-stimulated peripheral blood monocytes formed few mature TRAP+ multinucleated OCs that lacked actin rings *in vitro* (Fig. A.2). Failure of OC differentiation in this assay revealed that the defect was inherent to cells of hematopoietic origin because the addition of recombinant RANKL did not drive OC formation. The patient-derived cells produced full-length RANK protein, and sequencing revealed the genes that encode RANK and RANKL to be wild type. Interestingly, all other OPT-associated genes were sequenced, and no abnormalities were found.

Whole exome sequencing of this OC-poor OPT patient and his parents revealed a homozygous missense mutation in Transcription Factor EB, Tfeb, S401N, a transcription factor previously implicated in modulating OC bone resorption through disruption of lysosomal biogenesis. The goal of this study was to enhance our understanding of how Tfeb relates to OC formation as well as function, and investigate the link between this transcription factor and osteopetrotic phenotypes humans.

Introduction

Osteopetrosis (OPT):

Alteration of OC differentiation or function that is not matched by OB activity leads to a shift in bone composition toward low bone mass osteoporosis or high bone mass osteopetrosis (OPT), both of which have detrimental effects on skeletal health and quality of life for patients. Historically, OPT is attributed to mutations in a limited set of genes involved either in OC formation or function that contribute to OC-poor or OC-rich forms of the disease, respectively. Whether due to the absence of OCs or the presence of dysfunctional OCs, the ultimate phenotypic result is a failure of bone resorption that is associated with a set of clinical observations, including altered bone modeling, brittle bones prone to fracture, and anemia and bone marrow failure. Severe forms of OPT present in early childhood and are often fatal in early years as the bone marrow cavity is overcome by excess bone formation. In cases when the OPT-causing defect is intrinsic to the OC, bone marrow transplant can be an effective treatment to replace these cells of hematopoietic origin (reviewed in (Sobacchi et al., 2013)).

Whole exome sequencing (WES) was undertaken in our family from Shriners Hospitals for Children in St. Louis, and a small pool of candidate genes segregated with the homozygous inheritance pattern in the affected child and his parents. Two of the genes, Rab6c (a member of the Ras oncogene family) and Ubr5 (an E3 ubiquitin ligase), are not associated with bone biology in the literature. A third, however, was a missense mutation in Transcription Factor EB (Tfeb), a gene previously implicated in OC biology. While homozygous in the patient, the mutated Tfeb allele was heterozygous in both parents and absent in his unaffected sister. The particular mutation, S401N, falls within a relatively uncharacterized domain of the transcription factor (Fig. A.3). This serine residue is well conserved in mammals, birds, and reptiles, but not

fishes and amphibians. Evidence by mass spectrometry suggests that this serine residue is not phosphorylated (correspondence with Marco Sardiello, Ph.D.).

Transcription Factor EB (Tfeb):

Transcription Factor EB (Tfeb) is a highly conserved master regulator of lysosomal biogenesis and autophagy. In response to environmental cues, Tfeb is regulated post-translationally via sequestration in the cytoplasm or release into the nucleus. Here, under basal conditions it is localized to lysosomal surfaces by interaction with the lysosome nutrient sensing (LYNUS) machinery and phosphorylated by mammalian target of rapamycin complex 1 (mTORC1) on N-terminal residues S142 and S211 (Settembre et al., 2012). Upon mTORC1 inactivation due to cellular stress, starvation, or lysosomal inhibition, Tfeb becomes dephosphorylated and translocates to the nucleus to activate coordinated lysosomal expression and regulation (CLEAR)-network genes involved in lysosomal biogenesis and autophagy as well as amplify its own signal (reviewed in (Settembre et al., 2013)).

Another recently identified mechanism of post-translational Tfeb regulation in murine models relies on phosphorylation of several residues on the C-terminal end of the protein. Downstream of RANK signaling, these modifications by PKCβ are believed to stabilize Tfeb and facilitate nuclear translocation and therefore upregulation of lysosomal biogenesis factors. In the same murine model system, conditional deletion of Tfeb late in the OC lineage by cathepsin K-cre was associated with increased bone mass but unaltered OC number. Here, lack of Tfeb in OCs contributes to a high bone mass phenotype in mice through insufficient acidification of the OC resorption lacuna through decreased transcription of Tfeb target genes

required for lysosome formation, including H^+ ATPase and chloride channel subunits (Ferron et al., 2013).

Tfeb belongs to the Mitf family of four basic helix-loop-helix-leucine zipper (bHLH-Zip) transcription factors that regulate gene expression by binding to E-box regions as hetero- or homo-dimers. One family member, Mitf, is thought to modulate NFATc1 activity to promote osteoclast function downstream of RANK signaling (Lu et al., 2014). *In vivo*, dominant negative mutations in Mitf are associated with osteopetrotic phenotypes. These mutations disrupt residues that fall within the basic and helix-loop-helix domains of Mitf important for DNA binding, and murine femurs display excessive endochondral bone and lack a bone marrow cavity. These same mutations also hinder heterodimerization of Mitf with Tfe3 to eliminate Tfe3-DNA interactions *in vitro*, and OCs from these mice are small and stain weakly for TRAP compared to controls by histology. Interestingly, such phenotypes are not observed with Mitf of Tfe3 null mutations, but only in combined Mitf/Tfe3-null animals, or those harboring a dominant negative allele (Hemesath et al., 1994; Steingrimsson et al., 2003; 2002). It seems likely that a similar situation might occur with Tfeb. Complete disruption of Tfeb results in embryonic lethality in mice between E9.5-E10.5 due to defects in placental vascularization (Steingrímsson et al., 1998). Phenotypes are not observed in animals heterozygous for Tfeb loss in combination with Tfe3, Tfeb, or Mitf mutations. However, this does not discount the possibility that effects could arise when wild type Tfeb alleles are absent (Steingrimsson et al., 2002). As of yet, no such investigation has been documented.

Results

Tfeb was cloned into the pMX retroviral vector and site directed mutagenesis employed to create the S401N point mutation. Each vector was overexpressed in 293T cells and subsequent western blot analysis confirmed that Tfeb-S401N protein was stable and identical sizes between wild type and mutant suggests that phosphorylation forms between the two proteins are consistent (Fig A.4). Next, both pMX-Tfeb-WT and pMX-Tfeb-S401N TFEB were overexpressed in expanded wild type BMMs. Despite varying densities of seeded BMMs, exposure to RANKL enabled osteoclastogenesis in every condition, and no differences were seen in OC formation between vector controls and either version of Tfeb by TRAP staining (Fig A.5).

Due to the presence of endogenous Tfeb in the BMMs potentially obscuring our results, we obtained floxed Tfeb mice from the laboratory of Babak Razani, Ph.D., at Washington University in St. Louis. We were provided bone marrow from floxed controls and animals bearing the floxed plus LysM-cre alleles, $Tfeb^{fl/fl}$ and $Tfeb^{fl/fl}$;LysMcre, respectively. Using BMMs harvested from these animals, we repeated the infection protocol of pMX-Tfeb-WT and pMX-Tfeb-S401N and found no effect of the mutation on OC formation or function as assayed by TRAP stain, actin rings, and bone resorption pit assay (Fig A.6). Unexpectedly, overexpression of both wild type and S401N Tfeb in BMMs resulted in decreased osteoclastogenesis compared to empty vector controls. Furthermore, OC formation and function by actin ring and resorption pit staining were comparable between WT and S401N-infected cells on both wild type and $Tfeb^{fl/fl}$;LysMcre BMM backgrounds (Fig. A.6). However, qPCR of these BMMs revealed a residual 10% of Tfeb expression. Knockdown to 0.5% was achieved by adding additional cre to $Tfeb^{fl/fl}$;LysMcre BMMs *in vitro*. Here, resorption was slightly altered

but osteoclastogenesis left intact, phenocopying to a small degree the changes observed when Karsenty's group used Cathepsin K-cre (Fig. A.6). (Destaing et al., 2003)

To further probe the effect of mutant Tfeb on the OC, we assayed the expression of common Tfeb targets by quantitative real time PCR: p62 and ATP6v1h. No change in p62 or ATP6v1h expression was seen at basal levels in $Tfeb^{fl/fl}$ or $Tfeb^{fl/fl}$;LysMcre BMMs or OCs, or when levels were induced following cell starvation of 3 hrs with lowered percent FBS (2% compared to normal 10% in media) (Fig A.7). Here, as p62 and ATP6v1h levels rose in both cell types to a similar extent we wondered whether the residual 10% of Tfeb expression in the $Tfeb^{fl/fl}$;LysMcre samples was sufficient to create an effect. Further study was planned to generate animals harboring two LysM-cre alleles, to mitigate this possibility and further elucidate the contribution of Tfeb-S401N in the OC lineage when it is the only form of Tfeb present in a mouse or cultured cell. A knock-in mouse model was also considered.

Concurrent with our laboratory studies, the mother of the deceased OC-poor OPT patient gave birth to another son that was also affected with this condition, presenting with widened metaphyses and epiphyseal plates, as well as hypocalcemia and seizures at two weeks of age. His blood was sequenced for Tfeb, and it was found that he carried two wild type copies of the gene, thus, eliminating Tfeb as a disease-causing candidate. Tfeb studies in the laboratory were discontinued.

Discussion

The genetic etiology of this particular case of OC-poor osteopetrosis remains unclear, and further whole genome sequencing of the newborn affected child, parents, and unaffected sister will be highly informative. Here, we expect to uncover additional candidate genes that contribute to OC formation and thus, increase our general understanding of the differentiation of this important cell type. Until this becomes an option, however, we have comfort in knowing that the second affected child received a bone marrow transplant to allow OCs to form and function in this individual.

Figures and tables

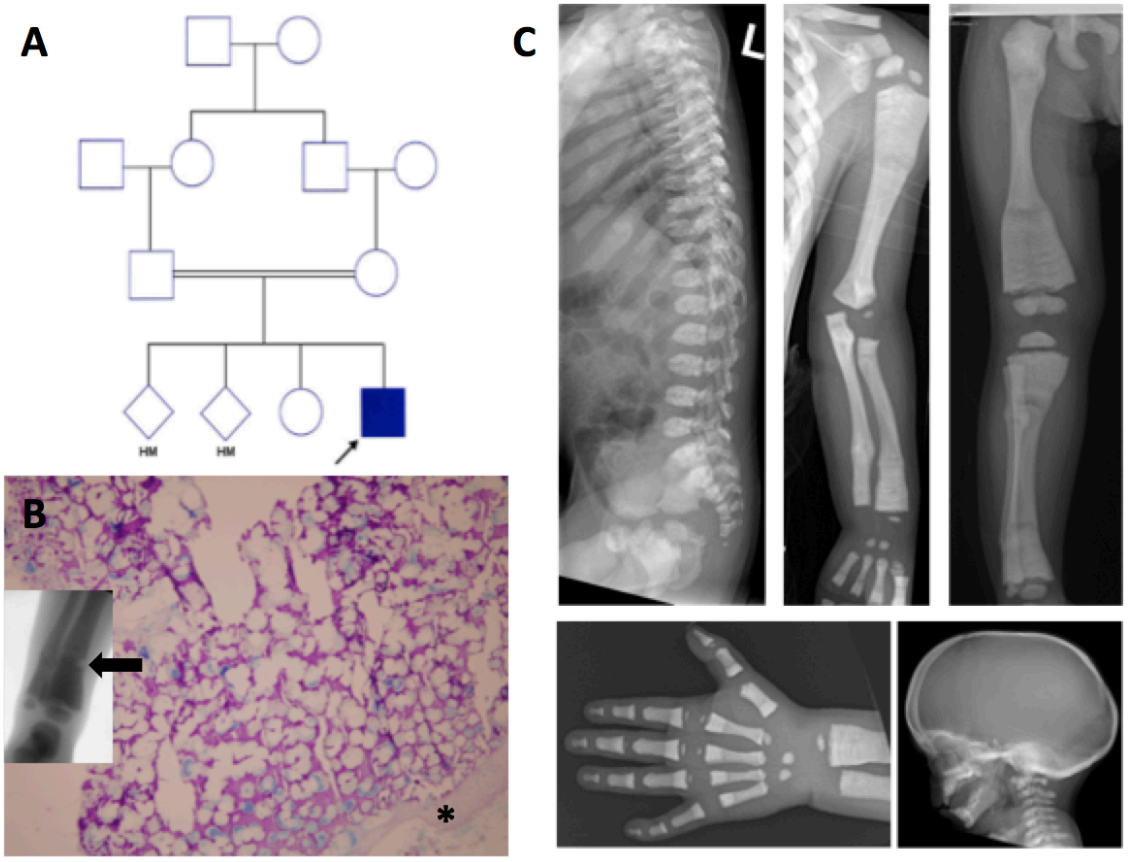

Figure A.1: Patient of consanguineous parents exhibits clinical signs of OPT

Family pedigree in which the four pregnancies from first cousins resulted in two hydatidiform molar (HM) pregnancies, a healthy girl, and boy with OC-poor OPT. B. Tibial bone core biopsy reveals disorganized trabeculae with minimal bone matrix (grey). Cartilage stains purple and cortex is thin (*). C. Radiographic imagine of patient's spine, upper and lower extremities, hand, and skull in which abnormally modeled metaphyses, as well as wide dense ribs, phalanges, and skill base. Figures modified from Gary Gottesman, M.D.

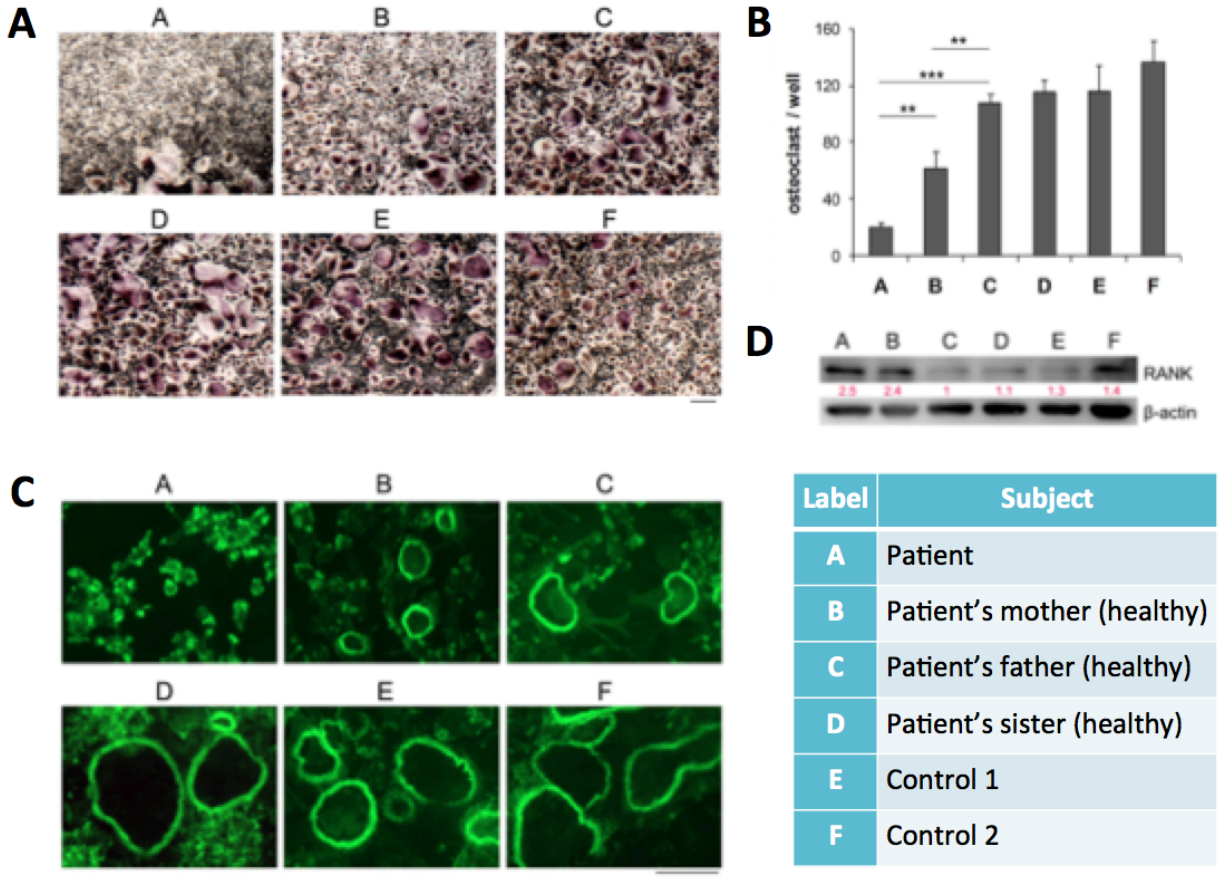

Label	Subject
A	Patient
B	Patient's mother (healthy)
C	Patient's father (healthy)
D	Patient's sister (healthy)
E	Control 1
F	Control 2

Figure A.2: CD14+ cells from patient carrying homozygous S400N Tfeb mutation do not differentiate into mature OCs with actin rings compared to healthy family members and unrelated controls

A-B). *In vitro* differentiation of CD14+ peripheral blood monocytes revealed patient has diminished TRAP+ OC numbers compared to unaffected family members and unrelated controls (quantified in B), with key to the bottom right, mean ± SD is representative of two experiments, **p<0.01, ***p<0.001, scale bars = 1 mm. C) When grown on bone, the patient's cells fail to form actin rings, as shown by FITC-phalloidin. D). Patient cells express RANK, as determined with primary OC cell lysates immunoblotted for RANK, and quantified by normalization to father in red. Figures modified from Gary Gottesman, M.D.

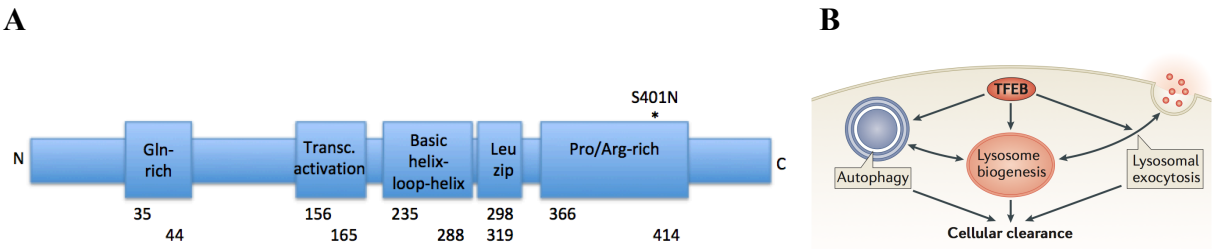

Figure A.3: Schematic representation of Tfeb

A. Amino acids lengths are shown and OC-poor OPT patient mutation location is identified. B. Depiction of Tfeb's role in autophagy, lysosome biogenesis, and exocytosis from (Settembre et al., 2013)

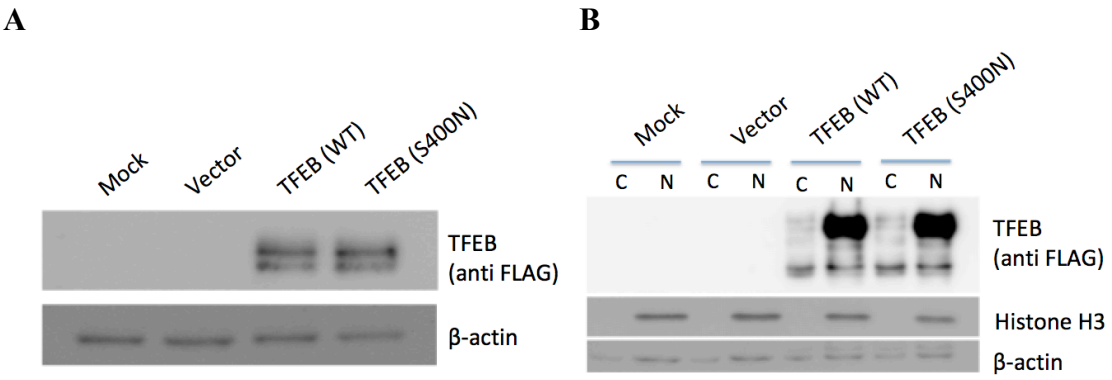

Figure A.4: Overexpression of S400N in 292T cells does not affect protein stability or nuclear localization

A). Western blots against Tfeb in whole cell lysates (A), or nuclear and cytoplasmic extracts (B), show no differences between WT and mutant forms of the protein.

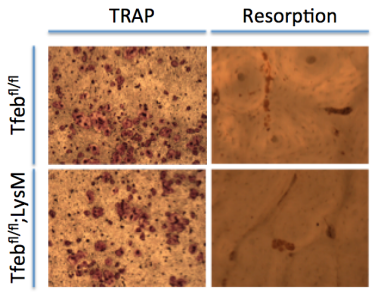

Figure A.5: *In vitro* addition of cre impacts bone resorption to a small degree while not altering osteoclastogenesis

Cre was added retrovirally in culture. TRAP at 2X, resorption pits at 20X.

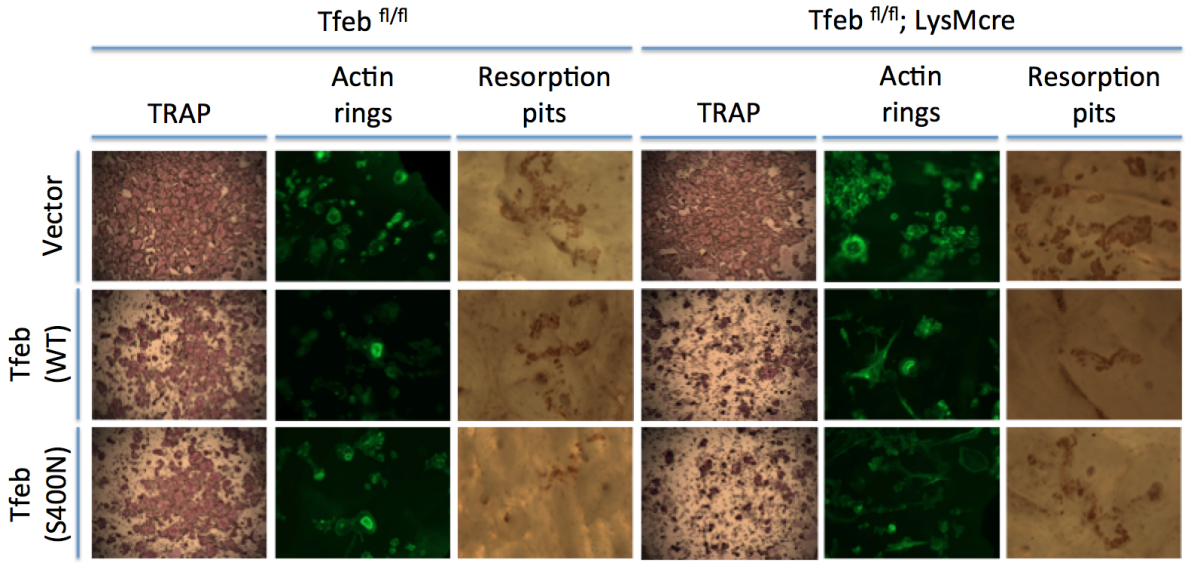

Figure A.6: Overexpression of Tfeb S400N does not alter osteoclastogenesis on WT or cKO backgrounds

Tfeb$^{fl/fl}$ and Tfeb$^{fl/fl}$;LysMcre BMMs were retrovirally infected with constructs and treated with 15 ng/ml RANKL for 5 days. TRAP stained wells are shown at 2X, actin rings and resorption pits at 20X.

A B

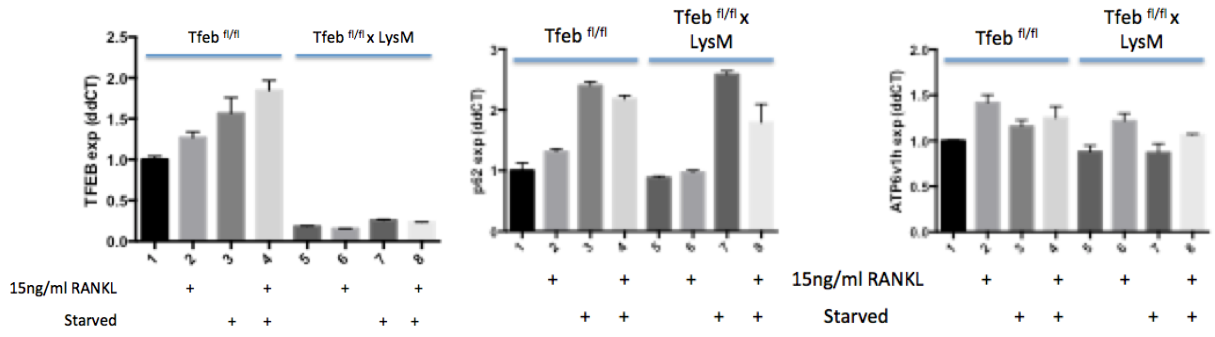

Figure A.7: Tfeb targets are altered with gene knockdown and induction with starvation

A). Tfeb expression is knocked down in cKO BMMs and OCs. B). p62 and ATP6v1h levels are induced when cells are starved in 2% serum, however no differences are seen between controls and cKO cells.

Appendix B –
Osteomyelitis

Abstract

Osteomyelitis (OM) is a severe bacterial infection of the bone associated with an inflammatory reaction and disruption of skeletal integrity in which *Staphylococcus aureus* (*S. aureus*) is the primary causative agent. Although *S. aureus* is considered to be an extracellular pathogen, recent evidence indicates it can persist intracellularly in many cell types, including osteoblasts (OB). Infected OBs produce RANKL and recruit osteoclasts (OCs) to the site of bone infection, but the role of OCs in OM, and in particular their ability to become infected, is not well understood. We hypothesized that *S. aureus* could infect OCs to contribute to OM pathogenesis. While previous work in the laboratory utilized *in vitro* assay of *S. aureus* infection of OCs, confirmation of the accuracy of this model between different bacterial and murine cells was lacking. Work was done to confirm previous findings and take steps toward developing an *in vivo* model of osteomyelitis.

Introduction

Bacterial osteomyelitis is associated with inflammation and pain, and leads to bone loss with increased susceptibility to atraumatic fractures. *S. aureus* is involved in over 60% of OM cases, and treatment generally involves surgical debridement and intravenous antibiotics (Calhoun et al., 2009; Lew and Waldvogel, 2004). Even so, recurrence is common, suggesting that the bacteria may evade antibiotic treatment or capture by the immune system, thereby allowing reactivation of disease at a later date. Surprisingly, little is known about mechanisms of OM etiopathology.

Much of the work in OM pathogenicity has made progress in elucidating bacterial survival strategies. For example, characterization of the *Sae* bacterial locus in *S. aureus* revealed that alpha-type phenol-soluble modulin toxins act osteolytically to promote infection of the bone, and epithelial cell infection studies showed that *S. aureus* organization into small colony variants increases intracellular survival. (Cassat et al., 2013; Tuchscherr et al., 2010). Interestingly, cultured OBs are susceptible to *S. aureus* infection, whereby the bacteria can alter these mammalian cells to promote bone resorption in two ways: triggering OB death, and inducing osteoclastogenesis (Alexander et al., 2003; Ellington, 1999; Hudson et al., 1995). In the latter, *S. aureus*-infected OBs increase expression of proinflammatory cytokines that activate RANKL to promote OC formation (Claro et al., 2013; Marriott et al., 2010; Somayaji et al., 2008). While the recruitment and activation of OCs clearly contributes the osteolytic lesions found in OM, we theorized there might be additional interactions between bacteria and the OC that hadn't yet been probed.

Previous work in our laboratory has used confocal imaging of decalcified calvaria sections from TRAP-Td-Tomato reporter mice injected with GFP-labeled *S. aureus* over the

periosteum to show that *S. aureus* is present within OCs following infection, *in vivo*. We have performed an *in vitro* infection protocol to assay the ability of *S. aureus* to reside in differentiating OCs. Primary expanded bone marrow macrophages (BMMs), cultured +/- RANKL, are infected with *S. aureus* for 30 min, extracellular bacteria killed with 1 hr gentamicin treatment, and cells cultured 16.5 hrs more prior to lysis; intracellular *S. aureus* growth is assessed by colony forming assay, comparing numbers immediately following gentamicin treatment with endpoint. We found that while BMMs cultured in M-CSF alone reduce *S. aureus*, the same cells stimulated with M-CSF + RANKL experience increases of ~50-fold (2 d RANKL) to ~500-fold (3 d RANKL) in intracellular bacteria. Further supporting the requirement for OC lineage differentiation, intracellular *S. aureus* levels are diminished to BMM levels in RANKL-treated cells lacking NFATc1 or NIK, which fail to form OC. To determine whether increased bacterial recovery in mature OCs represents intracellular *S. aureus* proliferation, we used a microscopy approach and observe replicating bacteria in infected OCs *in vitro* by transmission EM (Krauss & Roper, et al., manuscript in preparation).

Results

To probe the effect of *S. aureus* infection on the OC *in vitro*, our laboratory employs a proliferation assay in which bacteria are incubated with BMM, pre-OC, or OC cells for 30 min at a multiplicity of infection (MOI) of 1 or 10. Subsequently, gentamicin is added for 1 hour to kill extracellular bacteria, and cells are lysed. Bacteria residing in the mammalian cells are enumerated by plating on agar and growing colonies overnight. Wells not lysed are allowed to grow for another 16.5 hrs prior to lysis and colony enumeration (18 hrs post-infection) (Fig. B.1 A). Here, in comparing the bacterial burden between 1.5 and 18 hr timepoints we find that while BMMs are effective in killing bacteria, *S. aureus* replicates in day 2 pre-OCs and to an even greater extent in day 3 mature OCs (Fig B.1 B). This same trend is seen regardless of murine strain of BMMs or genetic modification of USA300 MRSA used in the laboratory (Fig B.2).

Because other groups using a similar gentamicin protection assay maintain the drug in the cell culture media throughout the duration of the experiment to prevent escape of internalized bacteria, we sought to attempt this alteration of the protocol (Elsinghorst, 1994). We repeated the assay with two conditions: pulse treatment of gentamicin at 300μg/ml for 1 hour, or continuous gentamicin at 30μg/ml for the duration of the assay. We find that continuous presence of gentamicin abolishes our phenotype of *S. aureus* growth from 1.5 to 18 hrs (Fig B.3). Importantly, cell culture media plated in each condition yielded no bacterial colonies, indicating that with or without gentamicin presence in the media, no extracellular *S. aureus* replication is occurring. As probed media only tested for free-floating *S. aureus*, this brought up the question of whether once-internalized bacteria are replicating on the surface of the OC cells, and prompted us to test whether additional washes of the culture wells would change our results. No differences were detected between bacterial yields at 18 hrs with or without washing, suggesting

all bacteria are truly internalized (Fig B.4). We conclude that the differences seen between pulse vs. continual gentamicin treatment is due to the drug also being internalized by mammalian cells, as has been reported by other groups (Kim et al., 2019). Here, our one-hour pulse gentamicin treatment is sufficient to eliminate extracellular bacteria, and removing it from the media is necessary to avoid its dual killing of intracellular bacteria.

To further support our theory that the OC provides a niche for *S. aureus* to persist and replicate, we turned to confocal microscopy to demonstrate *S. aureus* internalization. To do this we infected TRAP-TdTomato pre-OCs with a GFP-labeled USA300 MRSA strain, fixed cultures in 4% paraformaldehyde, and mounted coverslips with a Dapi nuclear stain. Z-stack images taken on Leica TCS SPE confocal system, and z-plane images confirm that green bacteria are within the same plane as red OCs (Fig B.5), supporting internalization of *S. aureus*. Seeking another method to further demonstrate the intracellularity of *S. aureus*, we fixed cultures of pre-OCs infected with GFP-USA300 with 70% ethanol, and performed flow cytometry. Gating specimens by size and Hoechst staining revealed almost 25% of the population was multinucleated (Fig B.6 A). Further, we detect a higher proportion of GFP-positive bacteria-containing cells in infected samples, confirming for the first time by cytometry that *S. aureus* resides directly within pre-OCs *in vitro* (Fig B.6 B).

As a goal of our laboratory is to develop an *in vivo* model of OM, we began developing an infection model of the calvaria, a procedure previously done in our laboratory for imaging of infected OCs *in vivo*. We anticipated that by inducing osteoclastogenesis at the calvaria with RANKL injection we would create more opportunities for *S. aureus* to preferentially invade OCs and replicate. We injected mice over the calvaria for 4 consecutive days prior to injecting $1.0x10^7$ *S. aureus* cells at the same site. Calvaria were harvested 48 hrs later and crushed via

bullet blending. Minced contents were plated on agar and colonies observed the next day. We find that the RANKL-treated calvaria yield more bacterial colonies that PBS-treated calvaria, suggesting the more abundant the OCs, the more likely *S. aureus* is to seed and replicate at that site (Fig B.7 A-B). To further probe whether the presence of OC at the calvaria alters infection by *S. aureus*, we repeated this model on animals lacking Nfatc1, the master transcriptional regulator of OCs. Surprisingly, no differences were observed in bacterial burden between control and Nfatc1 knockout calvariae (Fig. B.8). This may be due to a preference for bacteria to form an abscess on the skin at the infection site rather than infiltration into the calvaria itself. Many, but not all, animals had identifiable bacteria in the skin over the periosteum, likely masking any trends that would have been seen in the bone had bacteria colonized there instead.

Discussion

As our laboratory seeks to understand the etiopathology of OM in the OC, our primary objective was to establish a solid *in vitro* model. Here, work done to verify that multiple strains of *S. aureus* replicate in pre-OCs of different animal backgrounds brings confidence to the precision of our assay. Furthermore, confirmation that bacteria are truly residing intracellularly in our assay as well as demonstration of co-localization of *S. aureus* in OC cells by confocal microscopy and flow cytometry supports our hypothesis that the OC serves as a replicative niche for *S. aureus* during OM. Steps were also taken to begin developing an *in vivo* model of OM at the calvaria. While data are unreliable due to high variability in the amount of bacteria that seeded to the calvaria, the groundwork has been set for this work to continue. Currently, our laboratory is building on these *in vitro* and *in vivo* results to better demonstrate *S. aureus* intracellularity by microscopy and flow cytometry, as well as develop mouse models through depositing bacteria directly into the tibia as well as tail vein.

Figures and tables

A

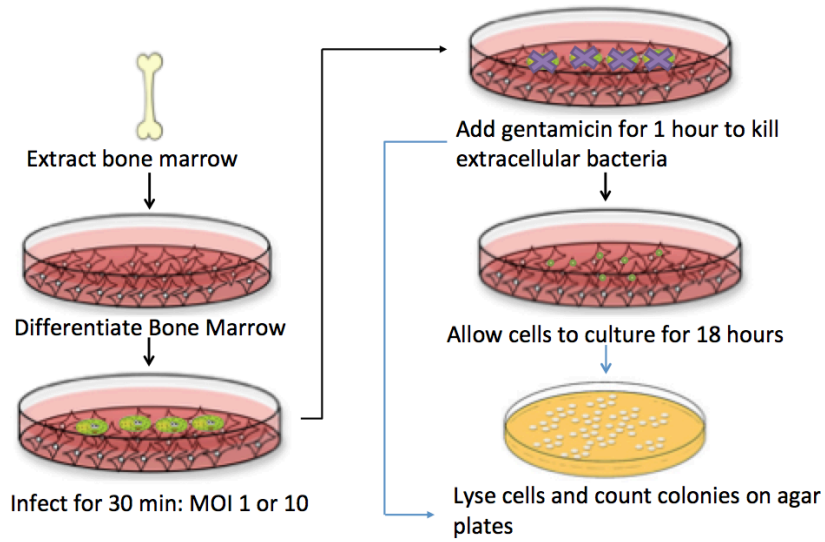

B

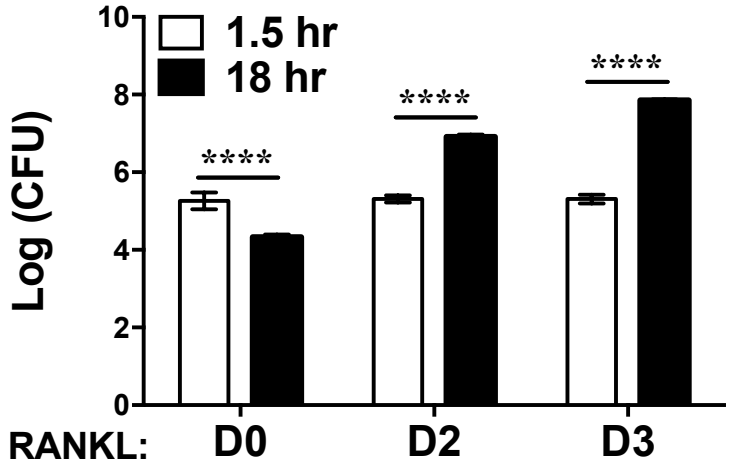

Figure B.1: In vitro infection protocol consistently captures S. aureus proliferation in maturing OCs

A). Bone marrow macrophages and differentiating OCs are infected with *S. aureus* for 30 min and extracellular bacteria killed by 1 h gentamicin treatment. Cells are lysed at 1.5 and 18 hrs post-infection, and colony formation enumerated to quantify *S. aureus* growth or killing in this 16.5 hr period. B). *S. aureus* growth within 16.5 hrs is observed in cells treated with at 2-3 days of RANKL exposure, while *S. aureus* is killed in BMMs cultures. Figure modified from work of Emily Goering and Jennifer Krauss.

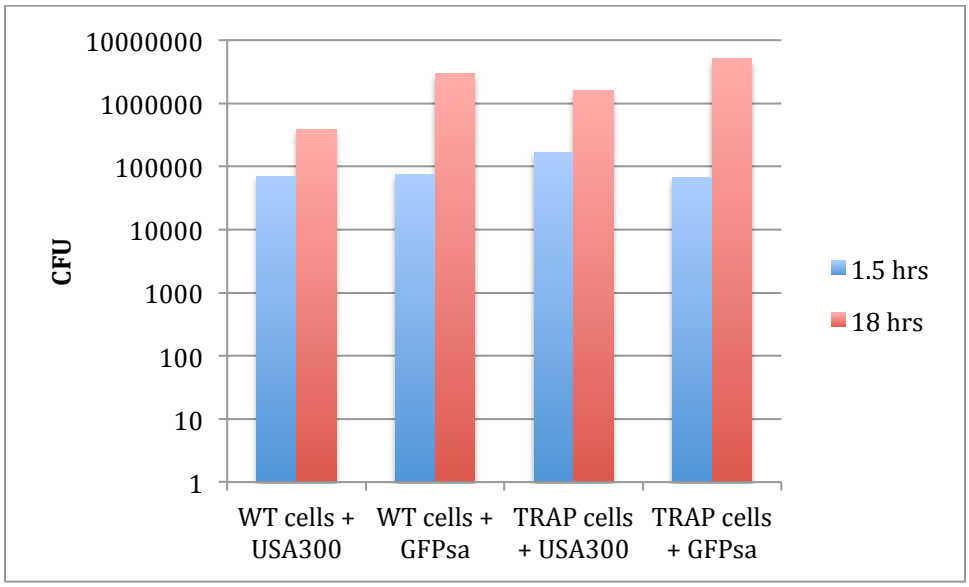

Figure B.2: Different strains of *S. aureus* are capable of growth in OCs derived from mice of different backgrounds

D3 OCs were generated from B6 and Trap-TdTomato mice and infected with USA300 or USA300-GFP *S. aureus.* Growth is seen in each condition.

A

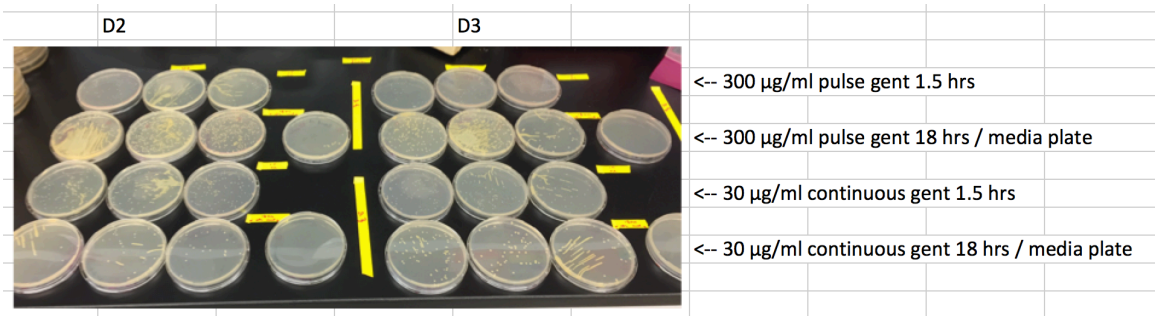

B

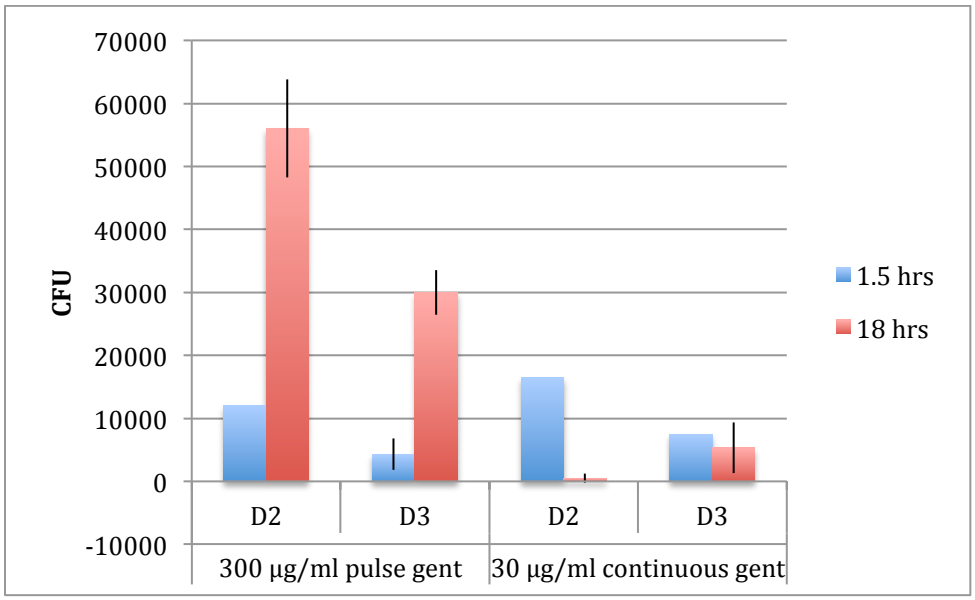

Figure B.3: *S. aureus* growth is lost when antibiotic is kept in culture media throughout infection timecourse

A). 1.5 and 18 hr agar plates display extensive growth in 1 hr 300 µg/ml pulse gentamicin treatment compared to little change when 30 µg/ml gentamicin is continuously in media following infection. B). CFU counts from D2 and D3 plates with different treatments are enumerated.

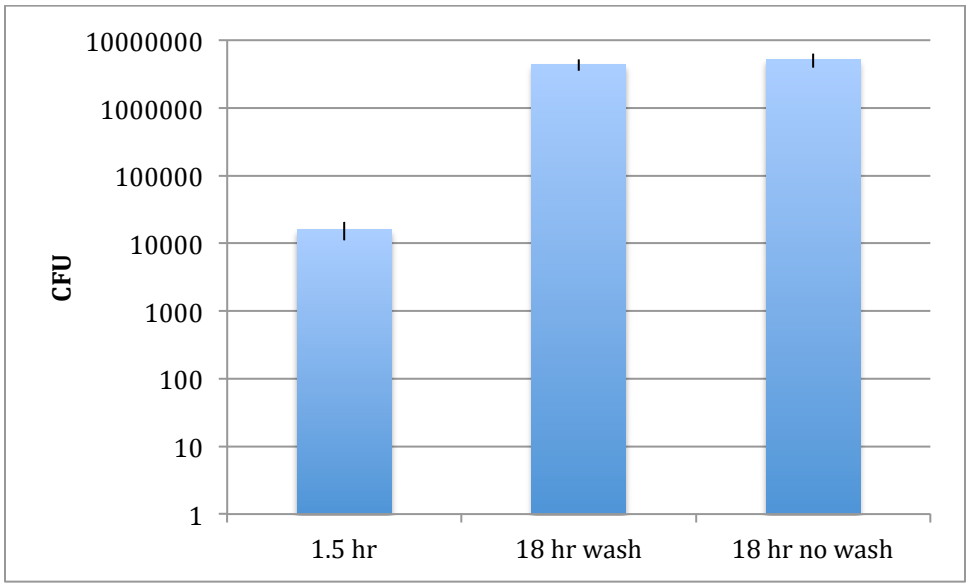

Figure B.4: Washing OCs at 18 hrs has no effect on recovered *S. aureus* by CFU assay

D3 OCs were infected with *S. aureus* and prior to OC lysis at 18 hrs, cells were or were not washed with PBS to eliminate non-intra-cellular bacteria. Identical growth is observed in each condition.

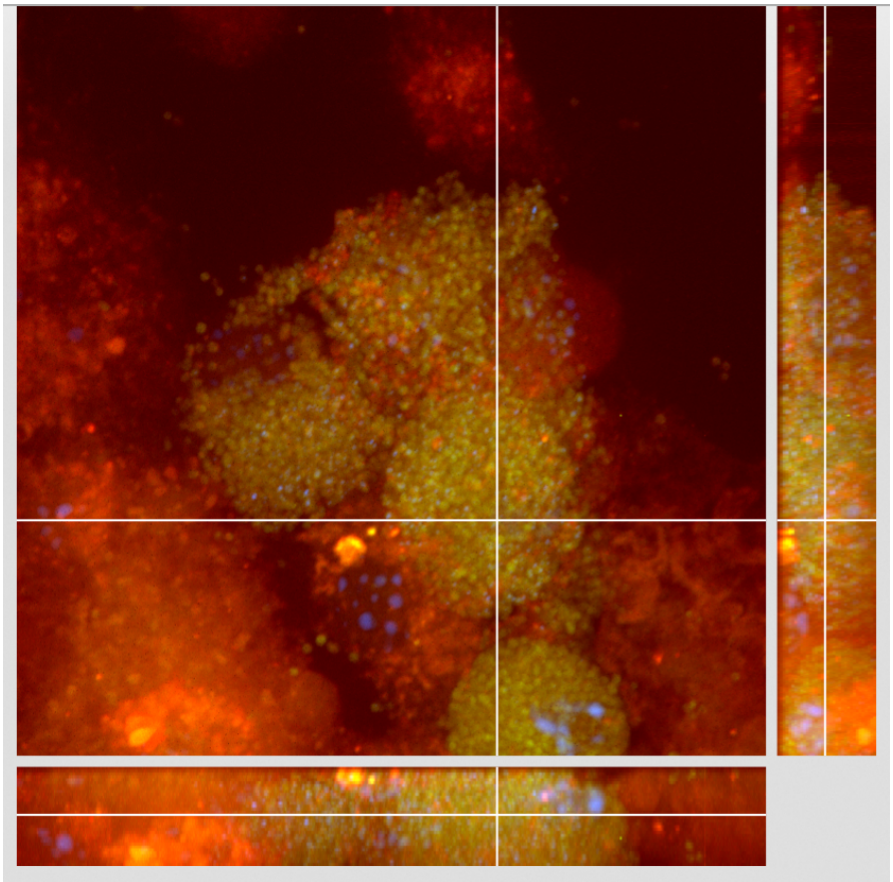

Figure B.5: GFP-labeled *St. aureus* found within OCs 18-hrs post infection

Z-stack confocal imaging was used to visualize D3 TRAP-TdTomato OCs infected with GFP-labeled *S. aureus*. Green bacteria lie within the same plane of red OCs and dapi-stained nuclei, suggesting bacteria are persisting within mammalian cells.

A

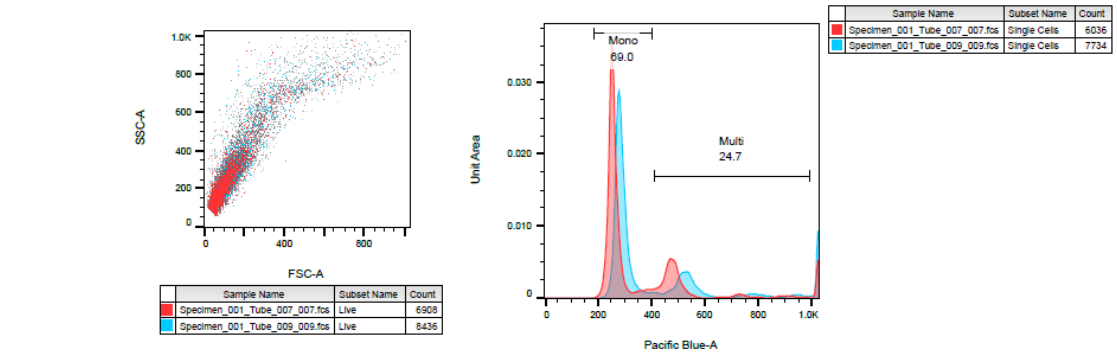

B

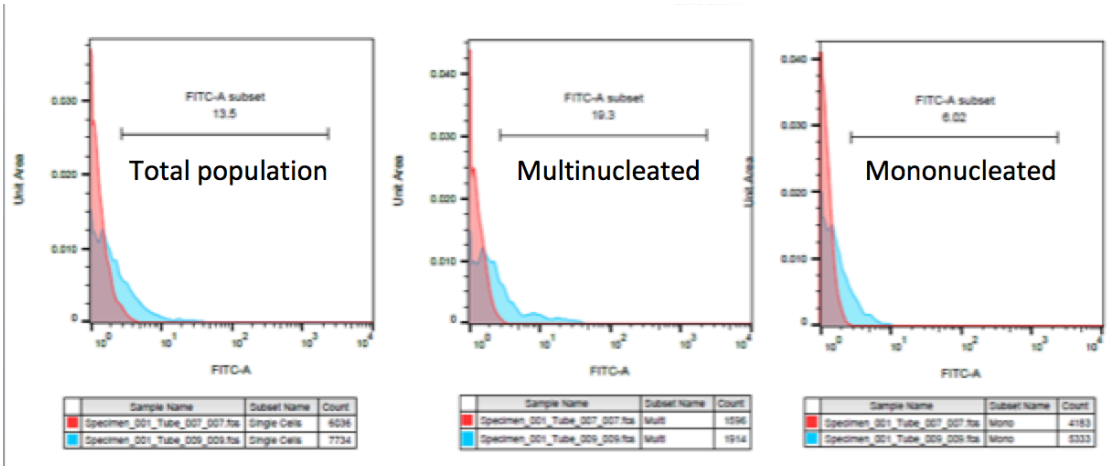

Figure B.6: *S. aureus* is detected by flow cytometry of D2 OCs

A). D2 OCs infected with GFP-labeled *S. aureus* were fixed with 70% ethanol and stained with Hoescht. Live cells were selected and Hoescht was used to gate on multinucleated cells. B). FITC green signal is detected to a greater extend in GFPstaph-infected OCs (blue) compared to uninfected OC cells (red) in total, multinucleated, and mononucleated cell populations.

A

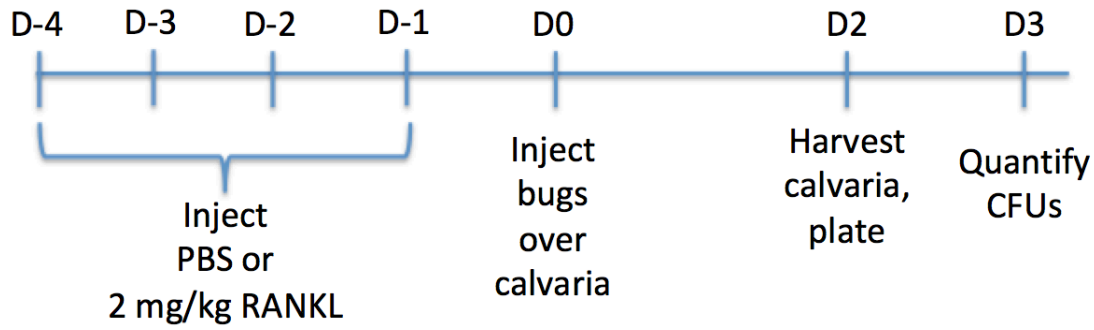

B

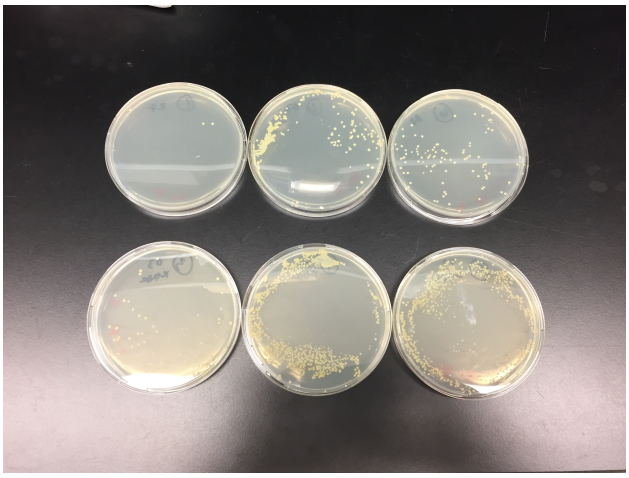

Figure B.7: RANKL-treated calvaria yield more *S. aureus* than PBS-treated calvaria

A). Schematic of experiment whereby 2 mk/kg RANKL or PBS was injected subcutaneously over the perisosteum of the calvaria prior to *S. aureus.* Bacteria were enumerated by CFU assay 48 hrs post infection. B). More *S. aureus* colonies are recovered from RANKL-treated calvaria (bottom) compared to PBS controls (top).

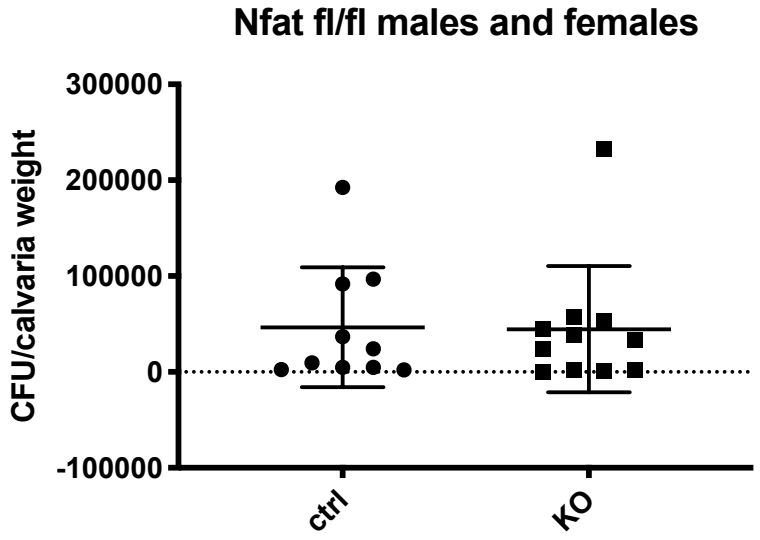

Figure B.8: Loss of Nfatc1 does not affect *S. aureus* infection of the calvaria

Nfatc1$^{fl/fl}$ (ctrl) and Nfatc1$^{fl/fl}$; cre (KO) mice were treated with RANKL over the calvaria for 4 days prior to inoculation with *S. aureus* in the same location. Enumeration of bacterial residence 48 hrs post-infection reveals no difference between groups of animals.

References

Adam, M.P., Ardinger, H.H., Pagon, R.A., Wallace, S.E., Bean, L.J., Stephens, K., Amemiya, A., and Züchner, S. (1993). Charcot-Marie-Tooth Neuropathy Type 2A.

Alexander, E.H., Rivera, F.A., Marriott, I., Anguita, J., Bost, K.L., and Hudson, M.C. (2003). Staphylococcus aureus - induced tumor necrosis factor - related apoptosis - inducing ligand expression mediates apoptosis and caspase-8 activation in infected osteoblasts. BMC Microbiol. *3*, 5.

Amend, S.R., Uluckan, O., Hurchla, M., Leib, D., Novack, D.V., Silva, M., Frazier, W., and Weilbaecher, K.N. (2015). Thrombospondin-1 regulates bone homeostasis through effects on bone matrix integrity and nitric oxide signaling in osteoclasts. J Bone Miner Res *30*, 106–115.

An, J.H., Yang, J.-Y., Ahn, B.Y., Cho, S.W., Jung, J.Y., Cho, H.Y., Cho, Y.M., Kim, S.W., Park, K.S., Kim, S.Y., et al. (2010). Enhanced mitochondrial biogenesis contributes to Wnt induced osteoblastic differentiation of C3H10T1/2 cells. Bone *47*, 140–150.

Anginot, A., Dacquin, R., Mazzorana, M., and Jurdic, P. (2007). Lymphocytes and the Dap12 adaptor are key regulators of osteoclast activation associated with gonadal failure. PLoS ONE *2*, e585.

Arai, F., Miyamoto, T., Ohneda, O., Inada, T., Sudo, T., Brasel, K., Miyata, T., Anderson, D.M., and Suda, T. (1999). Commitment and Differentiation of Osteoclast Precursor Cells by the Sequential Expression of C-Fms and Receptor Activator of Nuclear Factor κb (Rank) Receptors. Journal of Experimental Medicine *190*, 1741–1754.

Arnett, T.R., and Dempster, D.W. (1986). Effect of pH on bone resorption by rat osteoclasts in vitro. Endocrinology *119*, 119–124.

Arnett, T.R., and Orriss, I.R. (2018). Metabolic properties of the osteoclast. Bone *115*, 25–30.

Arnett, T.R., Gibbons, D.C., Utting, J.C., Orriss, I.R., Hoebertz, A., Rosendaal, M., and Meghji, S. (2003). Hypoxia is a major stimulator of osteoclast formation and bone resorption. J. Cell. Physiol. *196*, 2–8.

Ashrafi, G., and Schwarz, T.L. (2013). The pathways of mitophagy for quality control and clearance of mitochondria. Cell Death Differ. *20*, 31–42.

Bach, D., Pich, S., Soriano, F.X., Vega, N., Baumgartner, B., Oriola, J., Daugaard, J.R., Lloberas, J., Camps, M., Zierath, J.R., et al. (2003). Mitofusin-2 Determines Mitochondrial Network Architecture and Mitochondrial Metabolism. J. Biol. Chem. *278*, 17190–17197.

Bakkar, N., Ladner, K., Canan, B.D., Liyanarachchi, S., Bal, N.C., Pant, M., Periasamy, M., Li, Q., Janssen, P.M.L., and Guttridge, D.C. (2012). IKKα and alternative NF-κB regulate PGC-1β to promote oxidative muscle metabolism. The Journal of Cell Biology *196*, 497–511.

Ban, T., Ishihara, T., Kohno, H., Saita, S., Ichimura, A., Maenaka, K., Oka, T., Mihara, K., and Ishihara, N. (2017). Molecular basis of selective mitochondrial fusion by heterotypic action between OPA1 and cardiolipin. Nat Cell Biol *19*, 856–863.

Basso, V., Marchesan, E., Peggion, C., Chakraborty, J., Stockum, von, S., Giacomello, M., Ottolini, D., Debattisti, V., Caicci, F., Tasca, E., et al. (2018). Regulation of ER-mitochondria contacts by Parkin via Mfn2. Pharmacological Research *138*, 43–56.

Belteki, G., Haigh, J., Kabacs, N., Haigh, K., Sison, K., Costantini, F., Whitsett, J., Quaggin, S.E., and Nagy, A. (2005). Conditional and inducible transgene expression in mice through the combinatorial use of Cre-mediated recombination and tetracycline induction. Nucleic Acids Res. *33*, e51–e51.

Betz, C., Stracka, D., Prescianotto-Baschong, C., Frieden, M., Demaurex, N., and Hall, M.N. (2013). Feature Article: mTOR complex 2-Akt signaling at mitochondria-associated endoplasmic reticulum membranes (MAM) regulates mitochondrial physiology. Proc. Natl. Acad. Sci. U.S.a. *110*, 12526–12534.

Billia, F., Hauck, L., Konecny, F., Rao, V., Shen, J., and Mak, T.W. (2011). PTEN-inducible kinase 1 (PINK1)/Park6 is indispensable for normal heart function. Proc. Natl. Acad. Sci. U.S.a. *108*, 9572–9577.

Blair, H.C., Teitelbaum, S.L., Tan, H.L., Koziol, C.M., and Schlesinger, P.H. (1991). Passive chloride permeability charge coupled to H(+)-ATPase of avian osteoclast ruffled membrane. Am. J. Physiol. *260*, C1315–C1324.

Bossard, M.J., Tomaszek, T.A., Thompson, S.K., Amegadzie, B.Y., Hanning, C.R., Jones, C., Kurdyla, J.T., McNulty, D.E., Drake, F.H., Gowen, M., et al. (1996). Proteolytic activity of human osteoclast cathepsin K. Expression, purification, activation, and substrate identification. J. Biol. Chem. *271*, 12517–12524.

Boutant, M., Kulkarni, S.S., Joffraud, M., Ratajczak, J., Valera Alberni, M., Combe, R., Zorzano, A., and Cantó, C. (2017). Mfn2 is critical for brown adipose tissue thermogenic function. Embo J. *36*, 1543–1558.

Bouxsein, M.L., Boyd, S.K., Christiansen, B.A., Guldberg, R.E., Jepsen, K.J., and Müller, R. (2010). Guidelines for assessment of bone microstructure in rodents using micro-computed tomography. J Bone Miner Res *25*, 1468–1486.

BURSTONE, M.S. (1959). Histochemical demonstration of acid phosphatase activity in osteoclasts. J. Histochem. Cytochem. *7*, 39–41.

Calhoun, J.H., Manring, M.M., and Shirtliff, M. (2009). Osteomyelitis of the long bones. Semin Plast Surg *23*, 59–72.

Callaway, D.A., and Jiang, J.X. (2015). Reactive oxygen species and oxidative stress in osteoclastogenesis, skeletal aging and bone diseases. J Bone Miner Metab *33*, 359–370.

Cappariello, A., Maurizi, A., Veeriah, V., and Teti, A. (2014). Archives of Biochemistry and Biophysics. Archives of Biochemistry and Biophysics *558*, 70–78.

Cartoni, R., Arnaud, E., Médard, J.-J., Poirot, O., Courvoisier, D.S., Chrast, R., and Martinou, J.-C. (2010). Expression of mitofusin 2(R94Q) in a transgenic mouse leads to Charcot-Marie-Tooth neuropathy type 2A. Brain *133*, 1460–1469.

Cassat, J.E., Hammer, N.D., Campbell, J.P., Benson, M.A., Perrien, D.S., Mrak, L.N., Smeltzer, M.S., Torres, V.J., and Skaar, E.P. (2013). A secreted bacterial protease tailors the Staphylococcus aureus virulence repertoire to modulate bone remodeling during osteomyelitis. Cell Host Microbe *13*, 759–772.

Celsi, F., Pizzo, P., Brini, M., Leo, S., Fotino, C., Pinton, P., and Rizzuto, R. (2009). Mitochondria, calcium and cell death: A deadly triad in neurodegeneration. BBA - Bioenergetics *1787*, 335–344.

Chen, H., Chomyn, A., and Chan, D.C. (2005). Disruption of fusion results in mitochondrial heterogeneity and dysfunction. J. Biol. Chem. *280*, 26185–26192.

Chen, H., Detmer, S.A., Ewald, A.J., Griffin, E.E., Fraser, S.E., and Chan, D.C. (2003). Mitofusins Mfn1 and Mfn2 coordinately regulate mitochondrial fusion and are essential for embryonic development. The Journal of Cell Biology *160*, 189–200.

Chen, H., McCaffery, J.M., and Chan, D.C. (2007). Mitochondrial Fusion Protects against Neurodegeneration in the Cerebellum. Cell *130*, 548–562.

Chen, H., Vermulst, M., Wang, Y.E., Chomyn, A., Prolla, T.A., McCaffery, J.M., and Chan, D.C. (2010). Mitochondrial fusion is required for mtDNA stability in skeletal muscle and tolerance of mtDNA mutations. Cell *141*, 280–289.

Chen, Y., and Dorn, G.W. (2013). PINK1-phosphorylated mitofusin 2 is a Parkin receptor for culling damaged mitochondria. Science *340*, 471–475.

Chen, Y., Liu, Y., and Dorn, G.W., II (2011). Mitochondrial Fusion is Essential for Organelle Function and Cardiac Homeostasis. Circ. Res. *109*, 1327–1331.

Chim, S.M., Tickner, J., Chow, S.T., Kuek, V., Guo, B., Zhang, G., Rosen, V., Erber, W., and Xu, J. (2013). Angiogenic factors in bone local environment. Cytokine Growth Factor Rev. *24*, 297–310.

Claro, T., Widaa, A., McDonnell, C., Foster, T.J., O'Brien, F.J., and Kerrigan, S.W. (2013). Staphylococcus aureus protein A binding to osteoblast tumour necrosis factor receptor 1 results in activation of nuclear factor kappa B and release of interleukin-6 in bone infection. Microbiology (Reading, Engl.) *159*, 147–154.

Clausen, B.E., Burkhardt, C., Reith, W., Renkawitz, R., and Förster, I. (1999). Conditional gene targeting in macrophages and granulocytes using LysMcre mice. Transgenic Res. *8*, 265–277.

Czupalla, C., Mansukoski, H., Pursche, T., Krause, E., and Hoflack, B. (2005). Comparative study of protein and mRNA expression during osteoclastogenesis. Proteomics *5*, 3868–3875.

Dai, Q., Xie, F., Han, Y., Ma, X., Zhou, S., Jiang, L., Zou, W., and Wang, J. (2017). Inactivation of Regulatory-associated Protein of mTOR (Raptor)/Mammalian Target of Rapamycin Complex 1 (mTORC1) Signaling in Osteoclasts Increases Bone Mass by Inhibiting Osteoclast Differentiation in Mice. J. Biol. Chem. *292*, 196–204.

Daumke, O., and Roux, A. (2017). Mitochondrial Homeostasis: How Do Dimers of Mitofusins Mediate Mitochondrial Fusion? Current Biology *27*, R353–R356.

de Brito, O.M., and Scorrano, L. (2008). Mitofusin 2 tethers endoplasmic reticulum to mitochondria. Nature *456*, 605–610.

Decker, C.E., Yang, Z., Rimer, R., Park-Min, K.-H., Macaubas, C., Mellins, E.D., Novack, D.V., and Faccio, R. (2015). Tmem178 acts in a novel negative feedback loop targeting NFATc1 to regulate bone mass. Proceedings of the National Academy of Sciences 201511285–201511286.

Dempster, D.W., Compston, J.E., Drezner, M.K., Glorieux, F.H., Kanis, J.A., Malluche, H., Meunier, P.J., Ott, S.M., Recker, R.R., and Parfitt, A.M. (2012). Standardized nomenclature, symbols, and units for bone histomorphometry: A 2012 update of the report of the ASBMR Histomorphometry Nomenclature Committee. J Bone Miner Res *28*, 2–17.

DeSelm, C.J., Miller, B.C., Zou, W., Beatty, W.L., van Meel, E., Takahata, Y., Klumperman, J., Tooze, S.A., Teitelbaum, S.L., and Virgin, H.W. (2011). Autophagy proteins regulate the secretory component of osteoclastic bone resorption. Dev. Cell *21*, 966–974.

Destaing, O., Saltel, F., Géminard, J.-C., Jurdic, P., and Bard, F. (2003). Podosomes display actin turnover and dynamic self-organization in osteoclasts expressing actin-green fluorescent protein. Mol. Biol. Cell *14*, 407–416.

Dorn, G.W., II (2016). ScienceDirect Mitochondrial fission/fusion and cardiomyopathy. Current Opinion in Genetics & Development *38*, 38–44.

Dorn, G.W., II (2019). Evolving Concepts of Mitochondrial Dynamics. Annu. Rev. Physiol. *81*, 1–17.

Dorn, G.W., Vega, R.B., and Kelly, D.P. (2015). Mitochondrial biogenesis and dynamics in the developing and diseased heart. Genes & Development *29*, 1981–1991.

Drake, F.H., Dodds, R.A., James, I.E., Connor, J.R., Debouck, C., Richardson, S., Lee-Rykaczewski, E., Coleman, L., Rieman, D., Barthlow, R., et al. (1996). Cathepsin K, but not cathepsins B, L, or S, is abundantly expressed in human osteoclasts. J. Biol. Chem. *271*, 12511–12516.

Elefteriou, F., and Yang, X. (2011). Genetic mouse models for bone studies—Strengths and limitations. Bone *49*, 1242–1254.

Ellington, J.K.E.A. (1999). Mechanisms of Staphylococcus aureus invasion of cultured osteoblasts. 1–7.

Elsinghorst, E.A. (1994). Measurement of invasion by gentamicin resistance. Meth. Enzymol. *236*, 405–420.

Engelhart, E.A., and Hoppins, S. (2019). A catalytic domain variant of Mitofusin requiring a wildtype paralog for function uncouples mitochondrial outer-membrane tethering and fusion. J. Biol. Chem. jbc.RA118.006347–25.

Eschenbacher, W.H., Song, M., Chen, Y., Bhandari, P., Zhao, P., Jowdy, C.C., Engelhard, J.T., and Dorn, G.W. (2012). Two rare human mitofusin 2 mutations alter mitochondrial dynamics and induce retinal and cardiac pathology in Drosophila. PLoS ONE *7*, e44296.

Ferron, M., Settembre, C., Shimazu, J., Lacombe, J., Kato, S., Rawlings, D.J., Ballabio, A., and Karsenty, G. (2013). A RANKL-PKC -TFEB signaling cascade is necessary for lysosomal biogenesis in osteoclasts. Genes & Development *27*, 955–969.

Filadi, R., Greotti, E., and Pizzo, P. (2018a). Highlighting the endoplasmic reticulum-mitochondria connection: Focus on Mitofusin 2. Pharmacological Research *128*, 42–51.

Filadi, R., Greotti, E., Turacchio, G., Luini, A., Pozzan, T., and Pizzo, P. (2016). Presenilin 2 Modulates Endoplasmic Reticulum-Mitochondria Coupling by Tuning the Antagonistic Effect of Mitofusin 2. Cell Rep *15*, 2226–2238.

Filadi, R., Pendin, D., and Pizzo, P. (2018b). Mitofusin 2: from functions to disease. 1–13.

Franco, A., Kitsis, R.N., Fleischer, J.A., Gavathiotis, E., Kornfeld, O.S., Gong, G., Biris, N., Benz, A., Qvit, N., Donnelly, S.K., et al. (2016). Correcting mitochondrial fusion by manipulating mitofusin conformations. Nature *540*, 74–79.

Frisch, B.J., Porter, R.L., Gigliotti, B.J., Olm-Shipman, A.J., Weber, J.M., O'Keefe, R.J., Jordan, C.T., and Calvi, L.M. (2009). In vivo prostaglandin E2 treatment alters the bone marrow microenvironment and preferentially expands short-term hematopoietic stem cells. Blood *114*, 4054–4063.

Funalot, B., Magdelaine, C., Sturtz, F., Ouvrier, R., and Vallat, J.-M. (2009). [Ultrastructural lesions of axonal mitochondria in patients with childhood-onset Charcot-Marie-Tooth disease due to MFN2 mutations]. Bull. Acad. Natl. Med. *193*, 151–60–discussion160–1.

Gao, A.W., Canto, C., and Houtkooper, R.H. (2014). Mitochondrial response to nutrient availability and its role in metabolic disease. EMBO Molecular Medicine 1–10.

Gay, C.V., and Mueller, W.J. (1974). Carbonic anhydrase and osteoclasts: localization by labeled inhibitor autoradiography. Science *183*, 432–434.

Glantschnig, H., Fisher, J.E., Wesolowski, G., Rodan, G.A., and Reszka, A.A. (2003). M-CSF, TNFalpha and RANK ligand promote osteoclast survival by signaling through mTOR/S6 kinase.

Cell Death Differ. *10*, 1165–1177.

Gomes, L.C., Di Benedetto, G., and Scorrano, L. (2011). During autophagy mitochondria elongate, are spared from degradation and sustain cell viability. Nat Cell Biol *13*, 589–598.

Gong, G., Song, M., Csordas, G., Kelly, D.P., Matkovich, S.J., and Dorn, G.W. (2015). Parkin-mediated mitophagy directs perinatal cardiac metabolic maturation in mice. Science *350*, aad2459–aad2459.

Guo, X., Chen, K.-H., Guo, Y., Liao, H., Tang, J., and Xiao, R.-P. (2007). Mitofusin 2 Triggers Vascular Smooth Muscle Cell Apoptosis via Mitochondrial Death Pathway. Circ. Res. *101*, 1113–1122.

Gustafsson, Å.B., and Dorn, G.W., II (2019). Evolving and Expanding the Roles of Mitophagy as a Homeostatic and Pathogenic Process. Physiological Reviews *99*, 853–892.

Hemesath, T.J., Steingrímsson, E., McGill, G., Hansen, M.J., Vaught, J., Hodgkinson, C.A., Arnheiter, H., Copeland, N.G., Jenkins, N.A., and Fisher, D.E. (1994). microphthalmia, a critical factor in melanocyte development, defines a discrete transcription factor family. Genes & Development *8*, 2770–2780.

Henriksen, K., Karsdal, M.A., and John Martin, T. (2013). Osteoclast-Derived Coupling Factors in Bone Remodeling. Calcif Tissue Int *94*, 88–97.

Hogan, P.G., Chen, L., Nardone, J., and Rao, A. (2003). Transcriptional regulation by calcium, calcineurin, and NFAT. Genes & Development *17*, 2205–2232.

Hu, C., Huang, Y., and Li, L. (2017). Drp1-Dependent Mitochondrial Fission Plays Critical Roles in Physiological and Pathological Progresses in Mammals. Int J Mol Sci *18*, 144.

Hudson, M.C., Ramp, W.K., Nicholson, N.C., Williams, A.S., and Nousiainen, M.T. (1995). Internalization of Staphylococcus aureus by cultured osteoblasts. Microb. Pathog. *19*, 409–419.

Indo, Y., Takeshita, S., Ishii, K.-A., Hoshii, T., Aburatani, H., Hirao, A., and Ikeda, K. (2013). Metabolic regulation of osteoclast differentiation and function. J Bone Miner Res *28*, 2392–2399.

Ishida, N., Hayashi, K., Hoshijima, M., Ogawa, T., Koga, S., Miyatake, Y., Kumegawa, M., Kimura, T., and Takeya, T. (2002). Large scale gene expression analysis of osteoclastogenesis in vitro and elucidation of NFAT2 as a key regulator. J. Biol. Chem. *277*, 41147–41156.

Ivanova, A., Signore, M., Caro, N., Greene, N.D.E., Copp, A.J., and Martinez-Barbera, J.P. (2005). In vivo genetic ablation by Cre-mediated expression of diphtheria toxin fragment A. Genesis *43*, 129–135.

Jheng, H.-F., Tsai, P.-J., Guo, S.-M., Kuo, L.-H., Chang, C.-S., Su, I.-J., Chang, C.-R., and Tsai, Y.-S. (2012). Mitochondrial fission contributes to mitochondrial dysfunction and insulin resistance in skeletal muscle. Mol. Cell. Biol. *32*, 309–319.

Jin, S.M., and Youle, R.J. (2013). The accumulation of misfolded proteins in the mitochondrial matrix is sensed by PINK1 to induce PARK2/Parkin-mediated mitophagy of polarized mitochondria. Autophagy *9*, 1750–1757.

Karbowski, M., Norris, K.L., Cleland, M.M., Jeong, S.-Y., and Youle, R.J. (2006). Role of Bax and Bak in mitochondrial morphogenesis. Nature *443*, 658–662.

Kasahara, A., Cipolat, S., Chen, Y., Dorn, G.W., and Scorrano, L. (2013). Mitochondrial fusion directs cardiomyocyte differentiation via calcineurin and Notch signaling. Science *342*, 734–737.

Khosla, S., Melton, L.J., III, and Riggs, B.L. (2011). The unitary model for estrogen deficiency and the pathogenesis of osteoporosis: Is a revision needed? J Bone Miner Res *26*, 441–451.

Kim, H., Kim, T., Jeong, B.-C., Cho, I.-T., Han, D., Takegahara, N., Negishi-Koga, T., Takayanagi, H., Lee, J.H., Sul, J.-Y., et al. (2013). Tmem64 Modulates Calcium Signaling during RANKL-Mediated Osteoclast Differentiation. Cell Metab. *17*, 249–260.

Kim, J.-H., Chaurasia, A.K., Batool, N., Ko, K.S., and Kim, K.K. (2019). Alternative Enzyme Protection Assay To Overcome the Drawbacks of the Gentamicin Protection Assay for Measuring Entry and Intracellular Survival of Staphylococci. Infection and Immunity *87*, 173.

Kim, J.-M., Jeong, D., Kang, H.K., Jung, S.Y., Kang, S.S., and Min, B.-M. (2007). Osteoclast precursors display dynamic metabolic shifts toward accelerated glucose metabolism at an early stage of RANKL-stimulated osteoclast differentiation. Cell. Physiol. Biochem. *20*, 935–946.

Kobayashi, Y., Uehara, S., Udagawa, N., and Takahashi, N. (2016). Regulation of bone metabolism by Wnt signals. J Biochem *159*, 387–392.

Koshiba, T., Detmer, S.A., Kaiser, J.T., Chen, H., McCaffery, J.M., and Chan, D.C. (2004). Structural basis of mitochondrial tethering by mitofusin complexes. Science *305*, 858–862.

Kubli, D.A., Zhang, X., Lee, Y., Hanna, R.A., Quinsay, M.N., Nguyen, C.K., Jimenez, R., Petrosyan, S., Murphy, A.N., and Gustafsson, Å.B. (2013). Parkin protein deficiency exacerbates cardiac injury and reduces survival following myocardial infarction. J. Biol. Chem. *288*, 915–926.

Lee, H., and Yoon, Y. (2016). Mitochondrial fission and fusion. Biochemical Society Transactions *44*, 1725–1735.

Lee, H., and Yoon, Y. (2018). Mitochondrial Membrane Dynamics—Functional Positioning of OPA1. Antioxidants (Basel) *7*, 186–21.

Lee, S., Sterky, F.H., Mourier, A., Terzioglu, M., Cullheim, S., Olson, L., and Larsson, N.-G. (2012). Mitofusin 2 is necessary for striatal axonal projections of midbrain dopamine neurons. Human Molecular Genetics *21*, 4827–4835.

Lemma, S., Sboarina, M., Porporato, P.E., Zini, N., Sonveaux, P., Di Pompo, G., Baldini, N., and PhD, S.A. (2016). The International Journal of Biochemistry & Cell Biology. International

Journal of Biochemistry and Cell Biology *79*, 168–180.

Lerner, U.H., and Ohlsson, C. (2015). The WNT system: background and its role in bone. J Intern Med *277*, 630–649.

Lew, D.P., and Waldvogel, F.A. (2004). Osteomyelitis. Lancet *364*, 369–379.

Li, T., Han, J., Jia, L., Hu, X., Chen, L., and Wang, Y. (2019). PKM2 coordinates glycolysis with mitochondrial fusion and oxidative phosphorylation. Protein & Cell 1–12.

Loiseau, D., Chevrollier, A., Verny, C., Guillet, V., Gueguen, N., Pou de Crescenzo, M.-A., Ferré, M., Malinge, M.-C., Guichet, A., Nicolas, G., et al. (2007). Mitochondrial coupling defect in Charcot-Marie-Tooth type 2A disease. Ann. Neurol. *61*, 315–323.

Lu, S.-Y., Li, M., and Lin, Y.-L. (2014). Mitf regulates osteoclastogenesis by modulating NFATc1 activity. Experimental Cell Research *328*, 32–43.

Luchsinger, L.L., de Almeida, M.J., Corrigan, D.J., Mumau, M., and Snoeck, H.-W. (2016). Mitofusin 2 maintains haematopoietic stem cells with extensive lymphoid potential. Nature *529*, 528–531.

Lymperi, S., Ersek, A., Ferraro, F., Dazzi, F., and Horwood, N.J. (2011). Inhibition of osteoclast function reduces hematopoietic stem cell numbers in vivo. Blood *117*, 1540–1549.

Lymperi, S., Horwood, N., Marley, S., Gordon, M.Y., Cope, A.P., and Dazzi, F. (2008). Strontium can increase some osteoblasts without increasing hematopoietic stem cells. Blood *111*, 1173–1181.

Mahdaviani, K., Benador, I.Y., Su, S., Gharakhanian, R.A., Stiles, L., Trudeau, K.M., Cardamone, M., Enríquez Zarralanga, V., Ritou, E., Aprahamian, T., et al. (2017). Mfn2 deletion in brown adipose tissue protects from insulin resistance and impairs thermogenesis. EMBO Rep. *18*, 1123–1138.

Manczak, M., Calkins, M.J., and Reddy, P.H. (2011). Impaired mitochondrial dynamics and abnormal interaction of amyloid beta with mitochondrial protein Drp1 in neurons from patients with Alzheimer's disease: implications for neuronal damage. Human Molecular Genetics *20*, 2495–2509.

Marriott, I., Gray, D.L., Tranguch, S.L., Fowler, V.G., Jr, Stryjewski, M., Levin, L.S., Hudson, M.C., and Bost, K.L. (2010). Osteoblasts Express the Inflammatory Cytokine Interleukin-6 in a Murine Model of Staphylococcus aureus Osteomyelitis and Infected Human Bone Tissue. The American Journal of Pathology *164*, 1399–1406.

Martin, T.J., and Sims, N.A. (2005). Osteoclast-derived activity in the coupling of bone formation to resorption. Trends Mol Med *11*, 76–81.

Matsuda, N., Sato, S., Shiba, K., Okatsu, K., Saisho, K., Gautier, C.A., Sou, Y.-S., Saiki, S., Kawajiri, S., Sato, F., et al. (2010). PINK1 stabilized by mitochondrial depolarization recruits

Parkin to damaged mitochondria and activates latent Parkin for mitophagy. The Journal of Cell Biology *189*, 211–221.

Misko, A., Jiang, S., Wegorzewska, I., Milbrandt, J., and Baloh, R.H. (2010). Mitofusin 2 is necessary for transport of axonal mitochondria and interacts with the Miro/Milton complex. J. Neurosci. *30*, 4232–4240.

Molina, A.J.A., Wikstrom, J.D., Stiles, L., Las, G., Mohamed, H., Elorza, A., Walzer, G., Twig, G., Katz, S., Corkey, B.E., et al. (2009). Mitochondrial networking protects beta-cells from nutrient-induced apoptosis. Diabetes *58*, 2303–2315.

Monticelli, S., and Rao, A. (2002). NFAT1 and NFAT2 are positive regulators of IL-4 gene transcription. Eur. J. Immunol. *32*, 2971–2978.

Morita, S., Kojima, T., and Kitamura, T. (2000). Plat-E: an efficient and stable system for transient packaging of retroviruses. Gene Ther. *7*, 1063–1066.

Morten, K.J., Badder, L., and Knowles, H.J. (2013). Differential regulation of HIF-mediated pathways increases mitochondrial metabolism and ATP production in hypoxic osteoclasts. J. Pathol. *229*, 755–764.

Movérare-Skrtic, S., Henning, P., Liu, X., Nagano, K., Saito, H., Börjesson, A.E., Sjögren, K., Windahl, S.H., Farman, H., Kindlund, B., et al. (2014). Osteoblast-derived WNT16 represses osteoclastogenesis and prevents cortical bone fragility fractures. Nat Med *20*, 1279–1288.

Moyzis, A., and Gustafsson, Å.B. (2019). Multiple recycling routes: Canonical vs. non-canonical mitophagy in the heart. Biochim Biophys Acta Mol Basis Dis *1865*, 797–809.

Mozdy, A.D., and Shaw, J.M. (2003). A fuzzy mitochondrial fusion apparatus comes into focus. Nat. Rev. Mol. Cell Biol. *4*, 468–478.

Nakashima, T., Hayashi, M., Fukunaga, T., Kurata, K., Oh-hora, M., Feng, J.Q., Bonewald, L.F., Kodama, T., Wutz, A., Wagner, E.F., et al. (2011). Evidence for osteocyte regulation of bone homeostasis through RANKL expression. Nat Med *17*, 1231–1234.

Naon, D., Zaninello, M., Giacomello, M., Varanita, T., Grespi, F., Lakshminaranayan, S., Serafini, A., Semenzato, M., Herkenne, S., Hernández-Alvarez, M.I., et al. (2016). Critical reappraisal confirms that Mitofusin 2 is an endoplasmic reticulum-mitochondria tether. Proc. Natl. Acad. Sci. U.S.a. *113*, 11249–11254.

Narendra, D.P., Jin, S.M., Tanaka, A., Suen, D.-F., Gautier, C.A., Shen, J., Cookson, M.R., and Youle, R.J. (2010). PINK1 is selectively stabilized on impaired mitochondria to activate Parkin. PLoS Biol. *8*, e1000298.

Nazarian, A., Snyder, B.D., Zurakowski, D., and Müller, R. (2008). Quantitative micro-computed tomography: A non-invasive method to assess equivalent bone mineral density. Bone *43*, 302–311.

Nelson, C.A., Warren, J.T., Wang, M.W.H., Teitelbaum, S.L., and Fremont, D.H. (2012). RANKL Employs Distinct Binding Modes to Engage RANK and the Osteoprotegerin Decoy Receptor. Structure/Folding and Design *20*, 1971–1982.

Novack, D.V., and Faccio, R. (2011). Osteoclast motility: Putting the brakes on bone resorption. Ageing Research Reviews *10*, 54–61.

Novack, D.V., and Teitelbaum, S.L. (2008). The osteoclast: friend or foe? Annu. Rev. Pathol. Mech. Dis. *3*, 457–484.

Novack, D.V. (2010). Role of NF-κB in the skeleton. Nature Publishing Group *21*, 169–182.

Novack, D.V. (2011). Role of NF-κB in the skeleton. Cell Res. *21*, 169–182.

Novack, D.V., Yin, L., Hagen-Stapleton, A., Schreiber, R.D., Goeddel, D.V., Ross, F.P., and Teitelbaum, S.L. (2003). The IkappaB function of NF-kappaB2 p100 controls stimulated osteoclastogenesis. Journal of Experimental Medicine *198*, 771–781.

Ono, T. (2018). Recent advances in osteoclast biology. Histochemistry and Cell Biology *149*, 325–341.

Papanicolaou, K.N., Khairallah, R.J., Ngoh, G.A., Chikando, A., Luptak, I., O'Shea, K.M., Riley, D.D., Lugus, J.J., Colucci, W.S., Lederer, W.J., et al. (2011). Mitofusin-2 Maintains Mitochondrial Structure and Contributes to Stress-Induced Permeability Transition in Cardiac Myocytes. Mol. Cell. Biol. *31*, 1309–1328.

Papanicolaou, K.N., Kikuchi, R., Ngoh, G.A., Coughlan, K.A., Dominguez, I., Stanley, W.C., and Walsh, K. (2012a). Mitofusins 1 and 2 are essential for postnatal metabolic remodeling in heart. Circ. Res. *111*, 1012–1026.

Papanicolaou, K.N., Ngoh, G.A., Dabkowski, E.R., O'Connell, K.A., Ribeiro, R.F., Jr., Stanley, W.C., and Walsh, K. (2012b). Cardiomyocyte deletion of mitofusin-1 leads to mitochondrial fragmentation and improves tolerance to ROS-induced mitochondrial dysfunction and cell death. American Journal of Physiology-Heart and Circulatory Physiology *302*, H167–H179.

Pham, A.H., McCaffery, J.M., and Chan, D.C. (2012). Mouse lines with photo-activatable mitochondria to study mitochondrial dynamics. Genesis *50*, 833–843.

Quinn, J.M., Elliott, J., Gillespie, M.T., and Martin, T.J. (1998). A combination of osteoclast differentiation factor and macrophage-colony stimulating factor is sufficient for both human and mouse osteoclast formation in vitro. Endocrinology *139*, 4424–4427.

Rambold, A.S., Kostelecky, B., Elia, N., and Lippincott-Schwartz, J. (2011). Tubular network formation protects mitochondria from autophagosomal degradation during nutrient starvation. Proc. Natl. Acad. Sci. U.S.a. *108*, 10190–10195.

Rocha, A.G., Franco, A., Krezel, A.M., Rumsey, J.M., Alberti, J.M., Knight, W.C., Biris, N., Zacharioudakis, E., Janetka, J.W., Baloh, R.H., et al. (2018). MFN2 agonists reverse

mitochondrial defects in preclinical models of Charcot-Marie-Tooth disease type 2A. Science *360*, 336–341.

SALTEL, F., CHABADEL, A., BONNELYE, E., and JURDIC, P. (2008). Actin cytoskeletal organisation in osteoclasts: A model to decipher transmigration and matrix degradation. European Journal of Cell Biology *87*, 459–468.

Sandoval, H., Yao, C.-K., Chen, K., Jaiswal, M., Donti, T., Lin, Y.Q., Bayat, V., Xiong, B., Zhang, K., David, G., et al. (2014). Mitochondrial fusion but not fission regulates larval growth and synaptic development through steroid hormone production. eLife *3*, 211–223.

Saporta, M.A., Dang, V., Volfson, D., Zou, B., Xie, X.S., Adebola, A., Liem, R.K., Shy, M., and Dimos, J.T. (2015). Axonal Charcot-Marie-Tooth disease patient-derived motor neurons demonstrate disease-specific phenotypes including abnormal electrophysiological properties. Exp. Neurol. *263*, 190–199.

Schrepfer, E., and Scorrano, L. (2016). Mitofusins, from Mitochondria to Metabolism. Mol. Cell *61*, 683–694.

Seeling, M., Hillenhoff, U., David, J.P., Schett, G., Tuckermann, J., Lux, A., and Nimmerjahn, F. (2013). Inflammatory monocytes and Fcγ receptor IV on osteoclasts are critical for bone destruction during inflammatory arthritis in mice. Proc. Natl. Acad. Sci. U.S.a. *110*, 10729–10734.

Settembre, C., Fraldi, A., Medina, D.L., and Ballabio, A. (2013). Signals from the lysosome: a control centre for cellular clearance and energy metabolism. Nat. Rev. Mol. Cell Biol. *14*, 283–296.

Settembre, C., Zoncu, R., Medina, D.L., Vetrini, F., Erdin, S., Erdin, S., Huynh, T., Ferron, M., Karsenty, G., Vellard, M.C., et al. (2012). A lysosome-to-nucleus signalling mechanism senses and regulates the lysosome via mTOR and TFEB. Embo J. *31*, 1095–1108.

Sevillano Fernández, J.A., Paz Fraile, A., Cano Ballesteros, J.C., Villalba García, M.V., Otero Pérez, R., and Gilsanz Fernández, C. (1994). [Charcot-Marie-Tooth disease, dilated myocardiopathy and cardiac conduction disorders]. An Med Interna *11*, 455–456.

Shares, B.H., Busch, M., White, N., Shum, L., and Eliseev, R.A. (2018). Active mitochondria support osteogenic differentiation by stimulating β-catenin acetylation. J. Biol. Chem. *293*, 16019–16027.

Shashkova, E.V., Trivedi, J., Cline-Smith, A.B., Ferris, C., Buchwald, Z.S., Gibbs, J., Novack, D., and Aurora, R. (2016). Osteoclast-Primed Foxp3+ CD8 T Cells Induce T-bet, Eomesodermin, and IFN-γ To Regulate Bone Resorption. J. Immunol. *197*, 726–735.

Shirihai, O.S., Song, M., and Dorn, G.W. (2015). How mitochondrial dynamism orchestrates mitophagy. Circ. Res. *116*, 1835–1849.

Silver, I.A., Murrills, R.J., and Etherington, D.J. (1988). Microelectrode studies on the acid

microenvironment beneath adherent macrophages and osteoclasts. Experimental Cell Research *175*, 266–276.

Sobacchi, C., Schulz, A., Coxon, F.P., Villa, A., and Helfrich, M.H. (2013). Osteopetrosis: genetics, treatment and new insights into osteoclast function. Nat Rev Endocrinol *9*, 522–536.

Sole, G., Ferrer, X., Vital, C., Martin-Negrier, M.-L., Vital, A., and Latour, P. (2009). Ultrastructural mitochondrial modifications characteristic of mitofusin 2 mutations (CMT2A). J. Peripher. Nerv. Syst. *14*, 206–207.

Somayaji, S.N., Ritchie, S., Sahraei, M., Marriott, I., and Hudson, M.C. (2008). Staphylococcus aureus Induces Expression of Receptor Activator of NF- B Ligand and Prostaglandin E2 in Infected Murine Osteoblasts. Infection and Immunity *76*, 5120–5126.

Song, M., Mihara, K., Chen, Y., Scorrano, L., and Dorn, G.W. (2015). Mitochondrial fission and fusion factors reciprocally orchestrate mitophagic culling in mouse hearts and cultured fibroblasts. Cell Metab. *21*, 273–285.

Spencer, J.A., Ferraro, F., Roussakis, E., Klein, A., Wu, J., Runnels, J.M., Zaher, W., Mortensen, L.J., Alt, C., Turcotte, R., et al. (2014). Direct measurement of local oxygen concentration in the bone marrow of live animals. Nature *508*, 269–273.

Steingrimsson, E., Arnheiter, H., Hallsson, J.H., Lamoreux, M.L., Copeland, N.G., and Jenkins, N.A. (2003). Interallelic complementation at the mouse Mitf locus. Genetics *163*, 267–276.

Steingrimsson, E., Tessarollo, L., Pathak, B., Hou, L., Arnheiter, H., Copeland, N.G., and Jenkins, N.A. (2002). Mitf and Tfe3, two members of the Mitf-Tfe family of bHLH-Zip transcription factors, have important but functionally redundant roles in osteoclast development. Proceedings of the National Academy of Sciences *99*, 4477–4482.

Steingrímsson, E., Tessarollo, L., Reid, S.W., Jenkins, N.A., and Copeland, N.G. (1998). The bHLH-Zip transcription factor Tfeb is essential for placental vascularization. Development *125*, 4607–4616.

Strickland, A.V., Rebelo, A.P., Zhang, F., Price, J., Bolon, B., Silva, J.P., Wen, R., and Züchner, S. (2014). Characterization of the mitofusin 2 R94W mutation in a knock-in mouse model. J. Peripher. Nerv. Syst. *19*, 152–164.

Sugatani, T., and Hruska, K.A. (2005). Akt1/Akt2 and Mammalian Target of Rapamycin/Bim Play Critical Roles in Osteoclast Differentiation and Survival, Respectively, Whereas Akt Is Dispensable for Cell Survival in Isolated Osteoclast Precursors. J. Biol. Chem. *280*, 3583–3589.

Sun, N., Yun, J., Liu, J., Malide, D., Liu, C., Rovira, I.I., Holmström, K.M., Fergusson, M.M., Yoo, Y.H., Combs, C.A., et al. (2015). Measuring In Vivo Mitophagy. Mol. Cell *60*, 685–696.

Takayanagi, H., Kim, S., Koga, T., Nishina, H., Isshiki, M., Yoshida, H., Saiura, A., Isobe, M., Yokochi, T., Inoue, J.-I., et al. (2002). Induction and activation of the transcription factor NFATc1 (NFAT2) integrate RANKL signaling in terminal differentiation of osteoclasts. Devcel

3, 889–901.

Takeshita, S., Kaji, K., and Kudo, A. (2000). Identification and characterization of the new osteoclast progenitor with macrophage phenotypes being able to differentiate into mature osteoclasts. J Bone Miner Res *15*, 1477–1488.

Teitelbaum, S.L. (2011). The osteoclast and its unique cytoskeleton. Annals of the New York Academy of Sciences *1240*, 14–17.

Teti, A. (2013). Mechanisms of osteoclast-dependent bone formation. Bonekey Rep *2*, 449.

Tiedemann, K., Le Nihouannen, D., Fong, J.E., Hussein, O., Barralet, J.E., and Komarova, S.V. (2017). Regulation of Osteoclast Growth and Fusion by mTOR/raptor and mTOR/rictor/Akt. Front. Cell Dev. Biol. *5*, 227–10.

Trebec-Reynolds, D.P., Voronov, I., Heersche, J.N.M., and Manolson, M.F. (2010). VEGF-A expression in osteoclasts is regulated by NF-kappaB induction of HIF-1alpha. J. Cell. Biochem. *110*, 343–351.

Tuchscherr, L., Heitmann, V., Hussain, M., Viemann, D., Roth, J., Eiff, von, C., Peters, G., Becker, K., and Löffler, B. (2010). Staphylococcus aureusSmall‐Colony Variants Are Adapted Phenotypes for Intracellular Persistence. J Infect Dis *202*, 1031–1040.

Vaira, S., Johnson, T., Hirbe, A.C., Alhawagri, M., Anwisye, I., Sammut, B., O'Neal, J., Zou, W., Weilbaecher, K.N., Faccio, R., et al. (2008). RelB is the NF-kappaB subunit downstream of NIK responsible for osteoclast differentiation. Proc. Natl. Acad. Sci. U.S.a. *105*, 3897–3902.

van Vliet, A.R., and Agostinis, P. (2018). Mitochondria-Associated Membranes and ER Stress. Curr. Top. Microbiol. Immunol. *414*, 73–102.

Ventura-Clapier, R., Garnier, A., and Veksler, V. (2008). Transcriptional control of mitochondrial biogenesis: the central role of PGC-1alpha. Cardiovasc. Res. *79*, 208–217.

Ventura-Clapier, R., Moulin, M., Piquereau, J., Lemaire, C., Mericskay, M., Veksler, V., and Garnier, A. (2017). Mitochondria: a central target for sex differences in pathologies. Clin. Sci. *131*, 803–822.

Vettori, A., Bergamin, G., Moro, E., Vazza, G., Polo, G., Tiso, N., Argenton, F., and Mostacciuolo, M.L. (2011). Developmental defects and neuromuscular alterations due to mitofusin 2 gene (MFN2) silencing in zebrafish: a new model for Charcot-Marie-Tooth type 2A neuropathy. Neuromuscular Disorders *21*, 58–67.

Wang, X., Su, B., Lee, H.G., Li, X., Perry, G., Smith, M.A., and Zhu, X. (2009). Impaired Balance of Mitochondrial Fission and Fusion in Alzheimer's Disease. Journal of Neuroscience *29*, 9090–9103.

Wu, Y., Torchia, J., Yao, W., Lane, N.E., Lanier, L.L., Nakamura, M.C., and Humphrey, M.B. (2007). Bone microenvironment specific roles of ITAM adapter signaling during bone

remodeling induced by acute estrogen-deficiency. PLoS ONE *2*, e586.

Xu, F., and Teitelbaum, S.L. (2013). Osteoclasts: New Insights. Nature Publishing Group *1*, 11–26.

Xu, K., Chen, G., Li, X., Wu, X., Chang, Z., Xu, J., Zhu, Y., Yin, P., Liang, X., and Dong, L. (2017). MFN2 suppresses cancer progression through inhibition of mTORC2/Akt signaling. Nature Publishing Group 1–13.

Xue, R., Meng, Q., Lu, D., Liu, X., Wang, Y., and Hao, J. (2018). Mitofusin2 Induces Cell Autophagy of Pancreatic Cancer through Inhibiting the PI3K/Akt/mTOR Signaling Pathway. Oxidative Medicine and Cellular Longevity *2018*, 1–8.

Yagi, M., Miyamoto, T., Sawatani, Y., Iwamoto, K., Hosogane, N., Fujita, N., Morita, K., Ninomiya, K., Suzuki, T., Miyamoto, K., et al. (2005). DC-STAMP is essential for cell–cell fusion in osteoclasts and foreign body giant cells. Journal of Experimental Medicine *202*, 345–351.

Yang, Y.-M., Kim, M.S., Son, A., Hong, J.H., Kim, K.-H., Seo, J.T., Lee, S.-I., and Shin, D.M. (2009). Alteration of RANKL-Induced Osteoclastogenesis in Primary Cultured Osteoclasts From SERCA2 +/−Mice. J Bone Miner Res *24*, 1763–1769.

Yarmolinsky, M., and Hoess, R. (2015). The Legacy of Nat Sternberg: The Genesis of Cre-lox Technology.

Yoshida, H., Inagaki, M., Shukuya, M., Ono, S., Doba, N., Shimizu, N., Sugano, I., and Nagao, K. (1991). [Charcot-Marie-Tooth disease associated with dilated cardiomyopathy: an autopsy case report]. Kokyu to Junkan *39*, 295–298.

Zarei, A., Yang, C., Gibbs, J., Davis, J.L., Ballard, A., Zeng, R., Cox, L., and Veis, D.J. (2018). Manipulation of the Alternative NF-κB Pathway in Mice Has Sexually Dimorphic Effects on Bone. JBMR Plus *21*, 169–169.

Zeng, R., Faccio, R., and Novack, D.V. (2015). Alternative NF-κB Regulates RANKL-Induced Osteoclast Differentiation and Mitochondrial Biogenesis via Independent Mechanisms. J Bone Miner Res *30*, 2287–2299.

Zhang, Y., Rohatgi, N., Veis, D.J., Schilling, J., Teitelbaum, S.L., and Zou, W. (2018). PGC1β Organizes the Osteoclast Cytoskeleton by Mitochondrial Biogenesis and Activation. J Bone Miner Res *33*, 1114–1125.

Zou, W., DeSelm, C.J., Broekelmann, T.J., Mecham, R.P., Vande Pol, S., Choi, K., and Teitelbaum, S.L. (2012). Paxillin contracts the osteoclast cytoskeleton. J Bone Miner Res *27*, 2490–2500.

Züchner, S., Mersiyanova, I.V., Muglia, M., Bissar-Tadmouri, N., Rochelle, J., Dadali, E.L., Zappia, M., Nelis, E., Patitucci, A., Senderek, J., et al. (2004). Mutations in the mitochondrial GTPase mitofusin 2 cause Charcot-Marie-Tooth neuropathy type 2A. Nat Genet *36*, 449–451.